Development of a Wireless Sensor to Detect Cracks in Welded Steel

Connections

by

Lisa J. Novak, B.S.C.E.

Thesis

Presented to the Faculty of the Graduate School of

The University of Texas at Austin

in Partial Fulfillment

of the Requirements

for the Degree of

Master of Science in Engineering

The University of Texas at Austin

August 2002

Development of a Wireless Sensor to Detect Cracks in Welded Steel Connections

Approved by
Supervising Committee:

_____

Sharon L. Wood

_____

Dean P. Neikirk

_____

Karl. H. Frank

Dedication

To my parents, Robert and Loraine, for their advice, support, humor, and love.

To my sister, Karen, for providing the inspiration to get this written.

Acknowledgements

Abstract

Development of a Wireless Sensor to Detect Cracks in Welded Steel Connections

Lisa J. Novak, M.S.E.

The University of Texas at Austin, 2002

Supervisor: Sharon L. Wood

The objective of this thesis is to develop a prototype wireless sensor to detect cracks in welded steel moment resisting connections. These sensors are intended to be installed during construction after the connection has been welded. The sensor comprises two parts: a RF transmitter and a switch. Switches have been developed to monitor the formation of a crack at a single point, or distributed along the length of a weld. An electrical circuit model of the prototype sensor was also developed that provided an excellent representation of the measured characteristic frequency.

Table of Contents

List of Tables

List of Figures

CHAPTER 1
Introduction

1.1 INTRODUCTION

The 1994 Northridge earthquake caused extensive damage to a large number of steel moment-resisting frames. Before the earthquake, the welded flange - bolted web moment connections were widely believed to be able to undergo large rotations without damage based on laboratory tests (Fig 1.1).
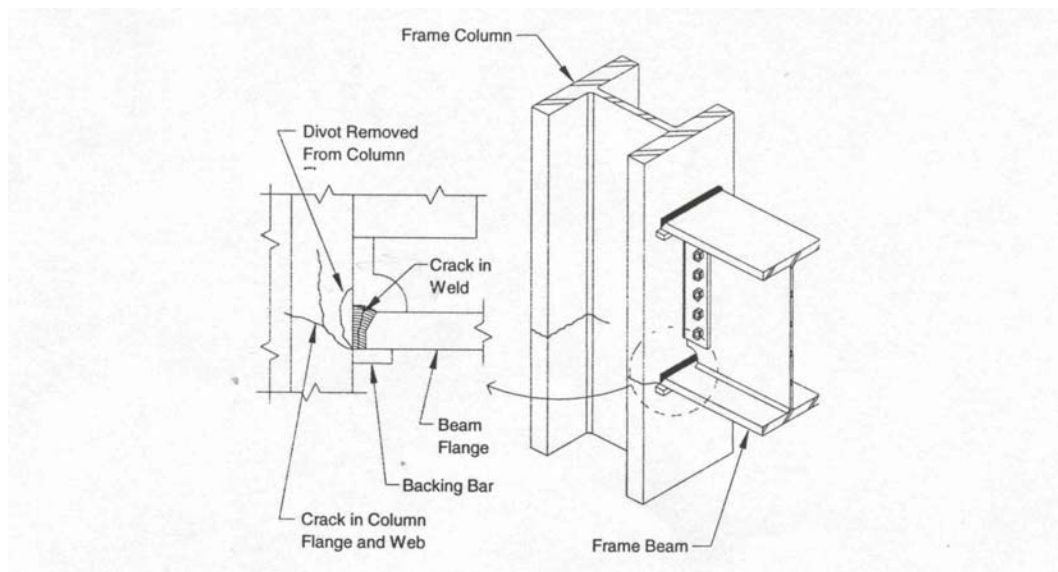
Figure 1.1 Typical Welded Flange – Bolted Web Moment Connection

(Sabol and Engelhardt, 1996)

The poor performance of these connections was first discovered in steel structures under construction at the time of the earthquake. Visual and ultrasonic inspection of other steel frame structures in the area revealed a large number of damaged connections. The damaged structures ranged from one to 26 stories in

height. Structures from 30 years of age to those under construction showed signs of damage upon inspection. Most alarmingly, structures on sites that experienced only moderate levels of ground shaking were damaged, the type of movement that the connections were designed to resist. This raised concerns that similar damage had occurred in other steel moment frame buildings due to past earthquakes. Reports of damage from the 1989 Loma Prieta and 1992 Landers earthquakes exist, but the extent of damage was not as widespread as that observed after the Northridge earthquake (SAC, 1995).

Over 200 welded moment-resisting frames in the epicentral region were discovered to have fractured welds within the beam/column connections. Damage reports indicate that in many cases brittle fractures were initiated at very low levels of plastic demand and in some cases while the structures were elastic. Many of the connection fractures were found in buildings that did not appear to have sustained serious structural damage. Upon inspection, the majority of the damage was found to have occurred at the bottom flange of the beam, with occasional failures at the top flange (SAC, 1995). The fractures appear to have initiated from the beam flange groove welds. Examples of the types of failures found at the bottom flange are shown in Fig. 1.2. Figures 1.2 (a) and (b) illustrate fractures in the base metal of the weld, typically near the column flange. Figures 1.2 (c) and (d) illustrate fractures starting at the weld, fracturing the column flange and creating a divot. Figures 1.2 (e) and (f) show fractures passing through the column flange and into the column web.
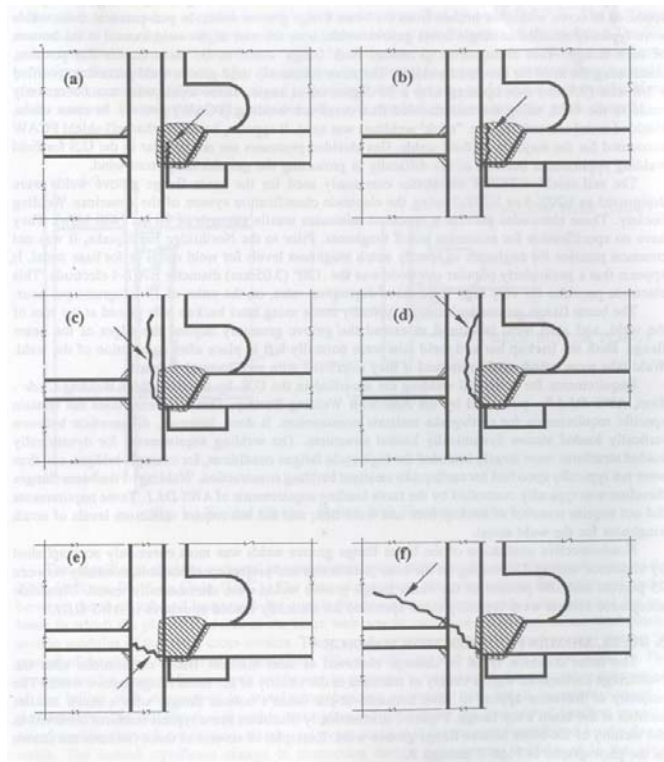
Figure 1.2 Common Fracture Types at Bottom Groove Weld of Beam

(Engelhardt and Sabol, 1995)

The recommended visual and ultrasonic inspection to determine damage to constructed buildings is very difficult. This requires removal of the interior architectural details and the fireproofing materials covering the steel. The cost to the building owner for these inspections ranged from $5,000 to $8,000 per joint and disrupted the building occupants (SAC, 1995). The potential loss in rent and high cost of inspection resulted in many owners opting to not inspect their buildings.

The SAC research program and building investigations have identified a number of problems that contributed to the poor behavior of welded moment-resisting connections. The difficulty of welding through the access hole at the

bottom flange often resulted in lack of fusion defects at the root of the weld. The backing bar on the bottom flange interfered with the ultrasonic inspection of the weld during construction, leaving many defects undetected. The weld metal used was found to have a very low fracture toughness, which combined with the typical welding flaws, greatly reduced the rotational capacity (SAC, 1995). A number of new connection details have been developed to address these issues (Fig. 1.3). The possibility that these welded connections will fracture during an earthquake remains, although the fractures are expected to occur at larger deformation levels.
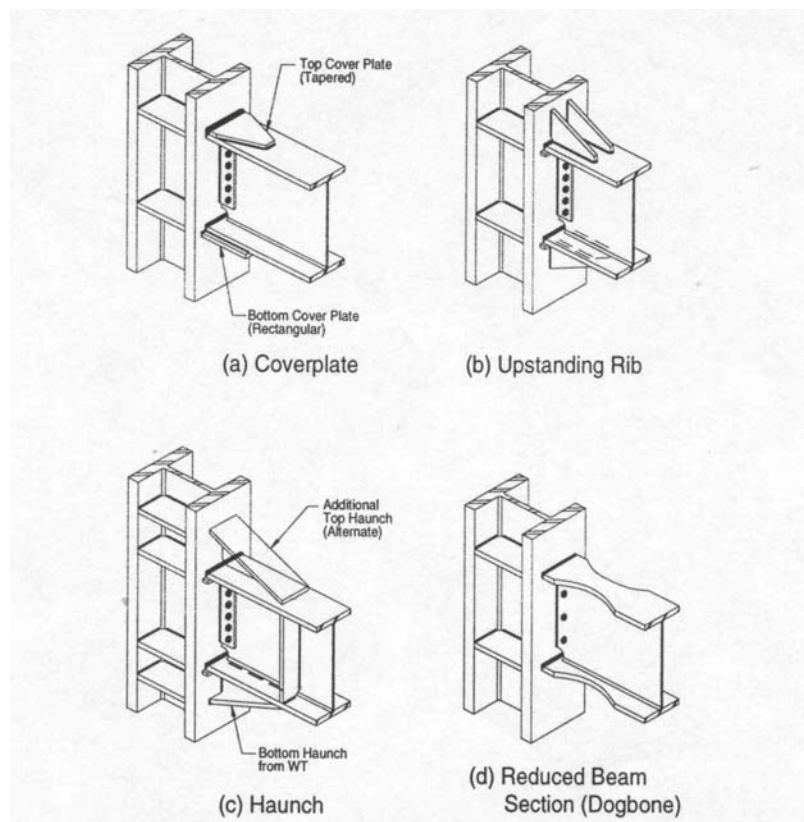
Figure 1.3 Connection Details Developed after the Northridge Earthquake

(Engelhardt and Sabol, 1997)

1.2 SCOPE OF WORK

Despite the improvements made to the connection details, weld fractures are still possible. Weld failure detection after an earthquake is necessary to determine the capacity of the building after a seismic event. A means of inspection that is economical and not disruptive to the building occupants is needed to ensure the safety of the building for its users. The proposed solution is to install crack detection sensors on the connections during construction.

The objective of this thesis is to develop a prototype passive wireless sensor to detect cracks in welded steel moment resisting connections. It was decided to focus on developing a sensor to detect failures at the weld toe and root. The sensors are to be placed at the top flange and bottom flange beam welds (Fig. 1.4).
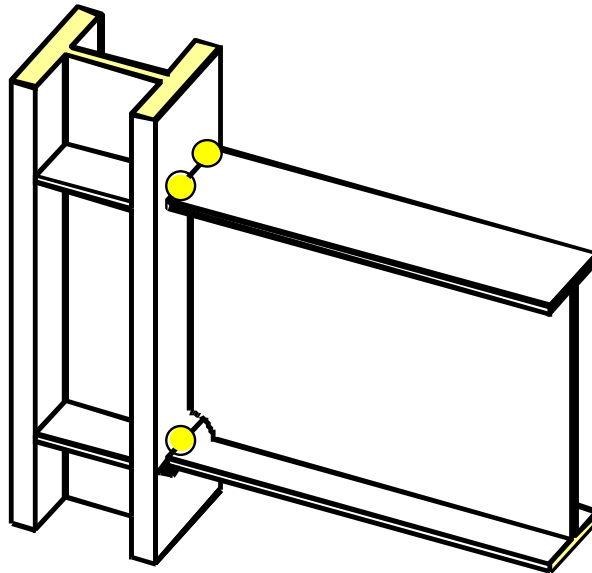
Figure 1.4 Location of Sensors on Welded Connection

These devices are intended to provide information quickly and reliably about the condition of the weld after an earthquake to identify the locations that need repairs. The most important features of this device are that it requires no

external power source; it is simple to apply in the field after the connection has been welded; and that both the condition of the device and the weld can be determined without accessing the connection. To be feasible for application, the sensor must be durable, affordable, require no external power, and reliable.

Numerous issues were investigated related to installing a fully functioning wireless sensor on the welded steel connection. There are two main functions this device must perform: detect when a crack is present in the weld and transmit that information to the inspector. This allows the sensor to be divided in two components, a data transmitter, and a crack detection device. The final sensor design must be reliable, durable, passive, and affordable. The following chapters of this thesis are an attempt to resolve these requirements.

The investigation into the electrical behavior and various types of wireless transmitters is presented in Chapter 2. The motivations behind selecting the Electronic Article Surveillance stickers as the data transmitter are presented. Included in this chapter is an overview of the crack detection switch development. The development of the point and distributed switch designs are also described.

The investigation of adhesives needed to affix the crack detector to the steel surface is discussed in Chapter 3. Three different testing conditions were used: a one-dimensional controlled displacement test, a two-dimensional dynamic displacement test, and a two-dimensional controlled displacement test. Modifications to the switch design and materials were made based on the results of each phase of testing. Results indicate that the combination of copper foil tape and high-strength tape adhesive combination has the potential of being able to detect small cracks.

Chapter 4 explores the behavior of the crack detection switch on welded steel specimens that were being tested as part of other ongoing investigations in Ferguson Laboratory. These tests were run concurrently with the testing program

6

discussed in Chapter 3. The behavior of the various crack detection switches improved as the design of the prototype switches was improved. These tests also demonstrated that the performance of a switch is significantly improved when the mill scale is removed. This may increase the cost of installation but improve the reliability of the switch.

The electrical circuit model for a complete sensor (transmitter and crack detector) was developed and evaluated in Chapter 5. The measured frequency response of point and distributed sensors was compared with the calculated response using the model. Two different crack progression patterns were investigated. In one case, the crack formed at one end of the switch and propagated along its length. In the other case, the crack formed near the middle of a distributed sensor and then propagated. The consequence of distributing capacitors along the length of the switch versus the addition of a single capacitor at the end was also explored. It was concluded that the prototype sensor was not reliable enough to be installed in the field. The soldered connection between the EAS tag and the switch was difficult to fabricate and tended to degrade with time. However, the prototype sensor did demonstrate that the objectives of the investigation could be accomplished.

Chapter 6 provides a summary of the information presented in this thesis as well as the conclusions of the testing program. Recommendations and suggestions for further testing are discussed.

CHAPTER 2

Design of Wireless Sensor

2.1 DESIRED ATTRIBUTES OF CRACK DETECTION SENSOR

The conceptual design of the crack detection sensor is presented in this chapter. The electrical behavior of different types of commercially available wireless transmitters is discussed and the development of the crack detection switch is introduced.

Wireless sensors have been used for a number of years to provide information about components in difficult environments. The versatility and durability of this technology makes it ideal for the case of a welded steel connection.

The most important features of this device are that it requires no external power; it is simple to apply in the field after the connection has been welded; and that both the condition of the device and the weld can be determined without accessing the connection. To be feasible for application, the sensor must be durable, affordable, require no external power, and reliable. Each of these requirements is described in detail in the following sections.

2.1.1 Durability Requirement

It is expected that the sensor will be installed during construction of the building. The sensor would be mounted on the exposed steel frame before the fireproofing is applied. The ruggedness of the job site requires that the sensor be able to withstand, as well as not interfere with, normal construction activities. Additionally, the sensor must have a life expectancy equivalent to that of the structure it is monitoring, which typically exceeds 50 years.

2.1.2 Affordability Requirement

The sensor needs to have a low initial cost compared with the cost of construction and the cost of inspection after an earthquake in order to be economical. To achieve this, the fabrication, installation, and maintenance costs of the sensor must be kept to a minimum. If the total cost becomes high, the owners will choose not to use the sensors, relying instead on traditional inspection methods after an earthquake.

2.1.3 Power Requirement

Access to the sensors will be blocked once the fireproofing is installed. Because of this limitation, the sensors cannot rely on exhaustible power supplies such as batteries. The cost of replacing the power supply or providing a power supply with the required life expectancy would be exorbitant. Additionally, replacing the power supply once the sensor is in place requires the fireproofing and architectural details to be removed, negating the purpose of the sensors. Connecting the sensors to external power supplies, such as electrical power from the building, creates the need for additional wiring. This raises the cost of installation and interferes with normal construction activities.

2.1.4 Reliability Requirement

The sensor must provide the inspector with reliable information about the condition of the welded connection. If the sensor indicates that a crack has formed, further inspection will be needed to determine the extent of the damage. The transmission of a false positive reading would unnecessarily increase the cost of inspection; a false negative would result in the failure to repair a damaged connection.

2.2   SELECTION OF DATA TRANSMISSION DEVICE

The sensor is viewed as having two main functions: detect when a crack is present in the weld and transmit that information to the inspector. For this reason the sensor was designed as two components, a data transmission device and a crack detection device. A cracked weld is a natural binary state, which is best determined by means of a simple on-off switch. The data transmission device must be able to transmit this binary information quickly and reliably. Radio frequency (RF) transmitters, which are wireless and passive, satisfy these requirements.

2.2.1   Radio Frequency Transmitters

Wireless transmitters are typically powered by means of an inductor. An alternating current driving coil in the transmission antenna produces an alternating current in the receiving sensor antenna, as depicted in Fig. 2.1. The induced current provides the sensor antenna with enough power to transmit the desired information back to the interrogating antenna. These devices are fabricated in three basic types: active, semi-passive, and fully passive. Active sensors are driven by an attached power source, typically a battery, and provide an unlimited amount of data. Semi-passive sensors typically require a minimum voltage to be induced in the circuit before transmission of data will occur. Fully passive sensors rely only on the induced current, which limits the amount of data that can be transmitted. Active sensors violate the requirement for the sensor to be passive, and thus were not considered. The latter types, semi-passive and fully passive, were investigated for use in this project.

10
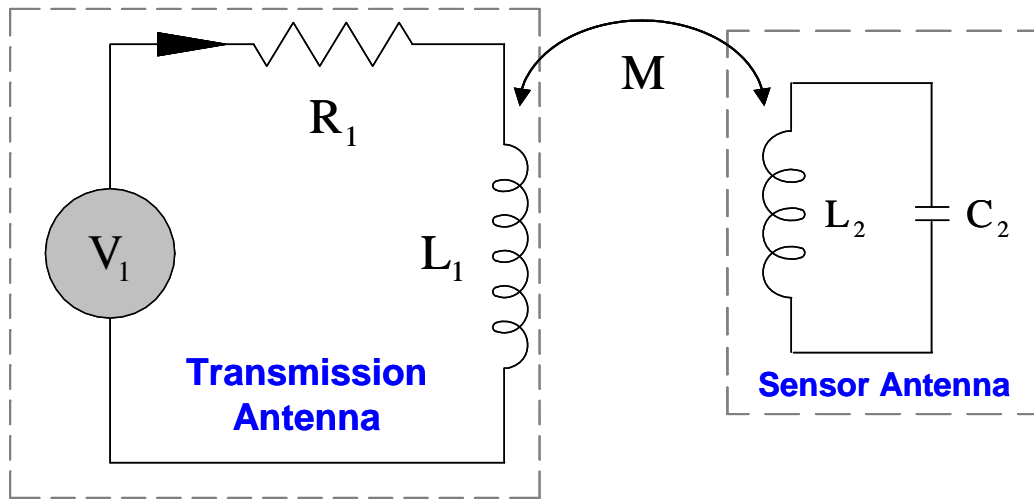
Figure 2.1 Electrical Model of Induced RF Power

Two types of wireless devices were investigated for use in this project, the semi-passive Radio Frequency Identification (RFID) tag and the fully passive Electronic Article Surveillance (EAS) sticker. These devices both satisfy the requirements of being durable, affordable, passive, and reliable as stated in Section 2.1.

2.2.2 RFID Tags

RFID tags contain a programmable silicon integrated circuit, encased in a protective plastic shell. The silicon chip transmits a unique identification code when prompted as described in Section 2.2.1. These tags are widely used for many applications, such as inventory control and equipment tracking, and are available in many different shapes and sizes (Fig. 2.2). RFID tags have been designed to accommodate an external switch device are also commercially available. It was initially postulated that a simple and commercially available device, such as a crack detection gage, would be connected to an RFID tag, and multiple tags, each with different unique codes, would be placed around the welded connection. At the time of writing, RFID tags cost $3.00 to $12.00 each.

11

Costs are expected to decrease as the technology is developed for additional applications.

Figure 2.2 Examples of Typical RFID Tags

The RFID tags require a minimum voltage to be induced at the antenna before they are activated, which has a significant impact on range. The required signal range of a RFID tag may be anywhere from less than an inch to 2 to 3 feet. To increase this range, the tag would have to be equipped with an additional power source, such as a battery. The limited range available to the detection antenna is viewed as a detriment, potentially requiring the inspector to remove architectural claddings in order to interrogate the sensor.

2.2.3   EAS Sticker

An EAS sticker consists of two printed elements: an inductor coil and a capacitor. These elements are encapsulated in a thin polymer film, to which a layer of adhesive is added for ease of placement. The inductor-capacitor (LC) circuit interacts with the transmission antenna as described in Section 2.2.1. When excited by electromagnetic energy, the tag will respond with a characteristic frequency signal. By changing the capacitance of the tag, the frequency is shifted.

Commercially available EAS stickers (Fig. 2.3) respond at the resonant frequency of approximately 8.0 MHz, have a range of 3 to 6 feet, and are available in a variety of shapes and sizes. The tags are inexpensive, with the average single sticker costing less than $0.10.

Figure 2.3 EAS Sticker Tag, Top and Side Views

Because these circuits are insulated with thin layers of polymer and adhesive, they are sensitive to metal surfaces. The currents in the tag are imaged in the base metal, producing parasitic inductance (Fig. 2.4). For this case the inductors from the tag and base metal are in parallel, and the total effective inductance is reduced as the gap between the tag and the metal surface is decreased. The reduction of inductance reduces the coupling efficiency and range of the tag. Preliminary testing found that an EAS sticker must be elevated at least 1 cm above a metallic surface in order to overcome the parasitic action of the metal surface.
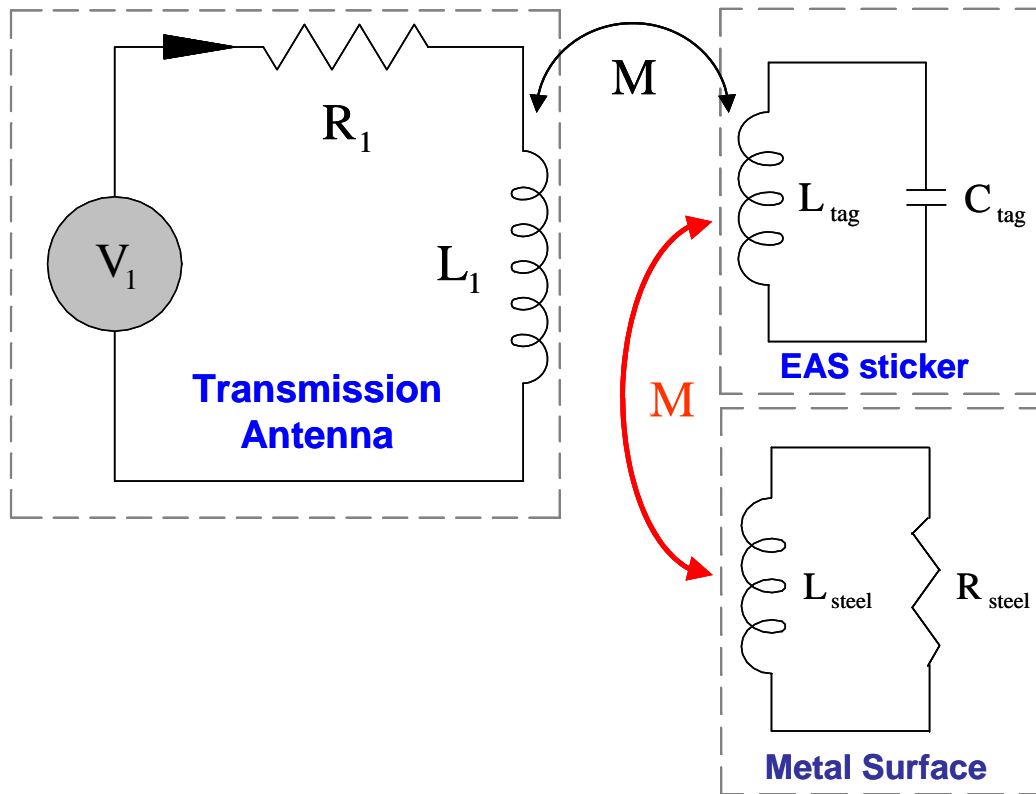
Figure 2.4 Electrical Model of Plate-Tag Interaction

The greater response range and reduced cost were motivating factors in choosing to use EAS tags as the data transmission device in the prototype sensor design. The stickers also satisfy the four admissibility requirements as stated in Section 2.1: they are durable, affordable, passive, and reliable. It was decided that a simple frangible switch with an attached capacitor would be connected to the EAS sticker (Fig. 2.5) to provide the desired frequency shift from the unmodified resonant frequency.
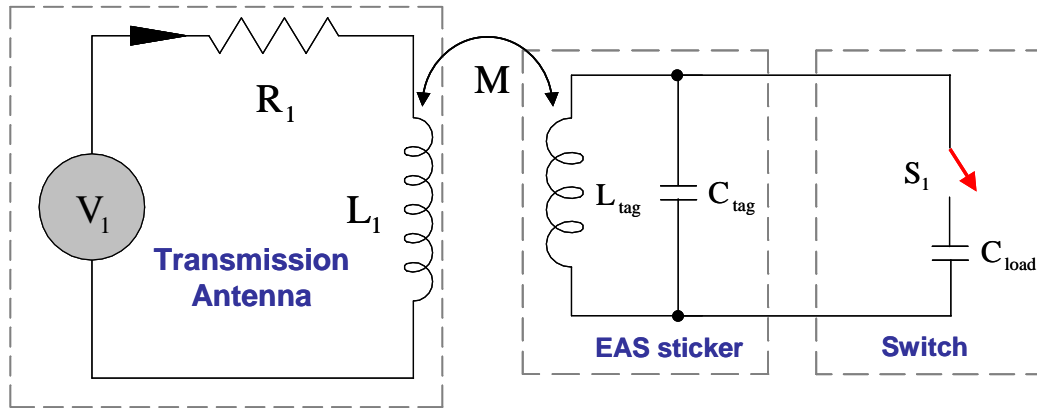
Figure 2.5 Electrical Circuit Model of EAS Sticker and Switch

2.2.4 Circuit Model of EAS Sticker and Switch

The EAS sticker is a simple LC circuit, composed of an inductor and a capacitor in series. A slight resistance is inherent to the circuit due to material effects and the circuit behaves as a series resistor-inductor-capacitor (RLC) circuit. Voltage in the EAS tag is generated by the magnetic output of the transmission antenna, driving the RLC circuit. The behavior of the sticker is determined by the electrical properties discussed in this section. Equations and definitions are from the textbook *Physics for Scientists and Engineers* by Serway (1982).

For a simple circuit composed of resistor R, and current i, the voltage, v_R, is calculated using Eq. 2.1.

$$v_R = iR \tag{2.1}$$

Similarly, the current i through a capacitor is related to the voltage through the capacitor, v_C, by the capacitive reactance, X_C (Eq. 2.2). The capacitive reactance has the SI unit of ohms.

$$v_C = iX_C \tag{2.2}$$

The capacitive reactance acts as a resistance to current but is not a true resistance because it is dependent on the angular frequency, ω, of the circuit and the capacitance of the capacitor, C (Eq. 2.3) and not an inherent property. The capacitor voltage, v_C, is out of phase with the current in the circuit, lagging i by 90°.

$$X_C = \frac{1}{\omega C} \tag{2.3}$$

Similarly, the current i through an inductor is related to the voltage through the inductor, v_L, by the inductive reactance, X_L (Eq. 2.4).

$$v_L = iX_L \tag{2.4}$$

The inductive reactance is dependent on the angular frequency, ω, of the circuit and inductance L of the inductor (Eq. 2.5). It also has the SI unit of ohm. The inductor voltage, v_L, is out of phase with the current, leading i 90°.

$$X_L = \omega L \tag{2.5}$$

Because of the phase differences, the total voltage, v_{max}, is properly calculated as a vector sum of the three element voltages. The total voltage through the RLC circuit is calculated using the phasor diagram shown in Fig. 2.x (a). The current is the same in all three elements and is represented by a single phasor. The total voltage is given in Eq. 2.6.

(a)	(b)
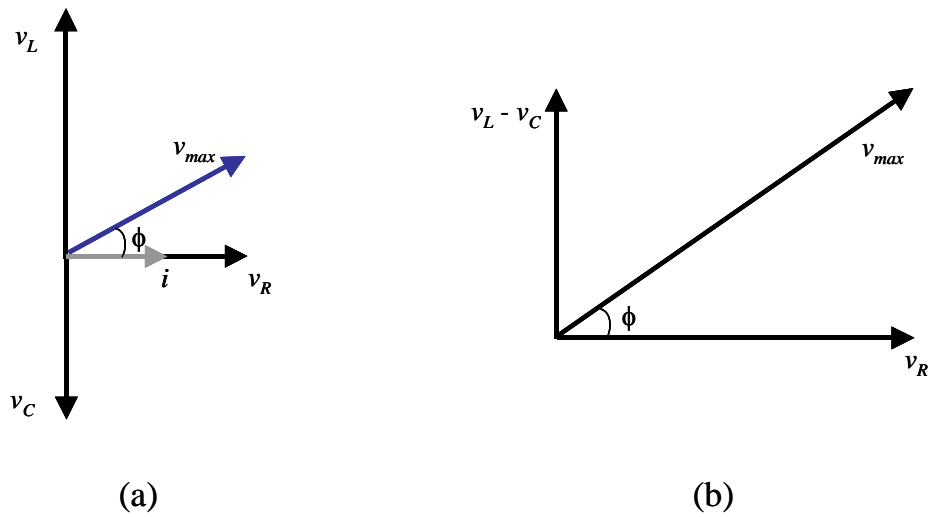
Figure 2.6 Phasor Diagram for Series RLC Circuit

$$v_{max} = \sqrt{v_R{}^2 + \left(v_L - v_C\right)^2} \qquad (2.6)$$

Substituting Eq. 2.1, 2.2, and 2.4 into Eq. 2.6 and factoring out current *i* yields Eq. 2.7.

$$v_{max} = i\sqrt{R^2 + \left(X_L - X_C\right)^2} \qquad (2.7)$$

The square root term in Eq. 2.7 is defined as the impedance, *Z*, of the RLC circuit (Eq. 2.8). The impedance, measured in ohms, is the effective resistance of the circuit. The value of the impedance of a circuit is dependent on the values of X_L and X_C, and therefore also dependent on the angular frequency, ω.

$$Z = \sqrt{R^2 + \left(X_L - X_C\right)^2} \qquad (2.8)$$

The frequency at which the magnitudes of the capacitor and inductor voltages completely cancel is called the resonant frequency. In other words, when $X_L = X_C$, the impedance equals the circuit resistance, the maximum current is produced, and the circuit is in resonance. Solving $X_L = X_C$ yields the resonant frequency of the circuit (Eq. 2.9).

17

$$\omega = \frac{1}{\sqrt{LC}} \qquad (2.9)$$

Resonant frequency is also defined as occurring when the phase angle, ϕ, between the maximum voltage, v_{max}, and the current in the circuit, i, becomes zero. This occurs when the voltages in the capacitor, v_C, and the inductor, v_L, become equal. Therefore, when the phase angle, ϕ, becomes zero, X_L is equal to X_C, the definition of resonance.

It is most common to measure frequency as cycles per second, or hertz. Equation 2.10 relates the angular frequency ω, measured in rad/sec, to frequency f, measured in Hz.

$$\omega = 2\pi f \qquad (2.10)$$

The inductance and capacitance of a typical EAS sticker were determined experimentally. The inductance, L_{tag}, is approximately 4 µH and the capacitance, C_{tag}, is approximately 100 pF. The resonant frequency of the unmodified EAS sticker is given in Eq. 2.11. Using these approximate values, the unmodified EAS tag responds at a frequency of 8 MHz.

$$f = \frac{1}{2\pi\sqrt{L_{tag}C_{tag}}} \qquad (2.11)$$

When the switch is added to the tag, the load capacitor, C_{load}, adds in parallel with the tag capacitor. The resonant frequency of the EAS sticker and switch combination is given in Eq. 2.12.

$$f = \frac{1}{2\pi\sqrt{L_{tag}(C_{tag}+C_{load})}} \qquad (2.12)$$

A 200 pF load capacitor was chosen to produce the desired frequency shift. This value of C_{load} causes the sticker to respond at a frequency of approximately 4.6 MHz. The sticker can now transmit two bits of data: 4.6 MHz

when the switch is closed and 8 MHz when the switch is open. If no signal is detected, then the sensor is not operative.

2.3 DEVELOPMENT OF CRACK DETECTION SWITCH

The crack detection switch must be able to provide the sensor antenna with the required information about the condition of the weld beneath the sensor. A crack size of 0.10 in. was arbitrarily chosen as the target width to be detected by the sensor. When the crack reaches this width, the switch breaks and the characteristic frequency of the switch changes.

2.3.1 Copper Foil Tape Designs

Initially, it was believed that 1-in. copper foil tape could be cut into a shape that would fracture at the desired crack width. The 1-in. wide 3M EMI Copper Foil Shielding Tape 1194 was selected for its electrical properties, ease of soldering, and insulated adhesive backing. Two shapes, the "bowtie" and "dog-bone," were cut out of 4-in. long sections of tape, as shown in Fig. 2.7. Samples of each shape, with taper distance, d, ranging from 1/8 in. to 1/2 in. in 1/16 in. increments, were tested in a one-dimensional displacement test. An additional shape, the hybrid bow-tie, was later developed to fit the geometry of the two-dimensional test setup.

bow-tie   **dog-bone**   **hybrid bow-tie**
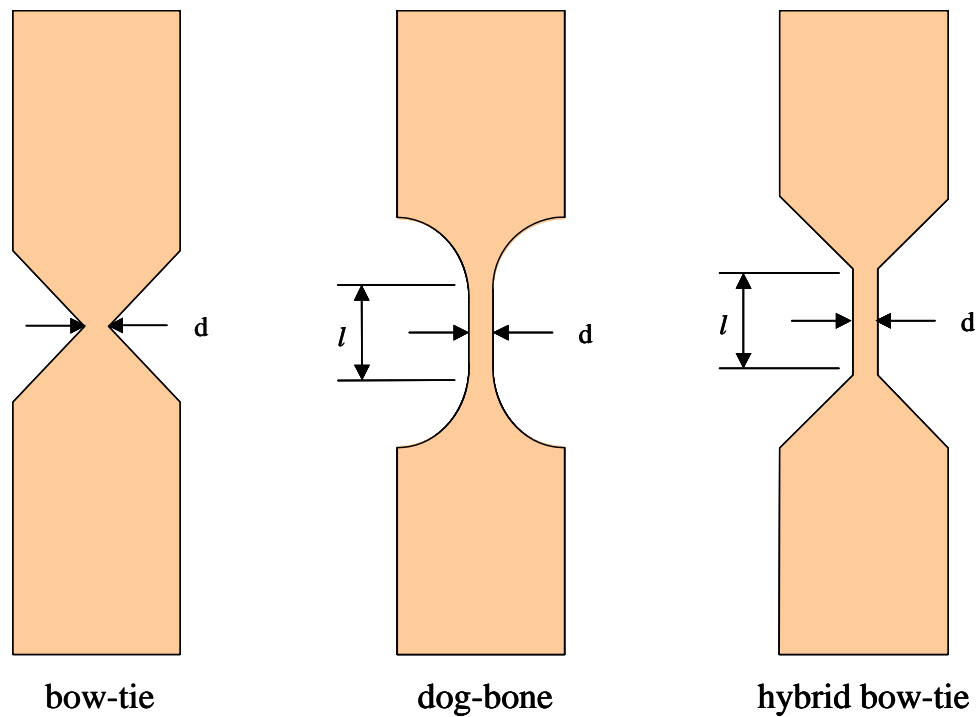
Figure 2.7 Copper Foil Tape Specimens

The specimens consistently delaminated from the surface of the steel before fracturing in subsequent two-dimensional tests (Chapter 3). In both the one- and two-dimensional test setups, the tapered region of the specimens lost contact with the steel surface and continued delaminating into the non-tapered regions, effectively removing the tape from the steel. It was proposed to affix the non-tapered regions with high-strength adhesive to reduce or eliminate this response.

One other limitation of this design was the need for wires to complete the electrical circuit. In order for the circuit to be completed, a wire would need to be placed across the weld to connect the switch to the EAS tag. It was originally thought that antenna would be placed at a distance away from the weld, to facilitate ease of reading. This separation created the need for external wiring,

which would be extremely sensitive to conditions in the field. The added wiring thus has the effect of reducing the durability of the overall sensor, violating one of the four basic requirements.

2.3.2   Copper Foil Tape Plus Additional Adhesive Design

A second design was developed using two copper foil tape strips placed parallel to each other and separated by 1/8 in. (Fig. 2.8). The use of the two copper strips eliminated the need for wiring across the weld. The strips were held in place with two large adhesive pads, one on each side of the weld. These adhesive pads hold the non-tapered areas of the copper foil strips in place while allowing the tapered regions to deform and break. To reduce the distance over which the copper foil tape delaminated, the adhesive pads were placed such that the edges would be placed on either side of the weld, holding the tapered copper foil strips in place across the weld. Small tabs of copper foil tape were left free at the ends of the adhesive pads, creating terminals for connecting the added capacitor and the EAS sticker. Although this switch has two copper strips running across the weld, their proximity to each other causes them to act in tandem, and thus the specimen is described as a point switch.
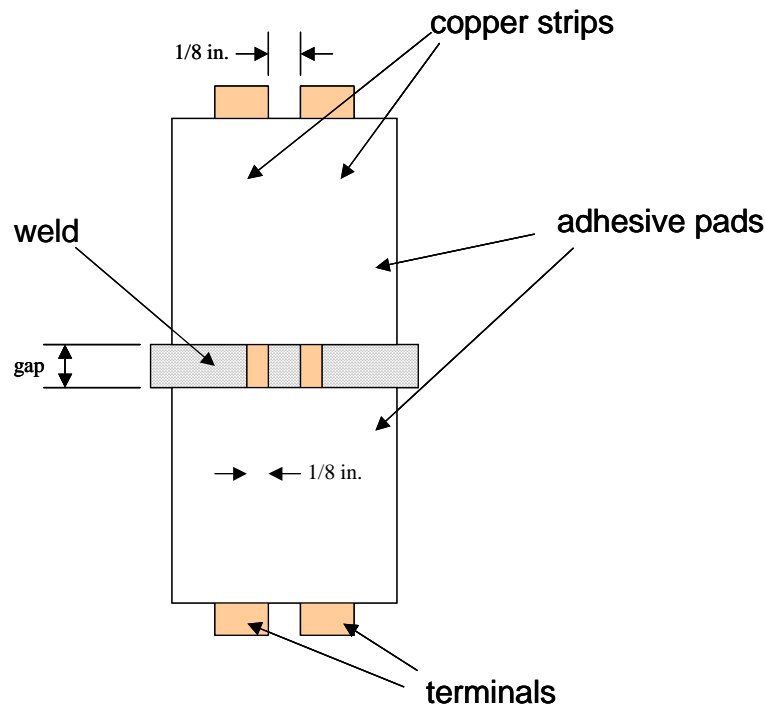
Figure 2.8 Design of Point Switch

The initial specimens were fabricated as described in Appendix A using heavy-duty carpet tape for the adhesive pads and packing tape as a protective layer on top. The width of the copper foil strips that span between the adhesive pads was 1/8 in., as thinner widths of foil could not be easily handled without breaking during fabrication or installation.

This switch design was tested in the two-dimensional setup, described in Chapter 3. Delamination in the packing tape and carpet tape layers of the switch was observed during testing. A higher strength adhesive, 3M VHB Adhesive Transfer Tape F-9473PC, was chosen to replace the carpet tape for the bottom layer and a thicker tape, 3M Polyester Film Tape 8412, was chosen as the top layer, to provide a distinct edge for the copper foil strips to break along.

2.3.3 Distributed Switch

After the development of the point switch, potential users suggested that a switch be created to monitor a larger area of the weld than a single location. A switch with multiple copper strips was designed for use as a distributed switch. The two copper strips in the distributed switch are oriented in a serpentine layout (Fig. 2.9). Cracks can now be detected at any of the locations where the pair of copper strips span between the adhesive pads.
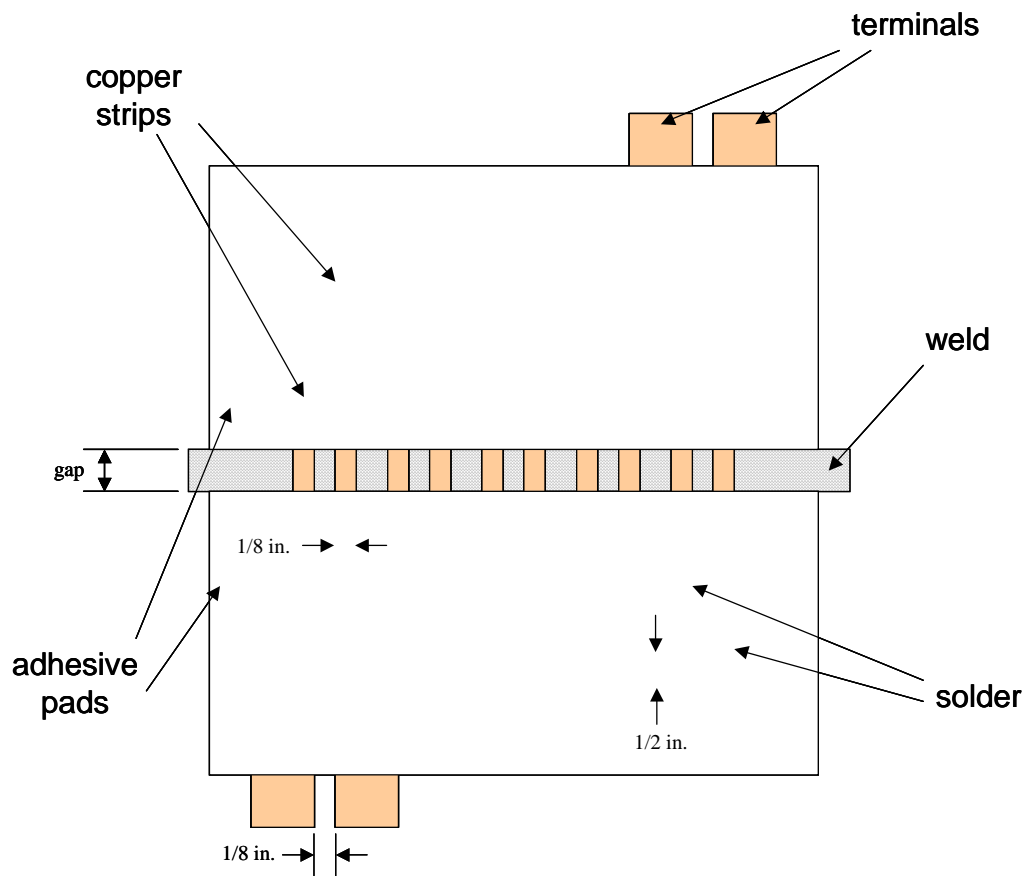
Figure 2.9 Distributed Switch Design

As the serpentine shape cannot be cut from the 1-in. copper foil tape used in this project, the serpentine was constructed from strips of copper foil and

23

soldered together to provide an electrical connection between the individual pieces. The construction process is described in detail in Appendix A. Many different lengths are possible with this pattern: during this project, distributed switches with three, five, seven, nine, ten, eleven, and thirteen pairs of copper strips were fabricated.

CHAPTER 3
Crack Detection Test

3.1 INTRODUCTION

The purpose of this test series is to determine the crack width at which the crack detection switch breaks and to determine if the results are repeatable. A crack size of 0.10 in. was chosen as the target width for the switch to fail. There were three main phases to this stage of the investigation. The first was to evaluate the performance of the simple shapes cut from copper foil tape, as described in Section 2.3.1, in a one-dimension test. In the second phase, the simple shapes cut from copper foil tape were tested in a dynamic two-dimensional situation, which was designed to simulate a weld fracturing. The third phase investigated the behavior of the point switch in a controlled two-dimensional environment. Results show that the point switches made from the 3M tapes failed at approximately the desired crack width.

3.2 PHASE ONE: ONE-DIMENSIONAL TESTS

In this phase, the behavior of simple shapes cut from copper foil was investigated in a one-dimensional setup. The objective was to determine which shapes, dimensions, and adhesives resulted in the smallest gap at failure.

3.2.1 Copper Foil Tape Shape Fabrication

Dog-bone and bow-tie copper foil shapes, as described in Chapter 2, with center width d equal to 1/16 in., 1/8 in., 3/16 in., 1/4 in., and 1/2 in., were evaluated during the first phase of testing. The length l of the reduced section of

25

the dog-bone shape was 1 in. during the first phase. Dimensions l and d are shown in Fig. 3.1.   Both the conductive (1181) and non-conductive (1194) adhesive 3M EMI copper foil tapes were investigated.   In addition, the factory adhesive was removed from some shapes and 3M 467MP double-sided tape was applied and tested.

bow-tie   dog-bone
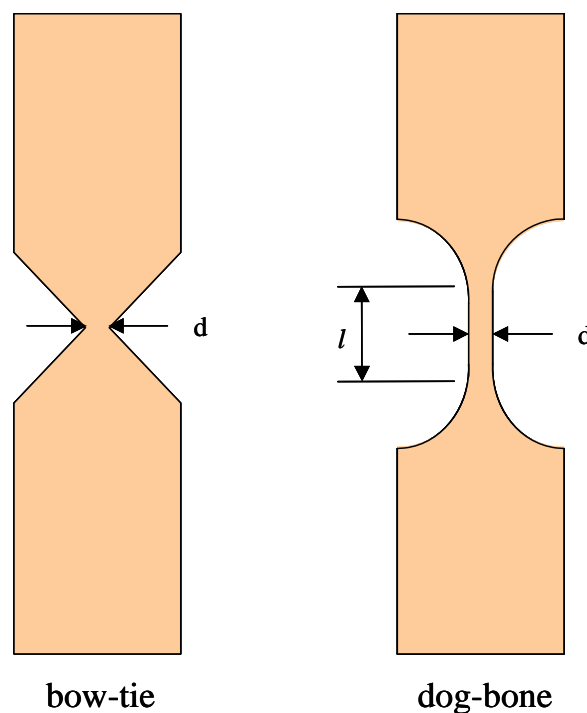
Figure 3.1 Simple Shapes Cut From Copper Foil Tape

3.2.2   Steel Plates for One-Dimensional Test

The one-dimensional displacement test was performed using two 1-in. thick 3-in. by 6-in. steel blocks set in a milling machine (Fig. 3.2).   The long edges of the blocks were machined for a tight fit and set flush to each other.   One block was held stationary by the quill, while the other was attached to move with the table.   A 3/8-in. diameter hole was drilled into the stationary block to accommodate the quill pin.

The gap between the blocks increased in size when the table was moved in the direction indicated in Fig. 3.2. The analog dial on the milling machine had a resolution of 0.001 in. and the digital meter had a resolution of 0.0001 in.

direction of movement
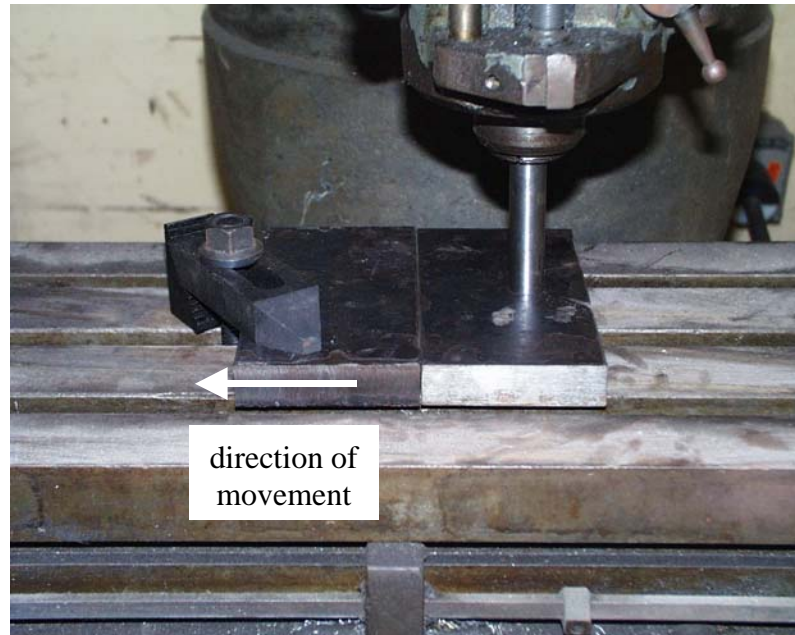
Figure 3.2 Steel Blocks Used in One-Dimensional Test

3.2.3   Testing and Results

The simple shapes cut from the copper foil tape were tested to failure in the one-dimensional test setup. Prior to installation, the top surface of the blocks was cleaned of dirt and machine oil with acetone. Two copper foil strip shapes were attached to the blocks, such that the middle of the strips was centered over the block boundary as shown in Fig. 3.3.
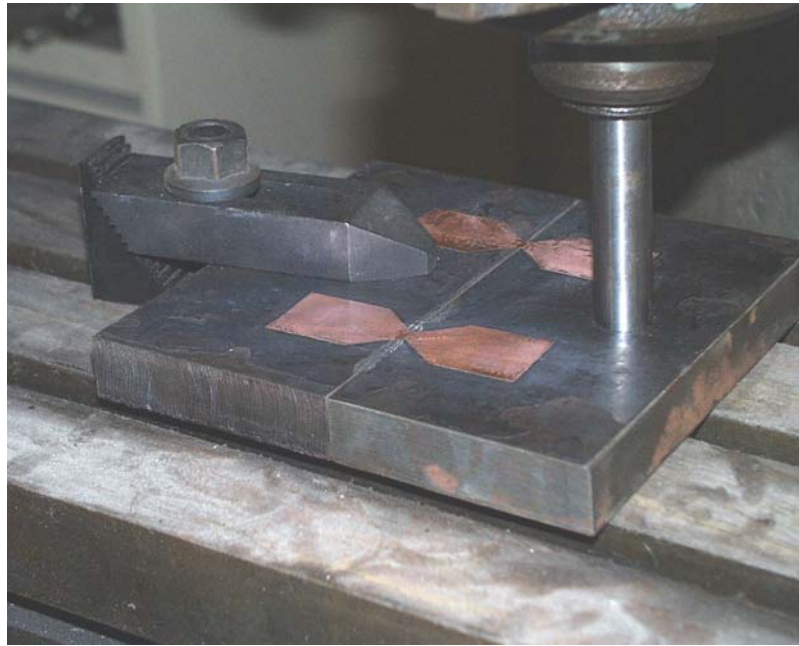
Figure 3.3 Bow-tie Specimens in One-Dimensional Test

The blocks were slowly separated until the two specimens had visibly failed. The distance the blocks were moved was recorded from the output of the digital meter. The failure modes were recorded for each test. The results are given in Table 3.1 and the observed failure patterns are shown in Fig. 3.4.

Table 3.1 Results from One-Dimensional Tests

adhesive tape	section width	bow-tie		dog-bone	
	(in.)	separation (in.)	failure mode	separation (in.)	failure mode
conductive	1/16	0.0293	(a)	0.0388	(a), (f)
non-conductive	1/16	0.0205	(a)	0.0310	(a), (f)
3M 467MP	1/16	0.0146	(a)	0.0309	(f)
conductive	1/8	0.0343	(a), (c)	0.0410	(a), (c)
non-conductive	1/8	0.0273	(a), (c)	0.0316	(a)
3M 467MP	1/8	0.0211	(a)	0.0511	(a), (f)
conductive	3/16	0.0339	(a)	0.0500	(a), (f)
non-conductive	3/16	0.0350	(a), (e)	0.0515	(a), (c), (f)
3M 467MP	3/16	0.0380	(a), (c)	0.0539	(a), (b), (c)
conductive	1/4	0.0374	(a)	0.0568	(a), (f)
non-conductive	1/4	0.0491	(a), (c)	0.0539	(a), (c), (f)
3M 467MP	1/4	0.0508	(a), (c)	0.0853	(b), (f)
conductive	3/8	0.0446	(a)	0.0646	(a), (b), (c), (f)
non-conductive	3/8	0.1175	(a)	0.2918	(a), (b), (c)
3M 467MP	3/8	0.0990	(c)	0.0839	(a), (b), (c), (f)
conductive	1/2	0.0520	(a), (c)	0.0728	(a), (b), (f)
non-conductive	1/2	0.1235	(a)	0.1175	(b), (c), (d)
3M 467MP	1/2	0.2203	(a)	0.1110	(a), (d), (f)
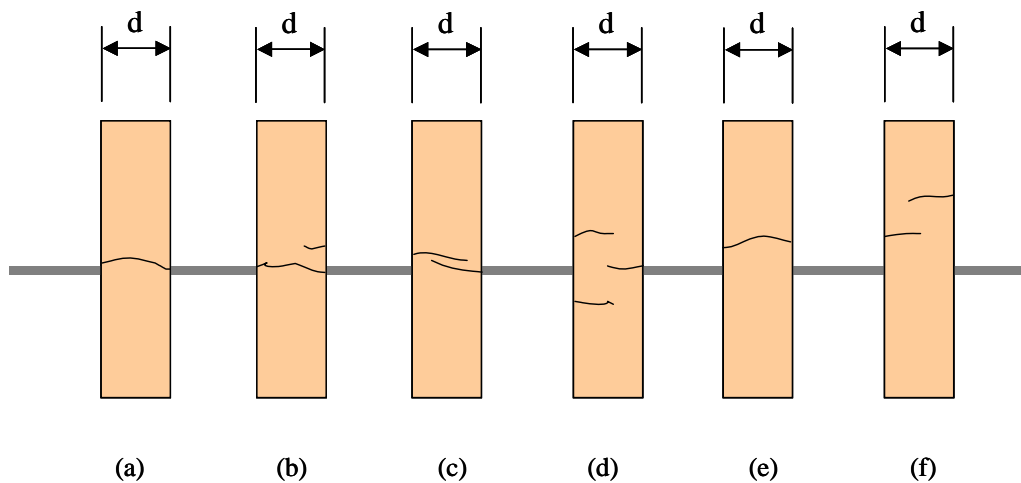
Figure 3.4 Failure Modes of Copper Foil Shapes

29

Overall, the bow-tie shapes failed at a smaller gap separation than the dog-bone shapes for all section widths and adhesive types. Only the 1/2-in. wide dog-bone shapes with the non-conductive and 3M 467MP adhesives outperformed the corresponding bow-tie designs. The most common failure mode for all shapes was mode (a), a single tear across the opened gap. The dog-bone shapes generally exhibited some combination of mode (a) and modes (b), (c), (d), and (f); the bow-tie shapes exhibited either mode (a) or a combination of mode (a) with mode (c) or (e).

Based on these results, the decision was made to continue testing the 1/16-in. and 1/8-in. wide strips. No significant difference was found at this stage between the adhesive types, thus the non-conductive 3M copper foil tape 1194 was used for the next round of testing.

3.3 PHASE TWO: TWO-DIMENSIONAL DYNAMIC TEST

In this phase, the simple shapes cut from copper foil tape from phase one were tested in a two-dimensional dynamic test. The bow-tie shape was modified into the hybrid bow-tie; a tapered section was added at the middle of the bow-tie (Fig. 3.5). This modification allowed a better fit for the bow-tie shape over the weld between the perpendicular steel plates. This test was intended to model the behavior of a weld during failure at a steel connection. This test included the strain in the steel before fracture, the dynamic behavior of weld failure, and the right angle geometry of the connection.
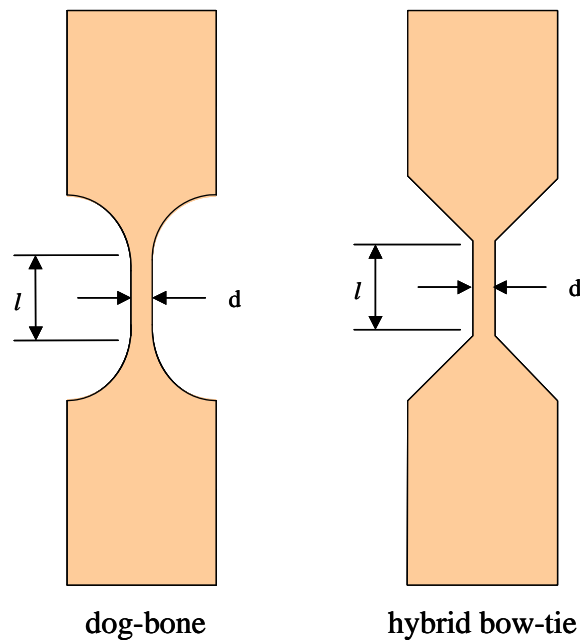
Figure 3.5 Hybrid Bow-tie and Dog-bone Shapes

3.3.1   Modified Bow-tie Shape

Dog-bone and hybrid bow-tie shapes with d equal to 1/16 in. and 1/8 in. and *l* equal to 1/4 in. and 1/2 in. were tested during this stage. All specimens were cut from the non-conductive 3M EMI copper foil tape 1194. Wire leads were soldered to the ends so that the resistance could be monitored using an ohmmeter. The ends were insulated with one-sided clear tape.

3.3.2   Cruciform Testing Platform for Two-Dimensional Test

To evaluate the performance of the switches for their intended configuration, a two-dimensional testing platform was devised. This platform consisted of a 1/2-in. thick steel tensile test specimen, cut in the center and welded to a 1-in. thick steel plate (Fig. 3.6). The weld size used was 3/16 in., which was the minimum size required for a weld on these shapes to fail in tension. On one

side of the 1-in. thick plate the welds were specified to be full-penetration, and partial-penetration welds were specified on the opposite side.
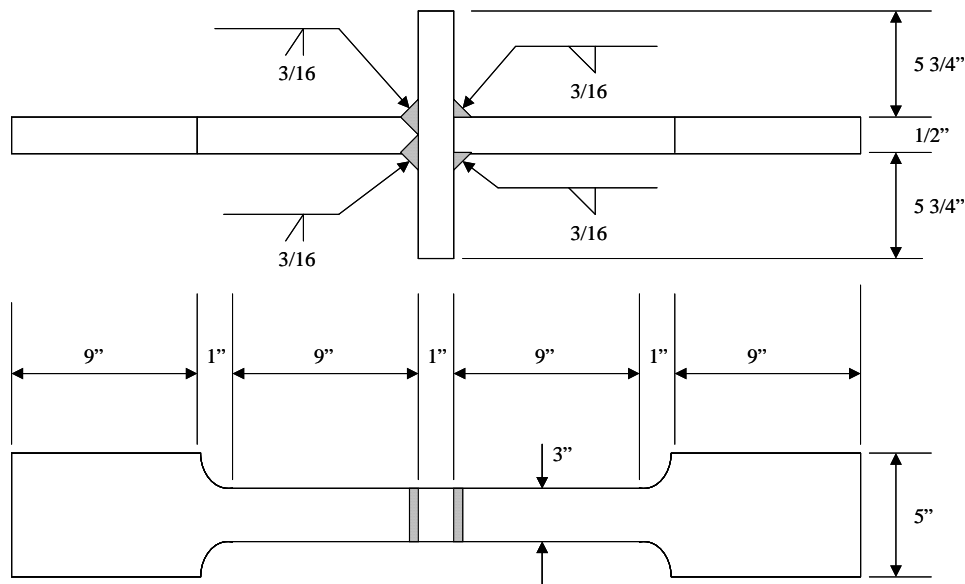
Figure 3.6 Cruciform Section Dimensions

The partial-penetration welds were designed to fail at a tensile load of approximately 50 kips. Three cruciform specimens were tested in this manner during this phase of the project.

3.3.3   Testing and Results

Each cruciform section was placed in a 600-kip testing machine. Two shapes cut from copper foil tape were positioned on each side of the partial-penetration weld after cleaning the area with acetone (Fig. 3.7). The wire leads were attached to an ohmmeter. The intact switch shapes had a resistance of approximately 1.3 ohms. At failure an open circuit is produced and the reading exceeded the range of the ohmmeter producing an effective reading of infinite resistance.

Figure 3.7 Installation of Copper Foil Shapes

Three tests were conducted (Table 3.2). In the first, two dog-bone and two hybrid bow-tie shapes were tested. The minimum width, d, was 1/8 in. for all four shapes. One dog-bone and one hybrid bow-tie had a length l of 1/4 in. and the remaining two shapes had a length l of 1/2 in. In the second test, the same shapes and lengths were used, except the minimum width, d, was reduced to 1/16 in. In the third test four dog-bone shapes were tested, which had a minimum width of 1/8 in. and a length of 1/4 in.

The fourth column in Table 3.2 indicates if the copper foil shapes tore during the tests. Six of the twelve simple shapes fractured, and the other six bridged over the weld (Fig. 3.8). The copper foil delaminated from the weld in all cases. This mode of response was not observed in the one-dimensional tests, but clearly could limit the reliability of the sensor.

33

Table 3.2 Results from Two-Dimensional Dynamic Tests

Test 1			
shape	l (in.)	d (in.)	failure
dog-bone	1/4	1/8	yes
dog-bone	1/2	1/8	no
hybrid bow-tie	1/4	1/8	yes
hybrid bow-tie	1/2	1/8	yes
Test 2			
shape	l (in.)	d (in.)	failure
dog-bone	1/4	1/16	no
dog-bone	1/2	1/16	yes
hybrid bow-tie	1/4	1/16	yes
hybrid bow-tie	1/2	1/16	yes
Test 3			
shape	l (in.)	d (in.)	failure
dog-bone	1/4	1/8	no
dog-bone	1/4	1/8	no
dog-bone	1/4	1/8	no
dog-bone	1/4	1/8	no
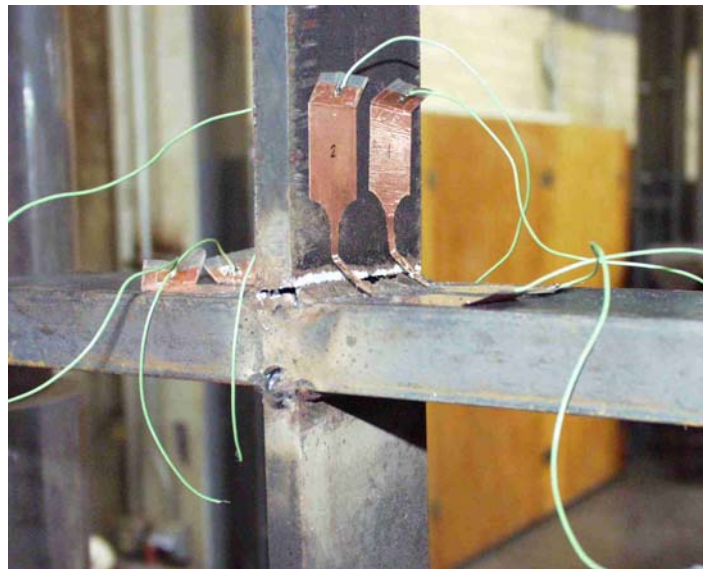
Figure 3.8 Delamination of Copper Foil Shapes from Surface of Steel Specimen

34

Based on the performance of the simple shapes cut from copper foil tape in the dynamic two-dimensional tests, it was decided that a controlled displacement test would be better suited for determining the width of a crack underneath the switch. The dynamic nature of the test setup caused the weld to break as soon as a crack occurred, precluding accurate measurement of width. The second decision based on these results was to alter the design of the switch to use two large adhesive pads. It was thought that if the copper foil was secured on either side of the weld, the foil crossing the weld was free to peel up but would break once the region of delamination reached the high strength adhesive. These observations and hypotheses led to the development of the point switch, where two thin strips of copper foil crossed the weld.

3.4   PHASE THREE: TWO-DIMENSIONAL CONTROLLED TEST

In this phase, fractured steel cruciform specimens tested in phase two were positioned in a milling machine and used to evaluate delamination of the switches under controlled displacements. The objective of this phase was to evaluate the behavior of the point switch design. Additionally, the two-dimensional tests were abandoned in favor of installing the switches directly onto welded specimens, as discussed in Chapter 4.

3.4.1   Two-Dimensional Testing Platform

To measure the crack size at which the point switches fail, a broken cruciform shape from phase two was mounted onto the milling machine as shown in Fig. 3.9. The broken specimen models the condition of a weld with a very small crack when the fractured pieces are placed together. Moving the plate adjacent to the broken partial-penetration weld increased the crack size at the

weld. A 3/8-in. hole was drilled in the adjacent plate to accommodate the quill pin.

Figure 3.9 Cruciform Mounted on Milling Machine

3.4.2 Fabrication of the Point Switch

As described in Chapter 2, two sets of point switches were used in the final testing phase (Fig. 2.8). The first set was constructed using carpet tape and packing tape; the second set was made from 3M VHB Adhesive Transfer Tape F-9473 and 3M Polyester Film Tape 8412. The switches were constructed using the method described in Appendix A.

3.4.3 Tests of Point Switches Fabricated Using Carpet Tape

The proposed point switch fabricated using high-strength carpet tape and packing tape was tested in this phase. Carpet tape was chosen as the base layer because of its high tack, low cost, and availability; packing tape was used for the top layer to provide insulation and protection to the copper strips and to facilitate

installation of the switch by providing a non-stick outer surface. Four specimens were tested and the geometric parameters are listed in Table 3.3. Each switch had a short wire soldered across the terminals at one end and wires were soldered to the terminals at the other end for connection to an ohmmeter. The weld and the surrounding areas on the steel were cleaned with acetone prior to installing the switch. Due to space constraints on the cruciform section, only one switch could be tested at a time.

The weld and surround steel surfaces were cleaned with acetone prior to installation of each switch. The switches were aligned on the test specimens and the adhesive pads were pressed against the steel surface using a roller. The dial gage on the table was used to measure the displacement of the cruciform sections. The table was moved manually until the ohmmeter gave a reading of infinity, indicating the switch had failed. Results are given in Table 3.3.

During testing, significant delamination occurred in the adhesive pad areas at the copper foil/adhesive tape interface for all specimens (Fig. 3.11). The copper foil tape peeled off the packing tape on top of the switch, and the copper foil tape delaminated from the carpet tape before fracturing. The gap size was no a factor in the response of the switch; however, it was a factor in the behavior of the switches during the inelastic tests discussed in Chapter 4. Based on these observations, four modifications to the switch design were proposed.

Table 3.3 Carpet Tape Switch Displacements

specimen ID	strip width (in.)	gap (in.)	displacement at failure (in.)	No. Strips Fractured	Delamination Observed
1	1/16	1/4	0.166	1	yes
2	1/8	1/4	0.260	2	yes
3	1/16	1	0.170	1	yes
4	1/8	1	0.261	2	yes
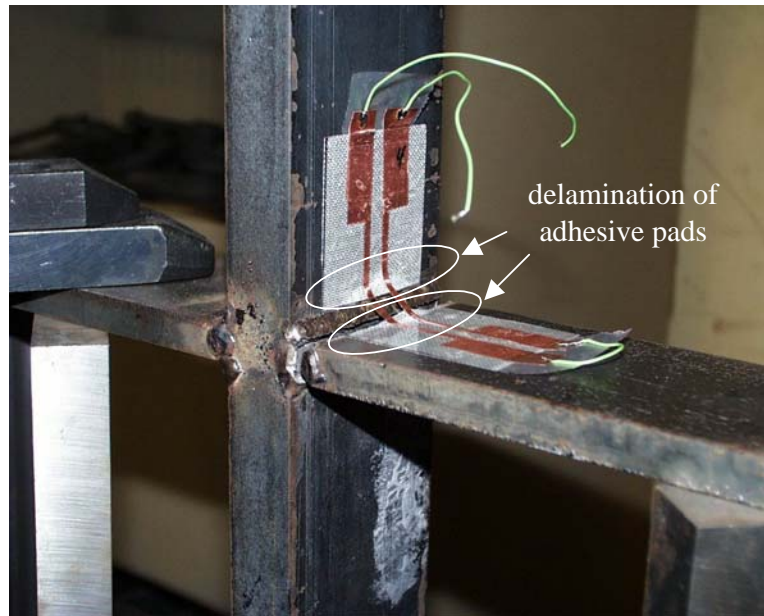
Figure 3.10 Delamination of Point Switch Fabricated Using Carpet Tape

3.4.4 Modifications to Point Switch Fabricated Using Carpet Tape

Four modifications to the basic point switch described in Section 3.4.3 were tested in an attempt to reduce the potential for delamination: perforating, scoring, and "cold working" the copper foil tape, and adding epoxy. A sharp utility knife was used to perforate and score the copper tape. A thin, blunt-ended tool was rubbed across the surface to cold work the copper tape. In all three cases, the copper tape was modified at the edges of the adhesive pads and at the center of the gap. For the fourth modification, a thin line of a two-part epoxy (JB Weld) was applied to the surface of the weld prior to installation and the copper strips pressed into the epoxy.

A total of five modified specimens were tested. The details are described in Table 3.4. In each case, the copper strips peeled off the carpet tape and the top packing tape layer delaminated in the vicinity of the copper strips. Figure 3.12

shows the region of delamination observed around the copper strips for the perforated specimen at failure.

Table 3.4 Measured Response of Modified Point Switches Fabricated Using Carpet Tape

specimen modification	strip width (in.)	gap (in.)	displacement at failure (in.)	No. Strips Fractured	Delamination Observed
perforated	1/8	1/4	0.230	2	yes
scored	1/8	1/4	0.228	2	yes
cold working	1/8	1/4	0.219	1	yes
epoxy	1/16	1/4	0.198	2	yes
epoxy	1/8	1/4	0.313	1	yes

delamination of adhesive pad
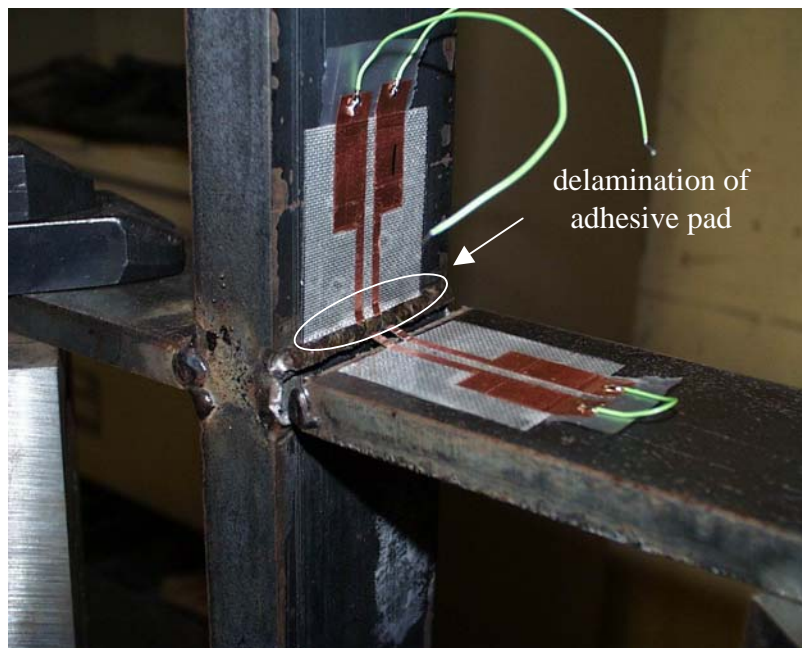
Figure 3.11 Point Switch with Perforated Copper Strips

The displacements at failure recorded for the three specimens with modifications to the copper foil tape were less than the displacements at failure of the original switches with 1/8-in. wide copper strips. The addition of epoxy to the copper strips did not have the expected response, the failure displacement

increased compared with the original switches with 1/8-in. wide copper strips. Despite the slight improvement in the first three specimens, the displacements of all specimens were still greater than the target crack size of 0.10 in.

One final modification to the point switch was tested: the factory-applied adhesive on the copper foil strips was removed, leaving the copper uninsulated across the weld. Four specimens were fabricated for this test. Details are given in Table 3.5. The switches were tested using the same procedure described earlier in this section. No disruption in the electrical response of the switch was observed due to the removal of the factory-applied adhesive.

Table 3.5 Measured Response of Point Switches When the Factory Adhesive
Was Removed from Copper Strips

specimen ID	strip width (in.)	gap (in.)	displacement at failure (in.)	No. Strips Fractured	Delamination Observed
1	1/8	1/4	0.346	2	yes
2	1/8	1/4	0.437	2	yes
3	1/16	1/4	0.262	2	yes
4	1/16	1/4	0.218	2	yes

No improvements in switch performance were obtained from this modification. The displacements at failure for each switch tested were greater than the values recorded for the other switches and delamination was observed during each test.

These observations led to the conclusion that delamination of the copper strips, packing tape, and carpet tape was inevitable. Higher strength adhesive was used to limit this type of behavior such that the copper strips broke at the desired crack size of 0.10 in. The behavior of point switches fabricated using tapes with stronger adhesives is described in the next section.

3.4.5   Point Switch Fabricated Using High Strength Adhesive Tapes

A total of eight point switch specimens were fabricated using tapes with high strength adhesives. All specimens were fabricated with 1/8-in. wide copper strips and a 1/4-in. gap. The 3M VHB Adhesive Transfer Tape F-9473PC was chosen for the bottom layer and the 3M Polyester Film Tape 8412 was chosen for the top layer. This stiff, thick tape was used to restrain the delaminating copper foil strips.

For these tests, the ohmmeter was abandoned in favor of a data acquisition system to measure the crack size at switch failure accurately. The switch was fabricated as before, but this time a 192-ohm resistor was attached to one of the wire leads. The addition of the resistor was used to reduce the current of the power source. Installation of the switch was similar to the method described in the previous section, except this time the adhesive pads were firmly pressed to the steel until the bottom adhesive was observed to extrude from beneath the top layer. This was done to simulate the 15 psi minimum installation pressure for the 3M VHB tape. Each switch was allowed to sit for 72 hours prior to testing to allow the 3M VHB tape to gain full bond strength.

A displacement transducer was mounted onto the cruciform shape, crossing the moveable weld. The wire leads from the switch were then connected to a 5-V power source. The test setup is shown in Fig. 3.12.
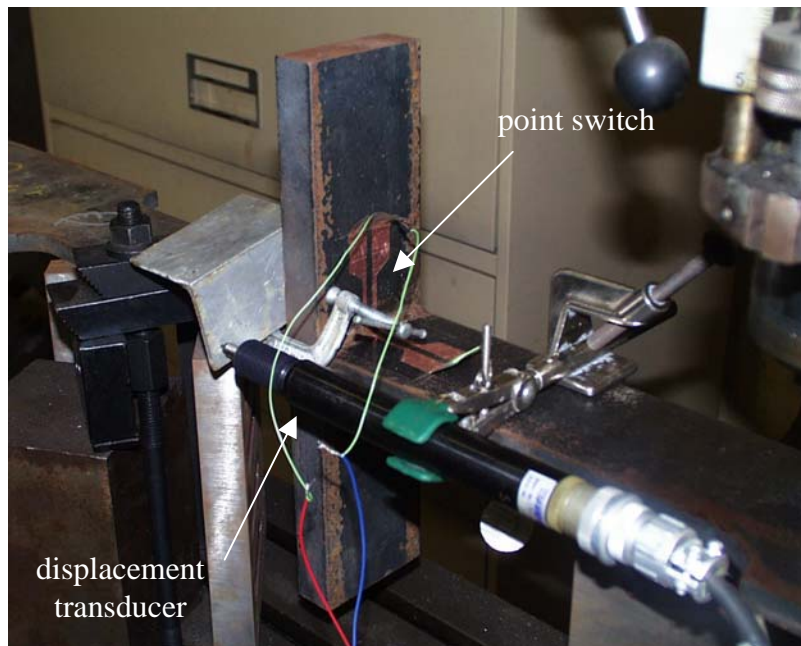
Figure 3.12 Data Acquisition Test Setup

Once again, the table was moved manually and stopped when the switch was visibly broken (Fig. 3.14). The displacement at failure of the copper strips was taken as the last value before the voltage deviated from 5 V. A representative plot is given in Fig. 3.15. The cruciform shape was replaced with another, previously untested in this setup, after tests 1 and 4 to determine the role of mill scale in causing the switch to peel from the steel surface. The results from these tests are given in Table 3.6.

Table 3.6 3M Adhesive Switch Performance

specimen ID	strip width (in.)	gap (in.)	displacement at failure (in.)	No. Strips Fractured	Delamination Observed
1	1/8	1/4	0.061	2	no
2	1/8	1/4	0.082	2	yes
3	1/8	1/4	0.110	2	yes
4	1/8	1/4	0.083	2	yes
5	1/8	1/4	0.091	2	yes
6	1/8	1/4	0.104	2	yes
7	1/8	1/4	0.098	2	yes
8	1/8	1/4	0.095	2	yes

Figure 3.13 Failure of Point Switch Fabricated Using 3M Tapes
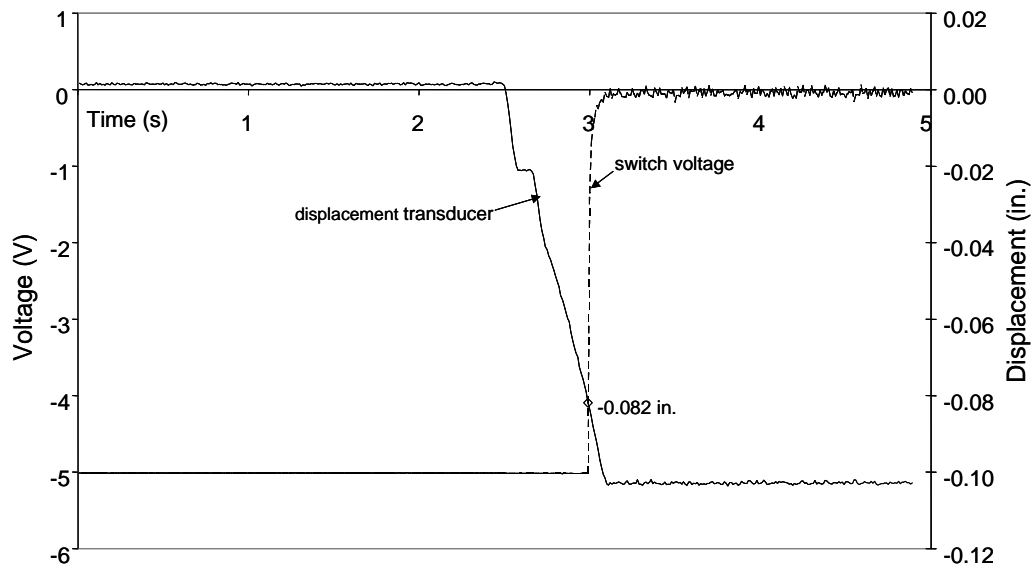
Figure 3.14 Voltage and Displacement of Specimen 2

The average displacement at failure for the switches was 0.09 in. The smallest displacement, 0.061 in., was recorded for specimen 1. The greatest displacement, 0.110 in., was recorded for specimen 3. No delamination was observed during the test of specimen 1. This was due to the removal of mill scale from the cruciform steel specimen during the previous experiments. Delamination was observed in all subsequent tests, most likely because mill scale was present on the surface of the steel.

The displacements recorded for specimens 2 and 4 were 0.082 in. and 0.083 in. respectively; in contrast, the displacement of specimen 3 was 0.110 in. These three specimens were all tested on the same cruciform specimen and experienced the same mill scale effects; therefore, insufficient application pressure was the likely cause for the higher displacement of specimen 3. This phenomenon also occurred in the test results of the last four specimens. A new cruciform specimen was installed after the fourth test, thus the amount of mill scale was similar for the last four specimens. The range of displacements for

44

specimens 5, 7 and 8 was between 0.09 in. and 0.10 in. Therefore, the slightly higher displacement of specimen 6, 0.104 in., was likely the result of insufficient installation pressure applied to the high strength 3M VHB tape layer.

3.5   CONCLUSION

The simple shapes cut from copper foil tape performed well in the one-dimensional tests. When the shapes were tested using the two-dimensional setup, the limitations of these designs became apparent. All specimens peeled away from the weld, and half bridged the crack without fracturing. The poor performance of the simple shapes during the two-dimensional dynamic tests led to the development of the point switch. The addition of the adhesive pads was intended to secure the copper strips on either side of the weld and limit the observed delaminations of the simple shapes cut from copper foil tape. The sections of copper foil tape crossing the weld were still expected to peel off, but would likely break once the region of delamination reached the high strength adhesive.

The point switch was initially fabricated using high-strength carpet tape and packing tape. The first specimens tested failed at simulated crack widths well above the target crack size of 0.10 in. All switches exhibited delamination at the copper foil/adhesive tape interface. Modifying the copper strips crossing the gap reduced the displacement at failure, but these displacements were still greater than the target size. Delamination of the adhesive pads continued to occur during testing. The addition of epoxy to the copper strips and the removal of the factory-applied adhesive from the copper strips actually increased the displacement at failure of the point switch. These observations led to the conclusion that

45

delamination of the copper strips, packing tape, and carpet tape was inevitable. Higher strength adhesive was chosen to limit this type of behavior.

The 3M adhesive tapes significantly improved the performance of the point switch design. The average displacement at failure for all specimens was 0.09 in., well below the target crack width of 0.10 in. No delamination occurred in the first test because the mill scale had been largely removed from the surface of the steel during the previous tests with switches constructed using carpet tape. The smallest displacement at failure, 0.061 in., was recorded for the first test. Delamination was observed during the remaining tests due to the presence of mill scale on the cruciform specimens. These observations indicate that mill scale should be removed in order to achieve the desired performance of the switch.

Only two of the specimens failed at a simulated crack width greater than the target width of 0.10 in. This was attributed to the application of insufficient pressure to the 3M VHB tape layer during installation. Thus, a uniform method of applying pressure to the high strength adhesive is needed.

CHAPTER 4

Performance of Switches Attached to Various Welded Steel Connections

4.1 INTRODUCTION

To be feasible, the crack detection device must be reliable, affordable, and durable. The switch must remain in position during an earthquake and open when a crack occurs beneath it. Ideally, the installer should need to do no more than clean the area with a solvent, peel off the tape backing, and affix the switch across the weld. Removing the mill scale or using a high strength epoxy may improve the operation of the switch, but this makes the procedure more complex and time-consuming, raising the cost of installation.

The objective of this phase of the investigation was to install switches on steel specimens in Ferguson Laboratory and observe the performance under a variety of loading schemes. This phase was performed concurrently with the testing program described in Chapter 3; therefore, three types of switches were evaluated: hybrid bow-tie shapes cut from copper foil tape, point switches fabricated using carpet and packing tape, and switches fabricated using the 3M tapes. The switches were installed on two types of welded specimen connections. One set of specimen was subjected to elastic stress and the other set was subjected to inelastic stress. The switches were inspected visually during and after the tests of the welded specimens. The observed response and difficulties encountered during installation are discussed in this chapter.

4.1.1 Tests of Welded Specimens

The first set of welded specimens was subjected to axial fatigue loads (Spadea, 2002). These specimens were designed to evaluate the fatigue response of fillet welds. Each specimen was constructed of a 1/2-in. thick 60-in. by 10 1/2-in. steel plate (Fig. 4.1). Six 1/4-in. plates were welded to the 1/2-in. plate dividing it into four quadrants on the front and back and creating four potential fracture locations at mid-height. The specimens were installed across the fillet welds at these locations.

Side Elevation   **Front Elevation**
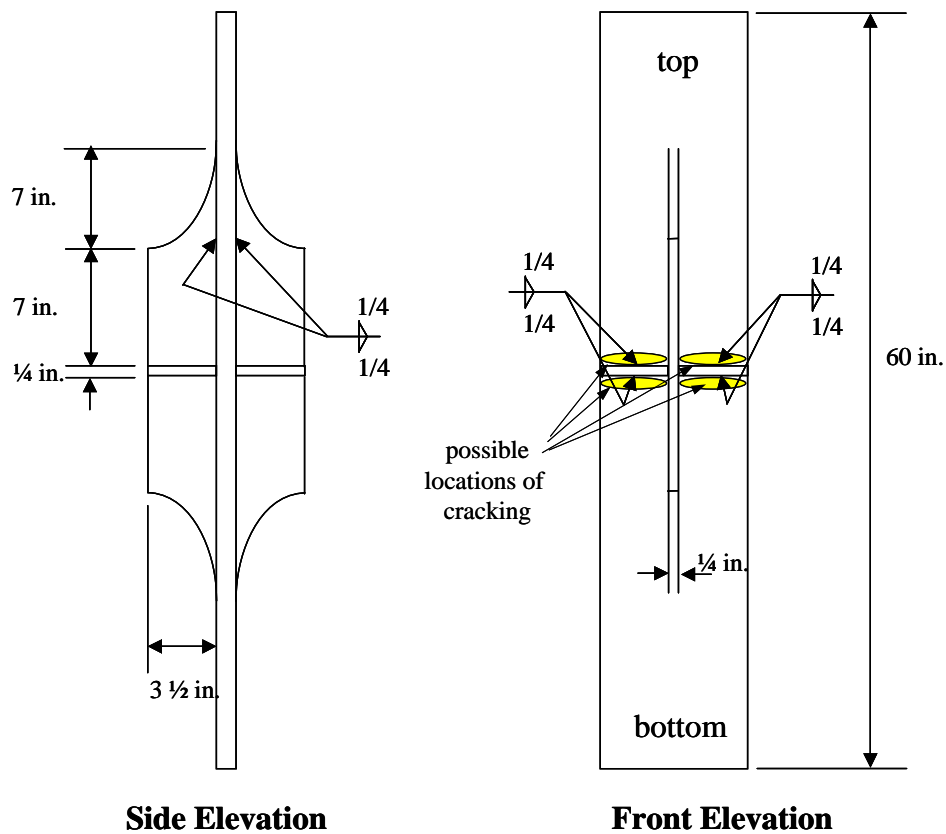
Figure 4.1 Welded Steel Specimen Tested by Spadea (2002)

The second set of welded specimens was subjected to cyclic lateral loads. Two different types of shear link connections were studied in these tests. The

48

first type of specimen was designed to test beam links in eccentrically braced frames (Arce, 2002). These link beams were welded to end plates for connection to the load frame. Switches were installed on the three specimens shown in Fig. 4.2. The typical beam to column connection detail of the specimens is shown in Fig. 4.3.

PL $9\frac{7}{16}$" x $1\frac{7}{8}$" x $\frac{3}{8}$"

PL $9\frac{7}{16}$" x $1\frac{7}{8}$" x $\frac{3}{8}$"

23"

30"

W10x19
Stiffeners: 3@$5\frac{3}{4}$"

W10x19
Stiffeners: 4@6"

(a)

(b)

PL $8\frac{13}{16}$" x $3\frac{13}{16}$" x $\frac{3}{8}$"

23"

W10x33
Stiffeners: 3@$5\frac{3}{4}$"

(c)
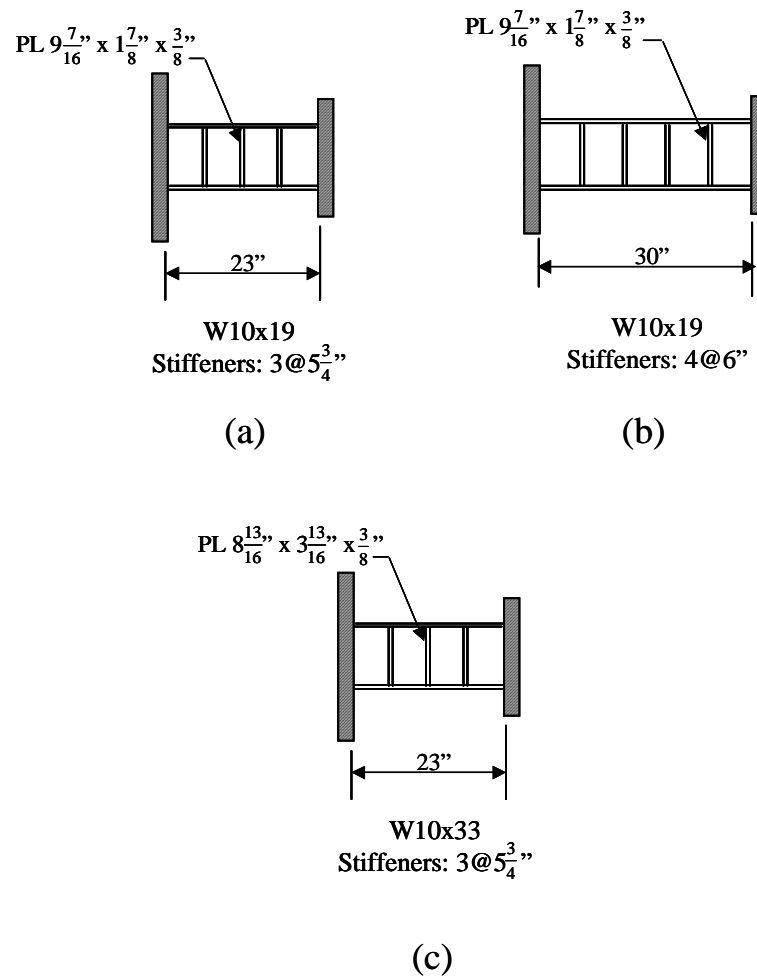
Figure 4.2 Welded Steel Link Beams Tested by Arce (2002)

49
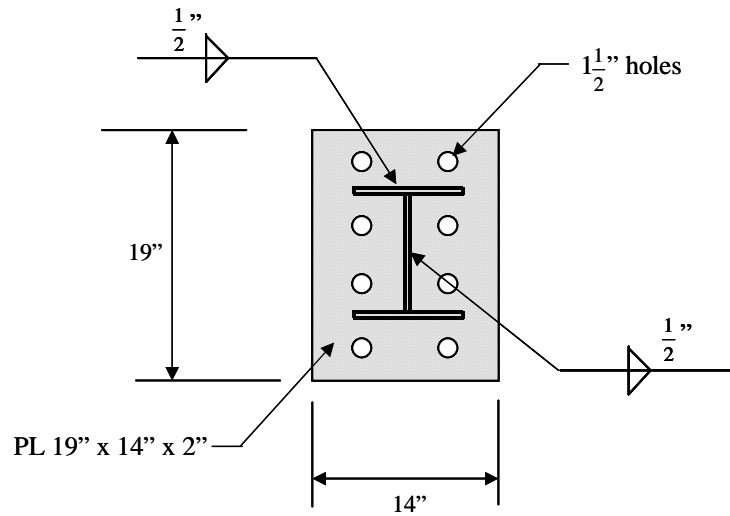
Figure 4.3 Typical Beam to End Plate Connection Detail (Arce, 2002)

The second type of specimen was designed to test the link to column connection for an eccentrically braced frame (Okazaki, 200x). The welded connections were fabricated according to pre-Northridge specifications. Figure 4.4 shows the details for the link and the connection of the specimen used to test the switches.

Link Beam   **Connection**
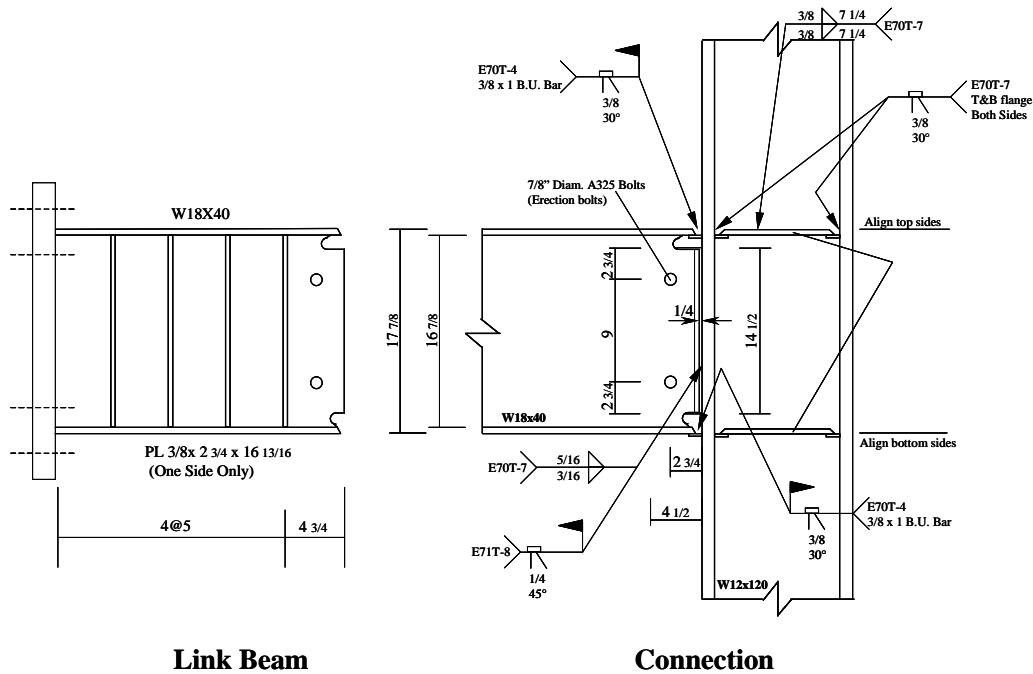
Figure 4.4 Link and Connection Details Tests by Okazaki (200x)

4.2 PERFORMANCE OF SIMPLE SHAPES CUT FROM COPPER FOIL TAPE

Hybrid bow-tie shapes cut from copper foil tape (Fig. 3.5) were installed on a specimen that was subjected to axial fatigue loads. One hybrid bow-tie shape was placed across the weld at each of the eight potential fracture locations at mid-height. Four specimens had a taper thickness, d, of 1/16 in. and the other four a taper thickness, d, of 1/8 in. All strips had a taper length, *l*, of 1/2 in.

Installation difficulties arose from the frangible, flexible nature of the switches. The first three specimens had to be replaced due to poor alignment across the weld or due to failure of the taper during installation.

The specimen failed when a fatigue crack formed in the toe of the top weld and propagated halfway across the specimen. The crack width at failure was

51

approximately 0.10 in. at the edge. The copper foil shapes located along the weld crack delaminated from the surface of the weld and the adjacent steel surfaces (Fig. 4.5 and 4.6). This behavior is similar to that observed during the dynamic two-dimensional tests (Section 3.3). The poor behavior of the shapes cut from copper foil tape under fatigue loading, combined with the results of the two-dimensional tests in Section 3.3, confirmed the need to develop an improved switch. The point switch design (Fig. 2.7) was used for all other tests described in this chapter. Fabrication of the point switch is discussed in Appendix A.

Figure 4.5 1/16-in. Wide Copper Shape over Crack, Top View
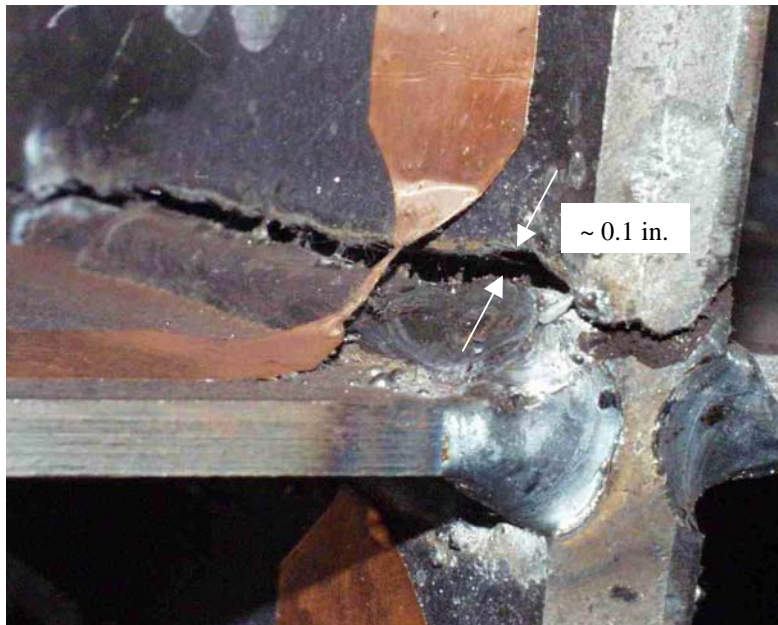
Figure 4.6 1/16-in. Wide Copper Shape over Crack, Side View

4.3 PERFORMANCE OF POINT SWITCH FABRICATED USING CARPET TAPE

Four point switches, constructed on heavy-duty carpet tape and covered with packing tape, were installed on one of the welded steel specimens tested by Spadea (2002). All of the switches had a gap size of 1/4 in. and copper strip width of 1/8 in. The switches were installed on the top weld, two on the front of the specimen and two on the back. As discussed in Section 3.4.4, the copper strips were modified in an attempt to limit the extent of delamination. One switch was fabricated with each of the modifications: perforating, scoring, and "cold working" the copper tape, and adding epoxy.

4.3.1 Installation of Modified Point Switches Fabricated Using Carpet Tape

The cold-worked switch was damaged during installation. A second cold-worked switch was fabricated and installed successfully. During installation, it was found that the flexibility of the carpet tape adhesive pads made positioning

53

difficult; the corners of the pad often would become adhered to the adhesive side
of the pad. Numerous weld splatters were present on this specimen near the weld,
which interfered with the adhesion of the pads. Thus, complete adhesion was not
possible with minimal preparation of the surface. These air pockets are circled in
Fig. 4.7 through 4.10.
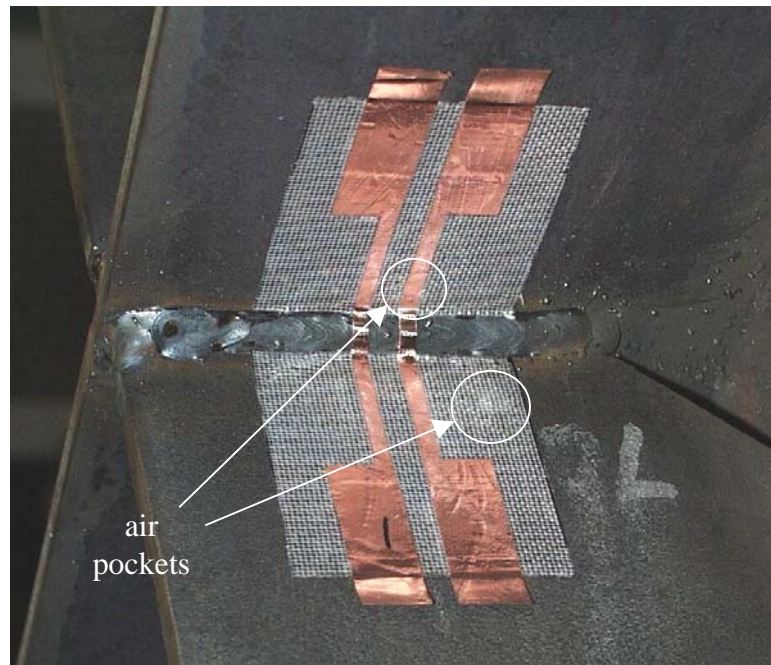
Figure 4.7 Point Switch Modified by Perforating
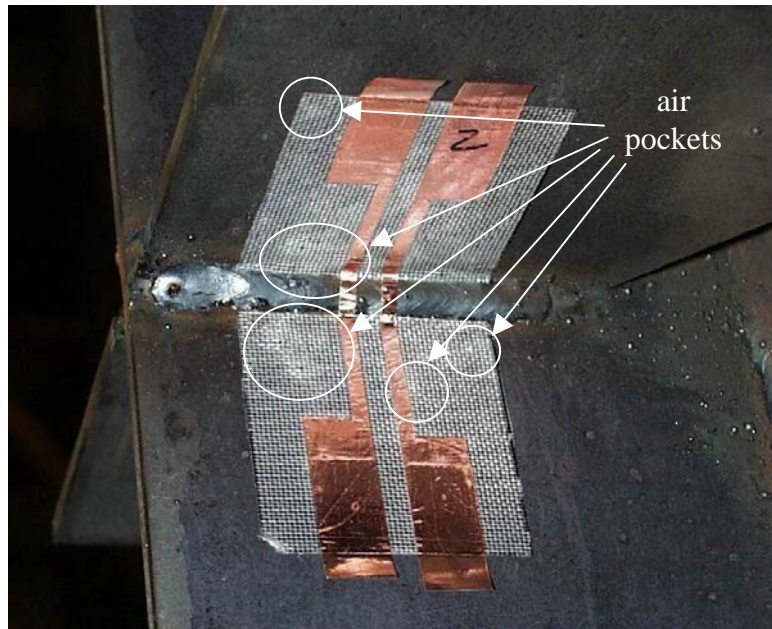
Figure 4.8 Point Switch Modified by Scoring
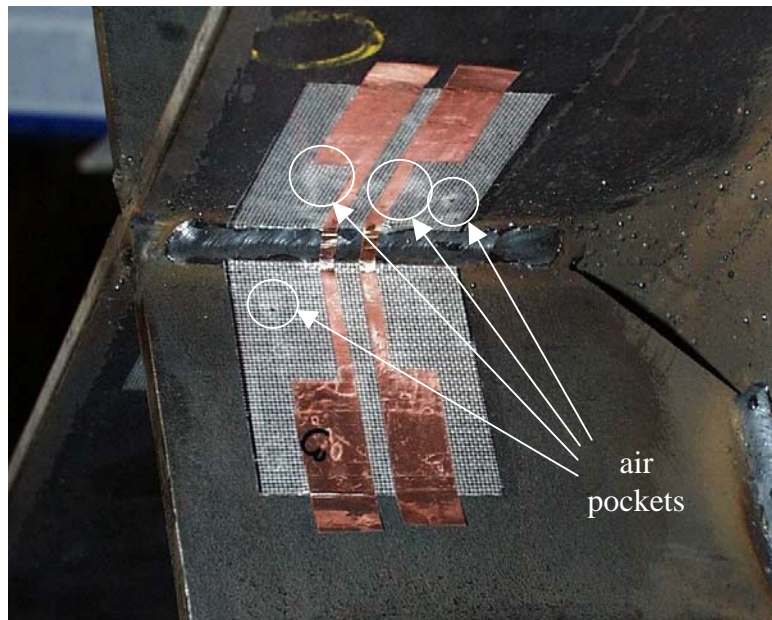
Figure 4.9 Point Switch Modified by Cold Working
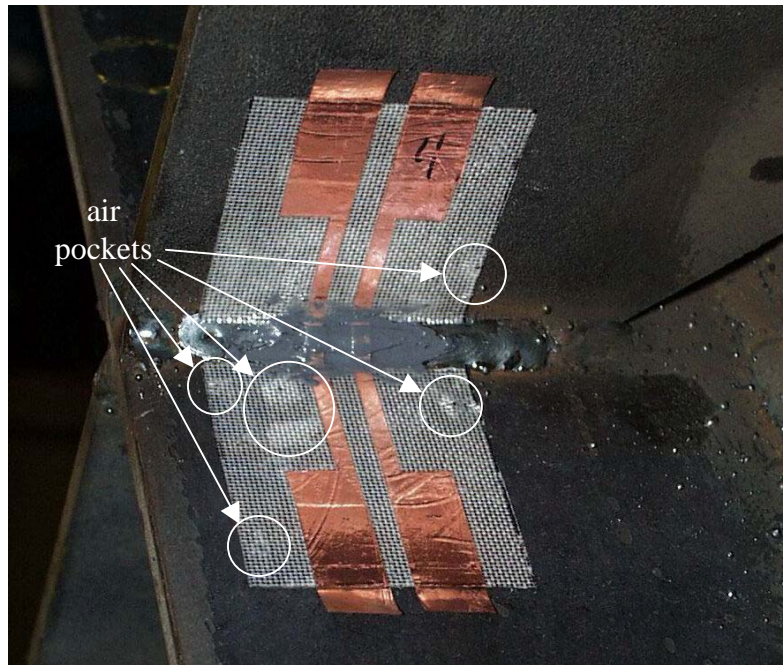
Figure 4.10 Point Switch Modified Using Epoxy

4.3.2   Observed Response of Modified Point Switches

The test specimen failed when a crack propagated across the entire width of the specimen (Fig. 4.11).   The copper strips in three of the point switches broke. The fourth switch remained intact because the crack propagated through the bottom portion of the weld at that location.   Very little delamination was observed on the three failed specimens. This was attributed to the rapid failure of the section during testing.

Figure 4.11 Test Specimen at Failure (Spadea, 2002)

The satisfactory performance of the modified switches in this test was negated by poor performance in the controlled two-dimensional displacement test (Section 3.4.4). The high delamination observed during the controlled tests led to the conclusion that delamination of the copper strips, packing tape, and carpet tape was inevitable. The behavior of point switches fabricated using higher strength 3M adhesive tapes for all other tests discussed in this chapter.

4.4 PERFORMANCE OF POINT AND DISTRIBUTED SWITCHES FABRICATED USING 3M TAPE

Point switches fabricated using 3M tape were also tested using the axial fatigue specimens (Spadea, 2002). Point and distributed switches were tested using shear link specimens that were subjected to cyclic lateral loads (Arce, 2002; Okazaki, 200x).

57

4.4.1   Performance on Axially Loaded Fatigue Specimens

The point switches were installed the same type of welded steel specimen described in the previous two sections. Two sets of four switches were installed on two different specimens. All switches were fabricated with 1/8-in. wide copper strips and a 1/4-in. gap.

(a) Installation of Point Switches

Four point switches were installed on the top weld of both specimens, two on the front and two on the back. Three of the four switches placed on the first specimen broke during installation. This occurred when the adhesive pads were applied; the pressure caused the polyester tape to press down on the exposed copper strips, snapping them along the edge of the pad. In addition, one switch failed during installation because of improper placement of the adhesive pads. All four switches on the second specimen were successfully installed. As with the switches fabricated using carpet tape, weld splatter prevented the complete adhesion of the adhesive pads (Fig. 4.12 (b) and 4.13).

(b) Observed Response of Point Switches

The first specimen failed when the crack propagated halfway across the plate. The switches that had failed during installation were located in the vicinity of the cracked weld; the weld beneath the intact switch did not crack. No delamination was observed on the intact switch from the fatigue loading. To evaluate the performance of the switches when a fatigue crack formed beneath them, four more switches were installed on the second test specimen.

The second test specimen failed along the toe of the top weld. The fatigue crack propagated halfway across the plate. The crack size was approximately 1/8-in. wide at the edge of the plate, reducing to 1/10 in. at the middle. Both switches located in this quadrant of the test specimen failed. The copper strips in these

switches failed at the copper tape/adhesive pad boundary (Fig. 4.12). This behavior was similar to the observed response of the point switches discussed in Chapter 3. The other two switches remained intact because the crack did not propagate into that half of the specimen (Fig. 4.13). No delamination was observed for either the intact or the failed switches.
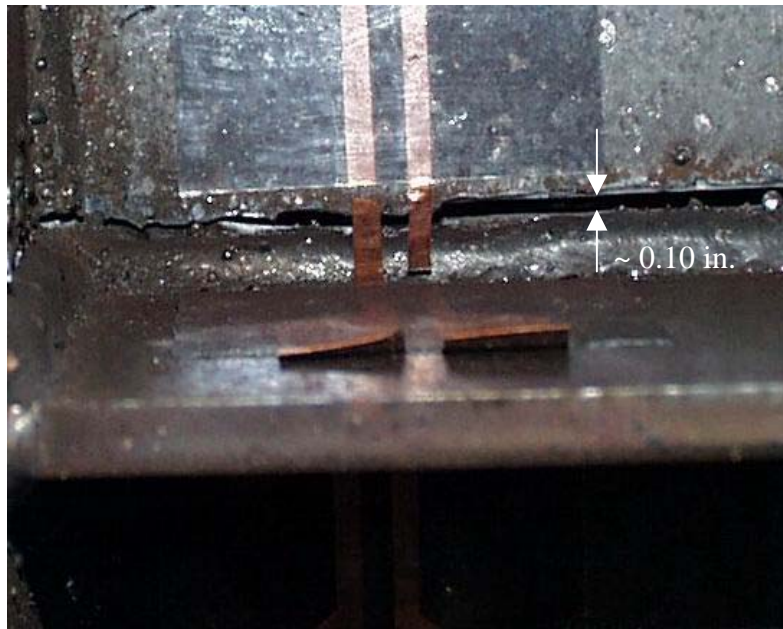
(a) Front of Test Specimen
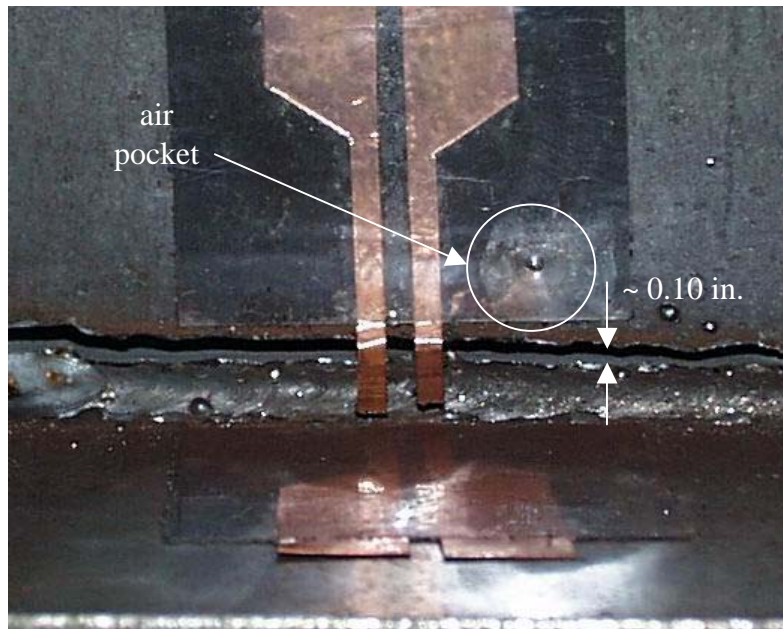
(b) Back of Test Specimen

Figure 4.12 Failure of Point Switches Fabricated Using 3M Tape
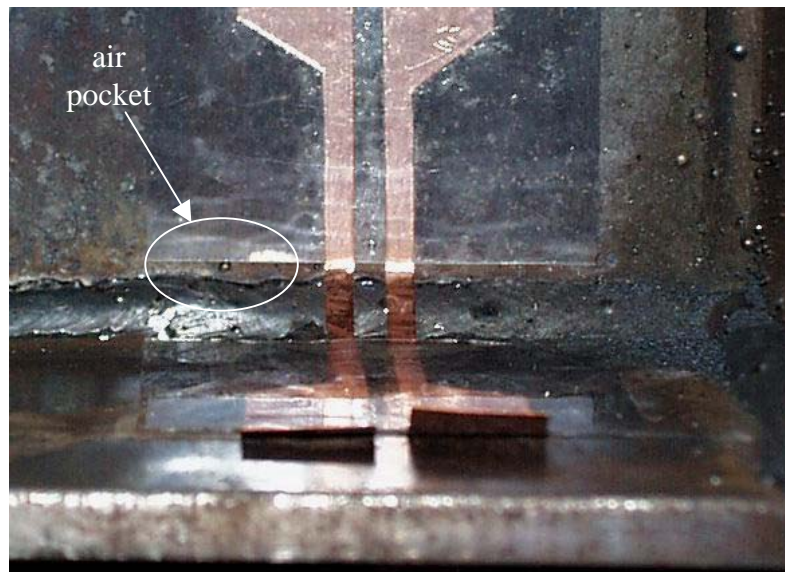
Figure 4.13 Point Switch Crossing Intact Weld

4.4.2   Performance on Shear Links Subjected to Cyclic Lateral Loads

Two different shear link connections were evaluated in ongoing tests by Arce (2002) and Okazaki (200x). The specimens tested by Arce were designed to test beam links in eccentrically braced frames, while the specimens tested by Okazaki were designed to test the link to column connection for an eccentrically braced frame. Point and distributed switches were fabricated using the high strength 3M adhesive tape. The switches were installed on four shear link specimens: three beam link specimens (Fig. 4.2) and one beam to column specimen (Fig. 4.3). Each specimen was whitewashed prior to testing. Details for each test are provided in Table 4.1. The switch gap was 1/8 in. larger than the weld size to provide a good fit over the weld geometry.

Table 4.1 Shear Link Test Details

test ID	shear link	Figure No.	No. of Point Switches Installed	No. of Distributed Switches Installed	weld size (in.)	gap (in.)
1	link beam	4.2 (a)	2	0	3/8	1/2
2	link beam	4.2 (b)	1	0	3/8	1/2
3	link beam	4.2 (c)	1	1	3/8	1/2
4	link to column	4.3	2	2	1/2	5/8

(a) First Shear Link Specimen

On the first connection (Fig. 4.2 (a)), one point switch was fabricated and installed on the top flange (Fig. 4.14). A second switch was installed underneath the beam on the bottom flange weld.

This link beam failed in the top flange first. The crack began near the toe of the weld at the edge of the flange and crossed beneath the adhesive pad attached to the top flange. However, the copper strips did not break (Fig. 4.15). The interface between the mill scale and the steel flange failed, thus the pad was not attached to the top flange at the end of the test (Fig. 4.16). The same phenomenon occurred with the second switch; the pad detached from the bottom flange and was hanging free at the end of the test (Fig. 4.17).

Figure 4.14 Point Switch with Minimal Surface Preparation in First Shear Link Specimen

Figure 4.15 Point Switch after Beam Flange Failed Near Top Flange Weld in First Shear Link Specimen

Figure 4.16 Photograph of Mill Scale Residue on Adhesive Pad on Top Flange

Figure 4.17 Photograph of Mill Scale Residue on Adhesive Pad on Bottom Flange

(b) Second Shear Link Specimen

Due the poor performance of the point switch on the first shear link, the mill scale was removed from the second specimen before the switch was attached. Patches of mill scale, approximately 1-in.^{2} in size, were removed from the top flange of the beam and the vertical end plate using a pneumatic grinder.

This shear link also failed in the top flange, with a 1/8-in. wide crack crossing beneath the adhesive pad on the beam. The pad remained attached to the top flange of the beam and both copper strips broke at the copper strip/adhesive pad interface (Fig. 4.17).
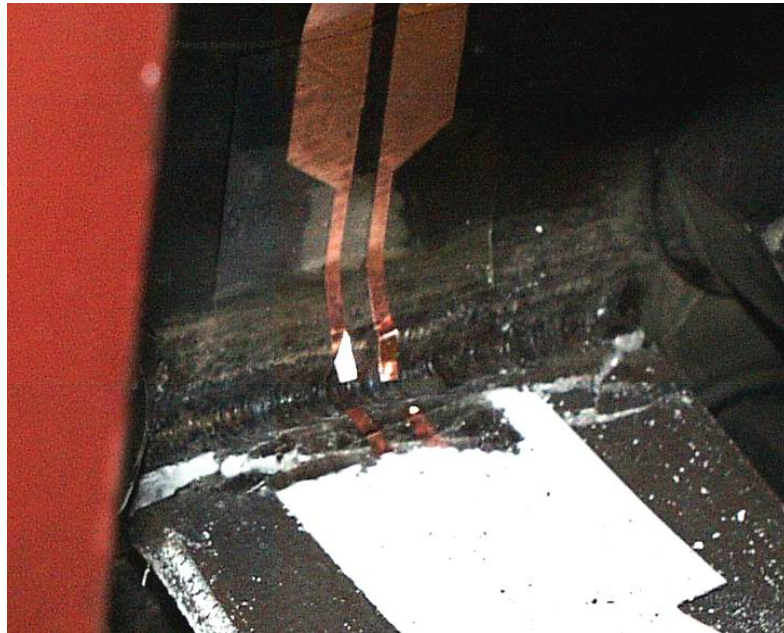
Figure 4.18 Point Switch After Beam Flange Failed Near Weld in Second Shear Link Specimen

(c) Third Shear Link Specimen

A point switch and a distributed switch with three pairs of copper strips were installed on the third shear link specimen. The point switch was installed on

the top flange of the beam. The distributed switch was too wide to fit on the beam flange, thus it was installed on the web along the bottom K-line.   At both locations, the mill scale was entirely removed from the steel with a pneumatic grinder before installation. Previous link beam specimens had failed along the K-line and the same mode of failure was expected to occur in this test.

None of the welds broke in this test and the point switch remained in place.   The K-line fracture occurred as expected, running along the top then crossing to the bottom of the web. However, the fracture did not extend into the area where the switch was located (Fig 4.19).

Figure 4.19 K-line Fracture on Web of Third Shear Link Specimen

(d) Fourth Shear Link Specimen

A total of four switches were attached to the fourth shear link specimen: two point switches and two distributed switches. The distributed switches were fabricated with three pairs of copper strips crossing the gap between the adhesive pads. The distributed switches were installed on the top flange of the beam, and the two point switches attached to the inside face of the bottom flange (Fig. 4.20).

66

Similarly to the second and third specimens, the mill scale was removed from the surrounding steel with a pneumatic grinder. Because the researcher was concerned about the integrity of the welds and possible adverse effects on behavior of the specimen, the areas immediately next to the weld were not cleaned of mill scale.
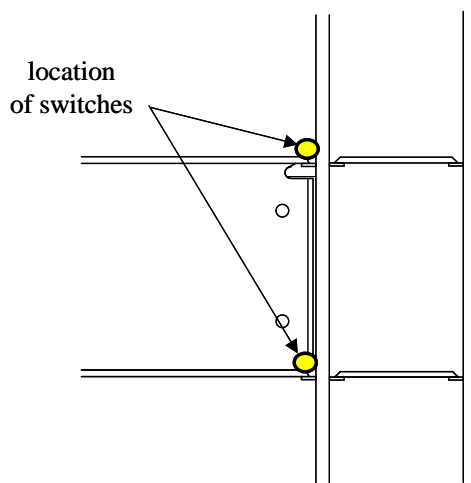
Figure 4.20 Location of Switches on Fourth Shear Link Specimen

During testing, a crack formed along the toe of the weld on the top flange. The test was stopped periodically to inspect the connection. During one pause, a 1/10-in. crack at the toe of the weld along the top flange was observed; however, none of the copper strips on the distributed switches was broken (Fig 4.21). During the next pause in testing, the crack width was observed to be to approximately 1/8 in. Upon inspection, the copper strips of the distributed switches were still intact but the adhesive pads had delaminated from the surface of the column flange near the weld (Fig. 4.22). The copper strips broke when the welds connecting the bottom flange to the column flange fractured, completely failing the connection (Fig. 4.23). The two point switches also delaminated from the column flange when a 1/10-in. crack formed at the weld (Fig. 4.24). The

copper strips failed when the bottom weld suddenly fractured and the resulting crack size was in excess of 1 in.

Figure 4.21 Distributed Switches Bridging a 1/10-in. Crack in Fourth Shear Link Specimen
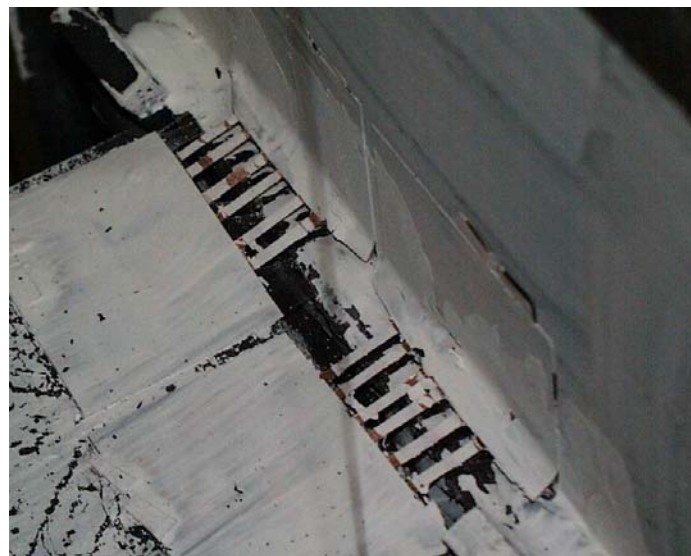
Figure 4.22 Delamination of the Adhesive Pads in the Fourth Shear Link Specimen

Figure 4.23 Distributed Switches after Failure of Top Beam Flange in the Fourth Shear Link Specimen

Figure 4.24 Point Switch Bridging 1/10-in. Wide Crack

4.5 CONCLUSION

The shapes cut from copper foil tape delaminated from the surface of the weld and the adjacent steel surfaces when a crack formed beneath them. These results are reasonable since the shapes tested in the dynamic two-dimensional tests of Chapter 3 delaminated in the same manner. The behavior of the shapes cut from copper foil tape under fatigue loading, combined with the results of the two-dimensional tests in Section 3.3, confirmed the need to develop an improved switch.

Modified point switches fabricated using carpet and packing tape all failed when a crack formed beneath them. Despite satisfactory performance on the welded steel specimen, the performance of the modified switches in the two-dimensional controlled tests in Section 3.4 was the reason the higher strength adhesives were chosen.

Switches fabricated using the high strength 3M adhesive tapes performed well on the axially loaded fatigue specimens. The point switches failed at the copper tape/adhesive pad interface when a crack opened beneath them. Also, there were no inelastic deformations in the axial fatigue specimens. Because the shear link connections experienced inelastic deformations, mill scale was a major factor in the performance of the switches. In the first shear link specimen test, the switches peeled from the beam flange when mill scale loosened from the steel during inelastic deformation. When the mill scale was removed from the steel in the second and third tests, the switches remained in place and failed when a crack formed beneath them. However, when not enough mill scale was removed from the surface adjacent to the weld on the fourth specimen, the switches all delaminated at the copper foil/adhesive tape interface, bridging the weld crack. Only when the crack size increased to 1 in. did the copper strips fail.

70

Adhesives are critical to the performance of the switches. In order for the adhesives to adhere properly, the mill scale must be removed from the steel. If not enough is removed, the switch will delaminate and the copper strips will bridge the crack. The probability that the copper strips will bridge a crack increases as the gap between the adhesive pads increases. Despite the improvement in switch performance when the mill scale is removed, the switches are likely to give inconsistent results for small crack widths.

CHAPTER 5

Measured Frequency Response of Prototype Sensor

5.1 INTRODUCTION

The previous two chapters have focused on the design of a switch to detect cracking in welded steel connections. This chapter investigates the characteristic frequency response of the complete sensor. The response is complicated by the fact that the steel structure induces a parasitic inductance in the sensor circuit. Additionally, attaching the strips of copper foil used to form the switch to the surface of the steel creates a parallel-plate capacitor within the circuit. Therefore, the interaction between the prototype sensor and the base metal must be evaluated experimentally.

Electrical circuit models of the prototype sensor are developed in Section 5.3 and the measured response is compared with the calculated response in Section 5.4. In all tests discussed in this chapter, cracks were simulated by cutting the copper strips in the switch. Most of the tests were conducted using distributed switches with the objective of identifying the location of the crack if only a portion of the cooper strips fracture.

5.2 DEFINITION OF TERMS

Terms and variables used in this chapter are defined below. A detailed sketch of a distributed sensor with five pairs of copper strips and a single added capacitor is given in Fig. 5.1. The same sensor with five added capacitors is

shown in Fig. 5.2 Many of the terms defined in this section are shown in these sketches.

A_{ij}:   Area of copper foil tape between potential zones of failure; mm^2. Copper foil tape is expected to tear in the gap between adhesive pads. i refers to the serpentine leg and j refers to the area. For a distributed sensor with n pairs of copper strips crossing the gap between adhesive pads, $i = 1, 2$ and $j = 1, n + 1$. For the distributed sensor, $j = 1$ corresponds to the area of copper foil that is furthest from the EAS tag.

C: Capacitance; pF.

C_{add}:   Capacitance of each capacitor added along a distributed switch (Fig. 5.2); pF.

C_{ij}:   Capacitance of area A_{ij} of copper foil tape; pF.

C_{load}:   Capacitance of single capacitor added at the end of a distributed switch (Fig. 5.1) or added to a point switch (Fig. 2.8); pF.

C_{tag}:   Measured capacitance of EAS tag; pF. For the EAS tags used in this investigation, $C_{tag} \approx 100$ pF.

C_{total}:   Total capacitance of sensor circuit, pF.

ε_o: Permittivity constant of free space; 8.85×10^{-12} F/m.

ε_r: Dielectric constant of the base layer of tape that fills the gap between the copper foil tape in the switch and the surface of the steel. Note that the value of ε_r may vary because the gap between the copper foil tape and the surface of the steel was not constant in the prototype sensors. The gap thickness was essentially zero in the region between the adhesive pads and equal to the thickness of the adhesive pads in other regions. For the purpose of this investigation the gap was assumed to be equal to the thickness of

73

the adhesive pads. Values of the dielectric constant were inferred from the measured frequency response of each sensor.

f: Frequency; MHz.

f_{ch}: Characteristic frequency of sensor; MHz. The characteristic frequency corresponds to the minimum value of the phase angle (Fig. 2.6).

f_r: Resonant frequency of an idealized RLC circuit; MHz. An idealized RLC circuit is in resonance when the current is at a maximum, the phase angle is zero, and the impedance is equal to the resistance of the circuit.

L: Inductance; μH.

L_{eff}: Effective inductance of EAS tag due placement on or near a steel plate; μH.

L_{steel}: Parasitic inductance produced by image currents in steel plate; μH.

L_{tag}: Inductance of EAS tag; μH. For the EAS tags used in this investigation, $L_{tag} \approx 4$ μH.

R_{bad}: Resistance induced in the sensor circuit by poor quality electrical connections between the switch and the EAS tag; ohms

S_i: Switch i in the electrical circuit model of the sensor. In the physical switch, location S_i corresponds to the ith copper strip that crosses the gap between adhesive pads. For a point sensor, $i = 1$, 2. For a distributed sensor with n pairs of copper strips crossing the gap between adhesive pads, $i = 1, 2n$ (Fig. 5.1 and 5.2). For the distributed sensors, $i = 1$ corresponds to the copper strip that is furthest from the EAS tag.

t: Thickness of base layer of tape that fills the gap between the copper foil tape in the switch and the surface of the steel; mm.
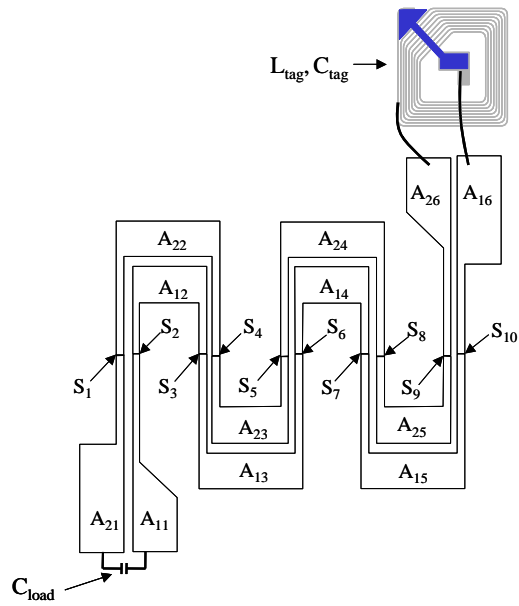
Figure 5.1 Components of a Distributed Sensor with Five Pairs of Switches and One Added Capacitor
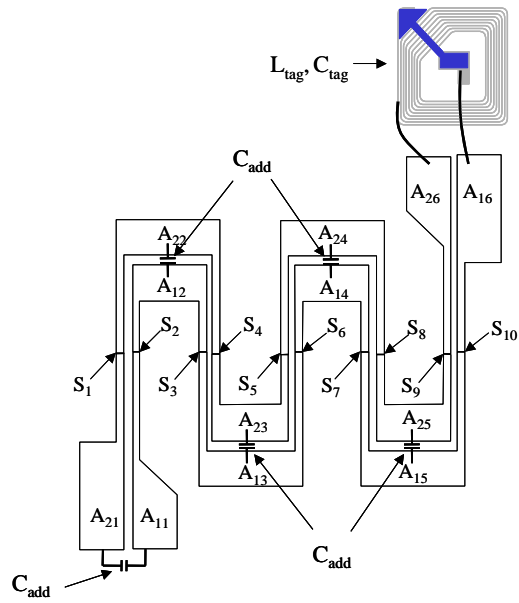
Figure 5.2 Components of a Distributed Sensor with Five Pairs of Switches and Five Added Capacitors

75

5.3 ELECTRICAL MODEL

The prototype sensor behaves as a series RLC circuit. Voltage in the sensor is generated by the magnetic output of the transmission antenna, producing a current in the EAS tag and attached switch. The circuit model of the sensor is developed in this section using these electrical properties.

The resonant frequency in a RLC circuit is:

$$f_r = \frac{1}{2\pi\sqrt{LC}}$$ (5.1)

When the sensor is placed on a steel surface, the copper tape strips in the switch interact with the steel forming parallel-plate capacitors within the circuit. As each copper strip is cut where it crosses the gap, total capacitance decreases as copper foil tape area is removed from the circuit. Assuming the inductance remains constant, this decrease in capacitance results in an increase in frequency.

The resonant frequency of the sensor is calculated by rewriting Eq. 5.1 as:

$$f_r = \frac{1}{2\pi\sqrt{L_{eff}C_{total}}}$$ (5.2)

where L_{eff} is the effective inductance of the EAS tag when placed on steel and C_{total} is the total capacitance of the sensor at a given switch state.

For an intact sensor not in contact with a steel surface, L_{eff} is equal to L_{tag} and C_{total} is the sum of C_{load} and C_{tag}; when all the switches are opened, and the sensors is not in contact with a steel surface, L_{eff} is equal to L_{tag} and C_{total} is equal to C_{tag}, the resonant frequency of the unmodified EAS tag. When the sensor is not in contact with a steel surface, a point or distributed sensor with a single added capacitor of 200 pF will transmit a resonant frequency of 4.6 MHz when the switch is closed and 8 MHz when the switch is open (Section 2.2.4).

It is assumed that L_{eff} remains constant while the sensor is on the steel surface. The currents in the tag are imaged in the base metal to produce a

parasitic inductance on the circuit (Fig. 2.4). The inductance and resistance of the copper foil tape was ignored in the development of this model; therefore, opening the switches only affects the capacitance of the circuit. As the copper foil strips on the switch are opened, C_{total} in Eq. 5.2 varies. Thus the frequency response of the sensor may be calculated if L_{eff} of the sensor and C_{total} of the current sensor state are known.

5.3.1 Effect of Steel Plate on Inductance of EAS Tag

The inductance of the tag is affected by the presence of the steel, which forms a parallel parasitic inductance on the circuit (Fig. 2.4). When the tag is placed on the steel, the inductance of the tag is lowered due to the transformer circuit between the steel and the EAS tag. Thus, the inductance of the circuit is transformed into an effective inductance, L_{eff}.

The inductance induced by the steel is related to the distance between the EAS tag and the surface of the steel. As the distance decreases, the transformer coupling factor increases, causing L_{eff} to decrease. A preliminary test found that an EAS sticker must be elevated at least 1 cm above a steel surface in order to overcome the parasitic action of the metal surface. Verification of this result is discussed in Section 5.5.1. It is assumed that the inductance L_{eff} remains constant once the EAS tag is attached to the steel surface and does not depend on the state of the switch.

5.3.2 Capacitance of Switches Fabricated from Copper Foil Tape

When the copper foil tape is attached to the surface of the steel, a parallel-plate capacitor is formed. The resulting capacitance is related to the area of the copper foil tape, the vertical gap between the foil tape and the steel surface, and the dielectric constant of the adhesive pads. Double-sided carpet tape was used to form the adhesive pads for all the tests reported in this chapter.

Because the potential exists for a crack to form at any location along the length of a distributed switch, the copper foil tape was divided into discrete areas, A_{ij}, as shown in Fig. 5.1 and 5.2. The capacitance associated with an area of copper foil tape is given by:

$$C_{ij} = \frac{\varepsilon_o \varepsilon_r}{t} A_{ij}$$ (5.3)

The distance separating the copper foil tape from the steel surface, t, was not constant within area A_{ij} because the strips of copper foil tape span between two adhesive pads and t is reduced in this region. The thickness was reduced beneath the copper foil areas on the adhesive pads due to the installation pressure applied to the carpet tape during the fabrication of the switch.

The dielectric constant, ε_r, and the distance separating the copper foil tape from the steel surface, t, for the adhesive pads were not known and had to be inferred from the measured data. Thus, ε_r and t were combined into a dielectric parameter, ε_r/t. Inferred values of ε_r/t are reported in Section 5.5.3.

5.3.3   Point Sensor on Steel Surface

The electrical model for the point sensor on the steel surface was developed first. The components of the point switch are defined in Fig 5.3. The corresponding circuit model for the point sensor on steel and added capacitor is shown in Fig. 5.4 (a). The EAS tag is modeled using L_{tag} and C_{tag}, the extra capacitor that is attached to the end of the switch is shown as C_{load}, and parasitic inductance of the steel plate is shown as L_{steel}. The capacitance of each leg of the switch, C_{ij}, is calculated using Eq. 5.3. A connection that links the legs of the switch is included in the circuit model to represent the influence of the steel surface to which the sensor is attached.
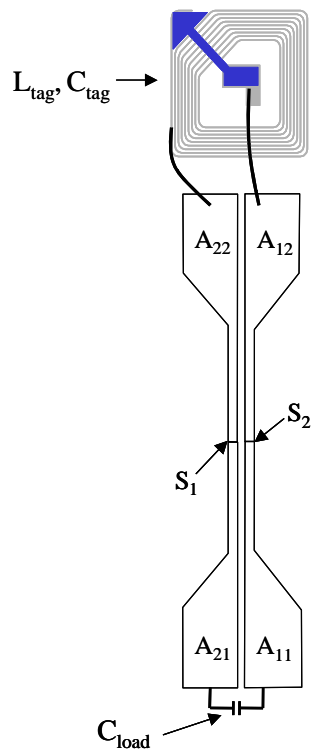
Figure 5.3 Components of a Point Sensor
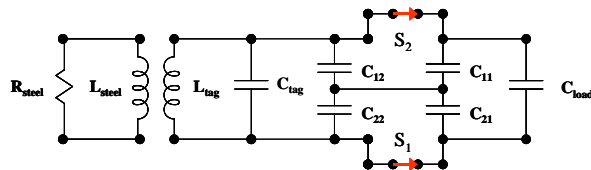
(a) Complete Electrical Circuit Model
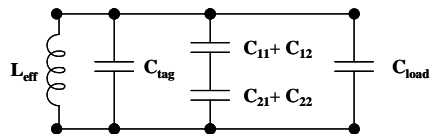
(b) Compressed Electrical Circuit Model

Figure 5.4 Electrical Circuit Models for a Point Sensor

The complete electrical circuit is simplified in Fig. 5.4 (b) by combining the inductance of the EAS tag and the parasitic inductance of the steel using Eq. 5.3 and adding the capacitance of each leg of the copper film tape in parallel. This circuit model can be further simplified by combining the capacitors into a single capacitor, C_{total}:

$$C_{total} = C_{tag} + \left[\frac{1}{C_{11} + C_{12}} + \frac{1}{C_{21} + C_{22}} \right]^{-1} + C_{load} \tag{5.4}$$

The circuit for the point sensor will change when the switches are opened. Switch S_1 is shown in the open position in Fig. 5.5 (a). The physical location of switch S_1 is shown in Fig. 5.3.
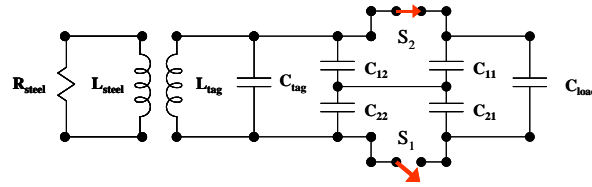
(a) Complete Electrical Circuit Model
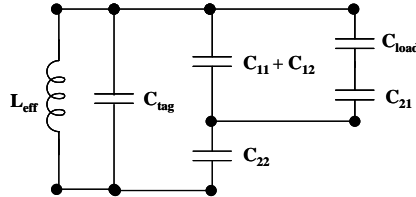
(b) Compressed Electrical Circuit Model

Figure 5.5 Electrical Circuit Models for a Point Sensor with One Switch Open

The consequence of opening switch S_1 is that the added capacitor, C_{load}, is now in series with the capacitor formed by area A_{21} of the copper foil tape, which in turn is in parallel with Leg 1 (Fig. 5.5 (b)). The total capacitance for this condition is given in Eq. 5.5.

$$C_{total} = C_{tag} + \left[\frac{1}{C_{22}} + \frac{1}{C_{11} + C_{12} + \left[\frac{1}{C_{21}} + \frac{1}{C_{load}} \right]^{-1}} \right]^{-1} \qquad (5.5)$$

Switch S_2 is shown in the open position in Fig. 5.6 (a) and the simplified circuit model for this condition in Fig. 5.6 (b). The added capacitor, C_{load}, plus the capacitance due to areas A_{11} and A_{21} of the copper foil tape are now removed from the circuit. The total capacitance of the circuit in this condition is given in Eq. 5.6.

$$C_{total} = C_{tag} + \left[\frac{1}{C_{12}} + \frac{1}{C_{22}} \right]^{-1} \qquad (5.6)$$
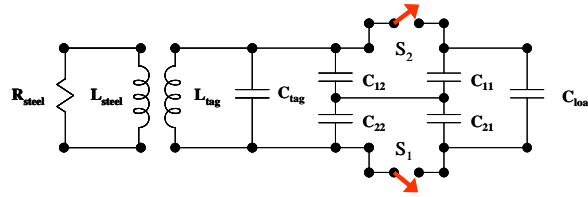
(a) Complete Electrical Circuit Model
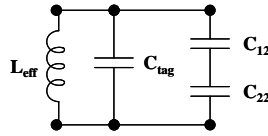
(b) Compressed Electrical Circuit Model

Figure 5.6 Electrical Circuit Models of a Point Sensor with Both Switches Open

5.3.4 Electrical Model for Distributed Sensor with One Added Capacitor

A circuit model for the distributed sensor with five pairs of copper strips (Fig. 5.1) and one added capacitor is shown in Fig. 5.7 (a). The EAS tag is modeled using L_{tag} and C_{tag} and the extra capacitor that is attached to the end of the switch is shown as C_{load}. The serpentine switch is modeled using a total of ten switches, representing each strip of copper foil tape that crosses the gap between the adhesive pads, and ten capacitors, representing the parallel-plate capacitors that form when the copper film tape is placed on the surface of the steel. Finally, the parasitic inductance of the steel plate is shown as L_{steel}. The capacitance of each leg of the serpentine switch, C_{ij}, is calculated using Eq. 5.3. A connection that links all legs of the serpentine switch is included in the circuit model to represent the influence of the steel to which the sensor is attached.
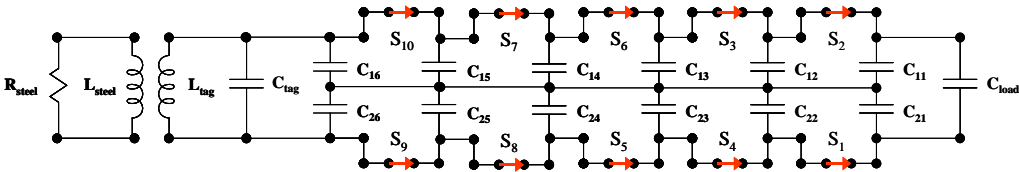
(a) Complete Electrical Circuit Model
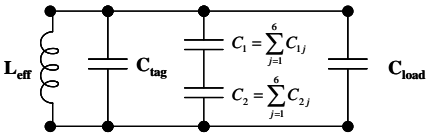
(b) Compressed Electrical Circuit Model

Figure 5.7 Electrical Circuit Models for a Distributed Sensor With Five Pairs of Copper Strips

The complete electrical circuit is simplified in Fig. 5.7 (b) by combining the inductance of the EAS tag and the parasitic inductance of the steel and adding the capacitance of each leg of the copper foil tape along each serpentine leg of the

82

switch. This circuit model can be further simplified by combining the capacitors into a single capacitor, C_{total}:

$$C_{total} = C_{tag} + \left[\frac{1}{\sum\limits_{j=1}^{6} C_{1j}} + \frac{1}{\sum\limits_{j=1}^{6} C_{2j}} \right]^{-1} + C_{load} \qquad (5.7)$$

(a) Circuit Model for Distributed Sensor When Switches Are Opened in Sequence

The circuit model for the distributed sensor will change as switches are opened. In this section, it is assumed that the switches open in sequence, which represents the initiation of a crack at one end of the distributed switch.

Switch S_1 is shown in the open position in Fig. 5.8 (a). The complete circuit model is otherwise identical to Fig. 5.3 (a). The physical location of Switch S_1 is shown in Fig. 5.1.
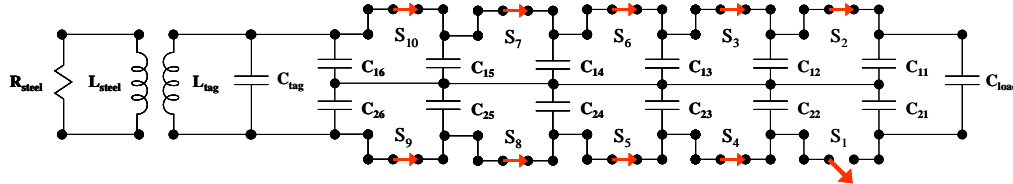
(a) Complete Electrical Circuit Model
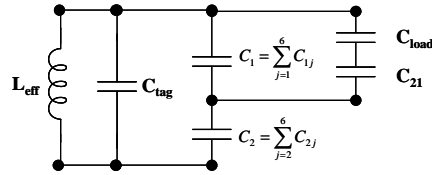
(b) Compressed Electrical Circuit Model

Figure 5.8 Electrical Circuit Models for a Distributed Sensor With Five Pairs of Copper Strips and One Switch Open

83

The consequence of opening switch S_1 is that the added capacitor, C_{load}, is now in series with the capacitor formed by area A_{21} of the copper foil tape, which in turn is in parallel with the capacitance of leg 2, C_2. The total capacitance, C_{total}, for this condition is given in Eq. 5.8.

$$C_{total} = C_{tag} + \left[\frac{1}{\sum_{j=1}^{6} C_{1j} + \left[\dfrac{1}{C_{load}} + \dfrac{1}{C_{21}} \right]^{-1}} + \frac{1}{\sum_{j=2}^{6} C_{2j}} \right]^{-1}$$ (5.8)

Switch S_2 is shown in the open position in Fig. 5.9 (a). The added capacitor, C_{load}, plus the capacitors due to areas A_{11} and A_{21} of the copper foil tape are now removed from the circuit. The simplified circuit model for this condition is shown in Fig. 5.9 (b). The total capacitance of the circuit in this condition may be calculated using Eq. 5.9.

$$C_{total} = C_{tag} + \left[\frac{1}{\sum_{j=2}^{6} C_{1j}} + \frac{1}{\sum_{j=2}^{6} C_{2j}} \right]^{-1}$$ (5.9)
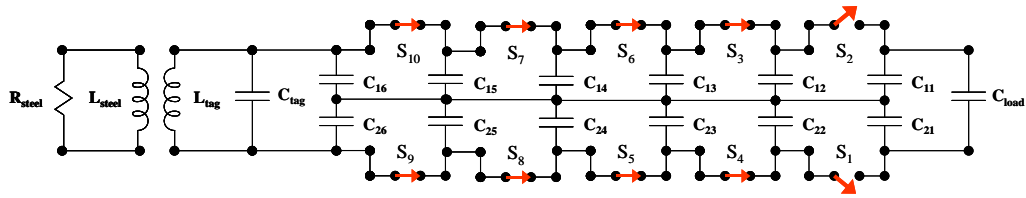
(a) Complete Electrical Circuit Model
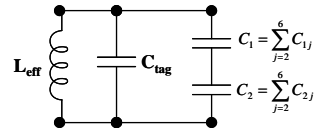
(b) Compressed Electrical Circuit Model

Figure 5.9 Electrical Circuit Models for a Distributed Sensor with Five Pairs of Copper Strips and Two Switches Open

When switch S_3 is opened, the capacitor due to area A_{12} of the copper foil tape is removed from the circuit (Fig. 5.10) and the total capacitance becomes:

$$C_{total} = C_{tag} + \left[\frac{1}{\sum\limits_{j=3}^{6} C_{1j}} + \frac{1}{\sum\limits_{j=2}^{6} C_{2j}} \right]^{-1} \tag{5.10}$$

(a) Complete Electrical Circuit Model

$$C_1 = \sum_{j=3}^{6} C_{1j}$$

$$C_2 = \sum_{j=2}^{6} C_{2j}$$
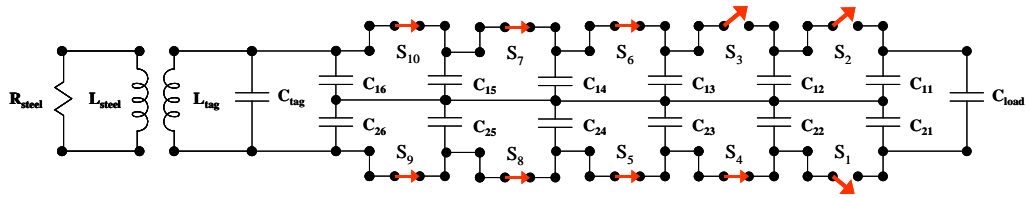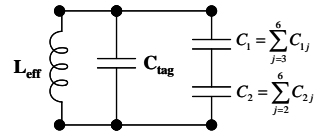
(b) Compressed Electrical Circuit Model

Figure 5.10 Electrical Circuit Models for a Distributed Sensor with Five Pairs of Copper Strips and Three Switches Open

Similarly, when switch S_4 is opened, the capacitance due to area A_{22} of the copper foil tape is removed from the circuit (Fig. 5.11) and the total capacitance becomes:

$$C_{total} = C_{tag} + \left[\frac{1}{\sum_{j=3}^{6} C_{1j}} + \frac{1}{\sum_{j=3}^{6} C_{2j}} \right]^{-1} \tag{5.11}$$

86

(a) Complete Electrical Circuit Model

$$C_1 = \sum_{j=3}^{6} C_{1j}$$

$$C_2 = \sum_{j=3}^{6} C_{2j}$$
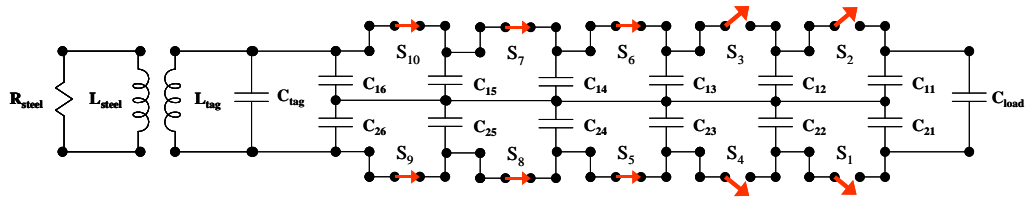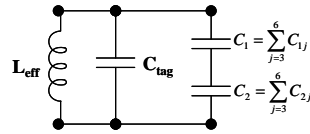
(b) Compressed Electrical Circuit Model

Figure 5.11 Electrical Circuit Models for a Distributed Sensor with Five Pairs of Copper Strips and Four Switches Open

This pattern repeats for the remaining switch locations until the total capacitance of the sensor is reduced to the capacitance of the EAS tag plus the two terminal end areas of the switch. As mentioned previously, the appropriate value of the total capacitance is used in Eq. 5.2 to calculate the resonant frequency of the sensor. Because the total capacitance changes each time a switch is opened, the frequency of the sensor will also change. Tests were conducted to determine if the length of a simulated crack could be identified using only the measured frequency of the sensor. Results of these tests are described in Section 5.5.3.

This electrical circuit model is easily adapted to accommodate distributed switches of varying lengths and provides a basis for evaluating the measured response of the sensor.

(b) Circuit Model for Distributed Sensor When Switches Are Opened in Random Order

The possibility also exists for a crack to form within the distributed switch, and electrical circuit models can be developed to represent this situation. The electrical model for the same distributed switch discussed in the previous section is shown in Fig. 5.12 (a), but now it is assumed that switch S_3 is the first switch opened.

The first simplification of this circuit is shown in Fig. 5.12 (b) where the capacitance of areas A_{11} and A_{12} of the copper foil tape have been combined and are shown in series with the added capacitor. A second simplification is shown in Fig. 5.12 (c) where the effective capacitance of the added capacitor and areas A_{11}, A_{12}, A_{21}, A_{22}, and A_{23} have been combined to form C_{eff}. C_{eff} is defined in Fig. 5.12 (d) and may be calculated as:

$$C_{eff} = \left(C_{23} + C_{22} + C_{21}\right) + \left[\frac{1}{C_{load}} + \frac{1}{C_{12} + C_{11}}\right]^{-1} \tag{5.12}$$

The total capacitance for this circuit is then defined as:

$$C_{total} = C_{tag} + \left[\frac{1}{C_{16} + C_{15} + C_{14} + C_{13}} + \frac{1}{C_{26} + C_{25} + C_{24} + C_{eff}}\right]^{-1} \tag{5.13}$$

If the crack propagates such that switch S_4 is opened next, then the total capacitance defaults to the case of switches opening in sequence, which was discussed in the previous section. If the crack propagates such that switch S_2 is opened next, then the model shown in Fig. 5.9 applies, but C_{eff} no longer depends on the capacitance of area A_{12} of the copper foil tape.
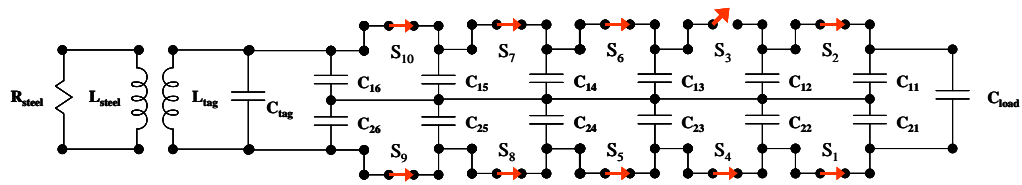
(a) Complete Electrical Circuit Model
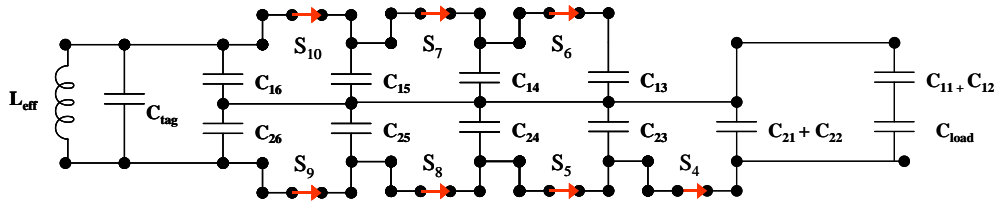
(b) First Simplification of the Electrical Circuit Model
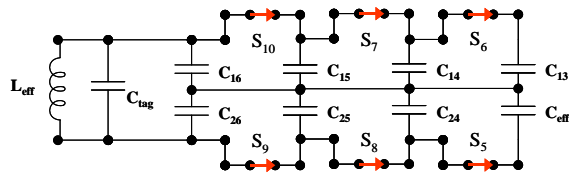
(a) Second Simplification of the Electrical Circuit Model
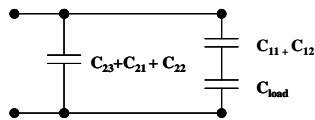
(d) Definition of C_{eff}

Figure 5.12 Electrical Circuit Model for a Distributed Sensor with Five Pairs of Copper Strips and Switch S_3 Opened First

5.3.5 Electrical Model for Distributed Sensor With Multiple Added Capacitors

A prototype distributed sensor was also developed with multiple added capacitors (Fig. 5.2). The electrical circuit model for this sensor is slightly different than that described in Section 5.3.4, which had a single added capacitor at one end of the switch. The electrical circuit model for the sensor with five pairs of copper strips and five added capacitors is shown in Fig. 5.13. It is assumed that each of the added capacitors has the same capacitance in this discussion, but capacitors with different capacitances could also be used.
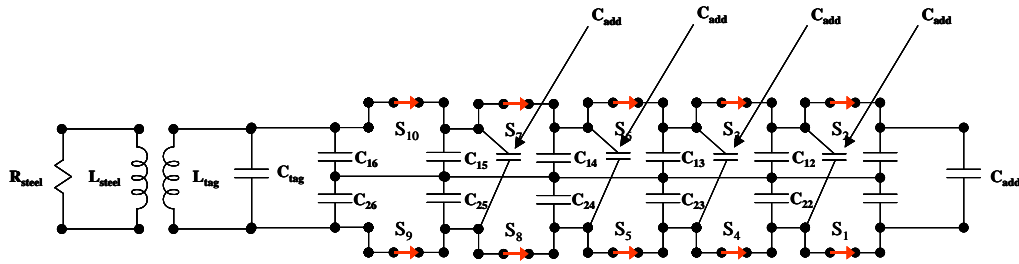
Figure 5.13 Electrical Circuit Model for a Distributed Sensor With Five Pairs of Copper Strips and Five Added Capacitors

The total capacitance of this circuit is similar to that shown in Fig. 5.7, but C_{load} is replaced with $5C_{add}$:

$$C_{total} = C_{tag} + \left[\frac{1}{\sum_{j=1}^{6} C_{1i}} + \frac{1}{\sum_{j=1}^{6} C_{2i}} \right]^{-1} + 5C_{add} \qquad (5.14)$$

Opening switch S_1 causes one of the added capacitors to be in series with C_{21}, resulting in a total capacitance of:

$$C_{total} = C_{tag} + \left[\frac{1}{\displaystyle\sum_{j=1}^{6} C_{1j} + \left[\frac{1}{C_{load}} + \frac{1}{C_{21}} \right]^{-1}} + \frac{1}{\displaystyle\sum_{j=2}^{6} C_{2j}} \right]^{-1} + 4C_{add} \qquad (5.15)$$

When switch S_2 is opened, C_{total} becomes:

$$C_{total} = C_{tag} + \left[\frac{1}{\displaystyle\sum_{j=2}^{6} C_{1j}} + \frac{1}{\displaystyle\sum_{j=2}^{6} C_{2j}} \right]^{-1} + 4C_{add} \qquad (5.16)$$

The total capacitance for the circuit when switch S_3 is opened becomes:

$$C_{total} = C_{tag} + \left[\frac{1}{\displaystyle\sum_{j=3}^{6} C_{1j}} + \frac{1}{\displaystyle\sum_{j=2}^{6} C_{2j} + \left[\frac{1}{C_{add}} + \frac{1}{C_{12}} \right]^{-1}} \right]^{-1} + 3C_{add} \qquad (5.17)$$

and when switch S_4 is opened, C_{total} becomes:

$$C_{total} = C_{tag} + \left[\frac{1}{\displaystyle\sum_{j=3}^{6} C_{1j}} + \frac{1}{\displaystyle\sum_{j=3}^{6} C_{2j}} \right]^{-1} + 3C_{add} \qquad (5.18)$$

This pattern is repeated as switches are opened in sequence. Similar electrical circuit models may be developed for the case when the switches are opened in random order, but that case was not investigated experimentally in this thesis.

91

5.3.6 Electrical Properties of a Sensor Inferred from the Measured Frequency Response

The transfer function of the circuit affects the coupling of the transmitter coil and the EAS tag; thus, the values obtained for impedance and phase angle in the circuit cannot be used to determine the resonant frequency. Therefore, a different feature of the impedance and phase angle curves was chosen to distinguish the characteristic frequency of the sensor. The characteristic frequency of the sensor was defined as the frequency corresponding to the minimum phase angle and inflection point of the impedance curve (Fig. 5.14). As will be demonstrated, Eq. 5.2 provides a reasonable estimate of the characteristic frequency.

The characteristic frequency depends on two parameters, the effective inductance of the circuit, L_{eff}, and the total capacitance, C_{total}. Neither of these quantities can be measured directly. As presented in Section 5.3.1, the effective inductance of a sensor depends on the inductance of the EAS tag, L_{tag}, and the parasitic inductance due to the steel, L_{steel}. Both values are assumed to be constant for a given sensor and will not change as switches are opened. Therefore, there is no need to estimate L_{tag} and L_{steel} individually; calculating L_{eff} from the measured frequency response is sufficient.
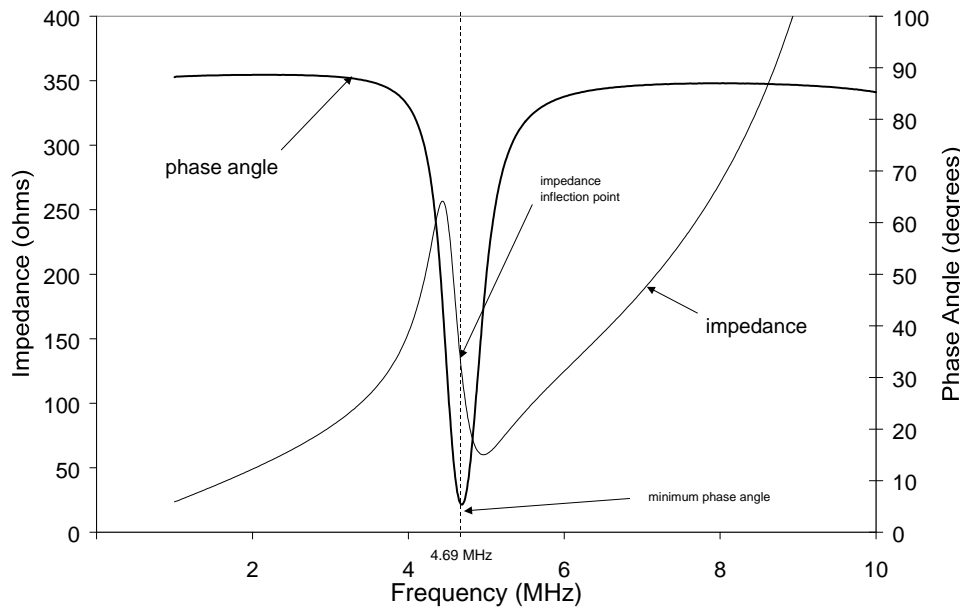
Figure 5.14 Frequency Response of EAS Tag with Point Switch Attached

In contrast, the total capacitance of the circuit depends on the state of the switches, as discussed in Sections 5.3.3 through 5.3.5. The capacitance of the EAS tag, C_{tag}, and the added capacitors, C_{load} or C_{add}, are known quantities. However, the capacitance of the parallel-plate capacitors that form when the copper foil tape is place on the surface of the steel, C_{ij}, depends on the dielectric parameter of the backing layer of adhesive tape, ε_r/t, defined in Section 5.3.2. The manufacturer of the carpet tape used to fabricate many of the prototype sensors did not report this information, so it was necessary to infer ε_r/t from the measured frequency response. Because the area of copper foil tape that contributed to the capacitance of the parallel-plate capacitors varies as switches are opened, a single distributed sensor will provide several data points from which ε_r/t can be inferred.

For a given switch configuration, the relationship between the effective inductance, L_{eff}, and the total capacitance, C_{total}, is given by:

93

$$L_{eff} = \frac{1}{C_{total}\left(2\pi f_{ch}\right)^2}$$ (5.19)

In the following discussion, it is assumed that the characteristic frequency of a distributed sensor with one added capacitor is measured as switches are opened in sequence beginning at switch S_1. Sensor states corresponding to all switches being closed and only switch S_1 being opened were not considered, in order to simplify the calculations.

Two arbitrary states of the sensor are considered, which are denoted a and b. The measured characteristic frequency is called f_a when the sensor is in state a, and the measured characteristic frequency is called f_b when the sensor is in state b. The corresponding values of total capacitance are C_a and C_b, respectively. Equation 5.21 may be rewritten as:

$$L_{eff} = \frac{1}{C_a\left(2\pi f_a\right)^2}$$ (5.20)

$$L_{eff} = \frac{1}{C_b\left(2\pi f_b\right)^2}$$ (5.21)

for sensor states a and b. Because the effective inductance does not depend on the state of the sensor, Eq. 5.20 and 5.21 may be rewritten as:

$$C_a f_a^{\,2} = C_b f_b^{\,2}$$ (5.22)

Because the states of all switches being closed and only switch S_1 being opened have been eliminated from consideration, the total capacitance for sensor states a and b may be expressed as:

$$C_{total} = C_{tag} + C_{cap}$$ (5.23)

which is a simplified version of Eq. 5.9 through 5.11, where C_{cap} represents the capacitance of the copper foil tape. As discussed in Section 5.3.2, the capacitance of the copper foil tape is related to the surface area, A_{cap}:

94

$$C_{cap} = \frac{\varepsilon_o \varepsilon_r}{t} A_{cap} \tag{5.24}$$

The total capacitance for sensor states a and b can therefore be expressed as:

$$C_a = C_{tag} + \frac{\varepsilon_o \varepsilon_r}{t} A_a \tag{5.25}$$

$$C_b = C_{tag} + \frac{\varepsilon_o \varepsilon_r}{t} A_b \tag{5.26}$$

Substituting the relationships for the total capacitance for sensor states a and b into Eq. 5.22 yields the following expression which contains one unknown parameter, the dielectric parameter of the backing tape, ε_r/t:

$$\frac{\varepsilon_o \varepsilon_r}{t}\left(A_a f_a^{\,2} - A_b f_b^{\,2}\right) = C_{tag}\left(f_b^{\,2} - f_a^{\,2}\right) \tag{5.27}$$

Solving for the dielectric constant yields:

$$\frac{\varepsilon_r}{t} = \frac{C_{tag}\left(f_b^{\,2} - f_a^{\,2}\right)}{\varepsilon_o\left(A_a f_a^{\,2} - A_b f_b^{\,2}\right)} \tag{5.28}$$

If the switches are opened in sequence and sensor state b corresponds to a state with more open switches than sensor state a, then A_a will be larger than A_b and f_b will be larger than f_a. Therefore, calculated values of ε_r/t will be positive if more switches are open in sensor state b than sensor state a.

Assuming that t is constant, then ε_r/t may be calculated from Eq. 5.28. If a distributed sensor is fabricated with a total of n switches and a single added capacitor is included in the circuit, then m combinations of sensor states may be used to calculate ε_r/t:

$$m = \frac{(n-1)!}{2(n-3)!} \tag{5.29}$$

where m is equal to the number of combinations of $(n - 1)$ sensor states taken in pairs. The number of combinations is based on $(n - 1)$ rather than n because the

95

sensor state corresponding to only switch S_1 being open was not considered in this analysis.

For each of the distributed sensors, a value of ε_r/t was calculated for each of the m combinations of sensor states. The mean value of ε_r/t was then used in all subsequent calculations for that sensor. Values of ε_r/t inferred from distributed sensors with three through thirteen pairs of copper strips are presented in Section 5.5.5. For a given sensor, the values of ε_r/t did exhibit scatter, but the average values did not vary appreciably.

Once the average dielectric parameter was determined for a given sensor, the effective inductance could be calculated. Because of the scatter in the measured frequencies and the dielectric parameter, the calculated values of L_{eff} for each sensor state exhibited a moderate amount of scatter; therefore the mean value of L_{eff} was used in subsequent calculations.

5.4 OVERVIEW OF TESTS OF PROTOTYPE SENSORS

The frequency response of sixteen prototype sensors was measured during this phase of the investigation. The overall objective of these tests was to determine if the electrical circuit models discussed in Section 5.3 represent the measured response of the prototype sensors. Three different sensor designs were tested: four point sensors (Fig. 5.3), eleven distributed sensors with a single added capacitor (Fig. 5.1), and one distributed sensor with multiple added capacitors (Fig. 5.2).

The point sensors were tested to verify that discrete and measurable changes in the characteristic frequency would occur when the switch was opened. This property is fundamental to the success of the sensor. It is envisioned that the frequency would be measured during construction of the building immediately

after the sensor is installed. After an earthquake, the characteristic frequency would be measured again. Provided that the switch did not bridge over a crack (as discussed in Chapter 4), the measured frequency after the earthquake would indicate if a crack had formed under the sensor. If the characteristic frequency measured after the earthquake was the same as the characteristic frequency measured before the earthquake, then the welded connection is intact. If the measured frequency after the earthquake exceeds the measured frequency before the earthquake, then the welded connection is cracked. It is important that the difference in frequencies between these two states is sufficiently different that the sensor reading provides a clear indication of the state of the switch. The size of the added capacitor was selected such that the characteristic frequency with the switch open was approximately twice the characteristic frequency with the switch closed.

The distributed sensors were tested to determine if the length of a crack could be determined from changes in the characteristic frequency. In most of the tests, a single capacitor was added to the circuit and the copper strips were opened in sequence as modeled in Section 5.3.4 (a). The data from these tests were used to calculate the two unknown electrical properties, L_{eff} and ε_r/t, and were used to evaluate the electrical circuit model. Six sensors, with three, five, seven, nine, ten, eleven, and thirteen pairs of copper foil strips, were tested. Four additional sensors with five pairs of copper foil strips were also tested by arbitrarily selecting the first switch opened, as modeled in Section 5.3.4 (b). These tests were included because the crack may not form at the end of the sensor and propagate in one direction. One distributed sensor with ten pairs of copper foil strips and ten added capacitors was also tested by opening the switches in sequence (Section 5.3.5) because the change in frequency each time a pair of switches was opened was expected to be larger.

5.4.1 Physical Characteristics of the Prototype Sensors

All sensors tested in this phase of the investigation were constructed using the procedures described in Appendix A. Double-sided carpet tape was used as the backing layer for the adhesive pads and clear packing tape was used for the top layer. The gap between adhesive pads was 1/4-in. for all switches.

The wires that were attached to an EAS tag were soldered to one set of terminals and a capacitor was soldered across the other set. Different EAS tags were used for each sensor, and the characteristic frequency of the EAS tags tended to vary between 8.0 and 8.4 MHz. When a single capacitor was added to the switch circuit, a 200 pF unit was used. When multiple capacitors were used in the sensor with ten pairs of switches, each had a capacitance of 22 pF. The exposed copper terminals were insulated with Scotch™ transparent tape to avoid contact with the underlying steel plate.

All switches were fabricated using strips of copper foil tape with the same nominal dimensions, as described in Appendix A. The area of each strip must be known to determine the parallel-plate capacitance attributable to the switches. Referring to Fig. 5.1 and 5.2, the nominal areas, A_{ij}, were measured to be:

- Tapered terminal sections (A_{11} and A_{26}) = 423 mm^2
- Rectangular terminal sections (A_{21} and A_{16}) = 585 mm^2
- Outer loops (A_{22}, A_{13}, A_{24}, and A_{15}) = 323 mm^2
- Inner loops (A_{12}, A_{23}, A_{14}, and A_{25}) = 202 mm^2

These values were assumed to be the same for all distributed switches. In reality, because these switches were fabricated by hand, variation in these quantities is expected. Also, these areas are calculated assuming that the switches were cut at consistent locations. The variation due to these assumed values is investigated in Section 5.5.3 (d).

A summary of the physical dimensions of each distributed sensor is given in Table 5.1 and shown in Fig. 5.15. The individual sensors are identified by the number of pairs of copper foil strip switches (3P thought 13P).

Table 5.1 Summary of Physical Dimensions of Distributed Sensors

number of switch pairs	length of switch (in.)	length of serpentine leg (in.)
3P	1.50	19.5
5P	2.75	29.0
7P	4.00	39.5
9P	5.25	49.5
10P	5.88	54.5
11P	6.50	59.5
13P	7.75	69.5

length of serpentine leg (in.)

length of switch (in.)
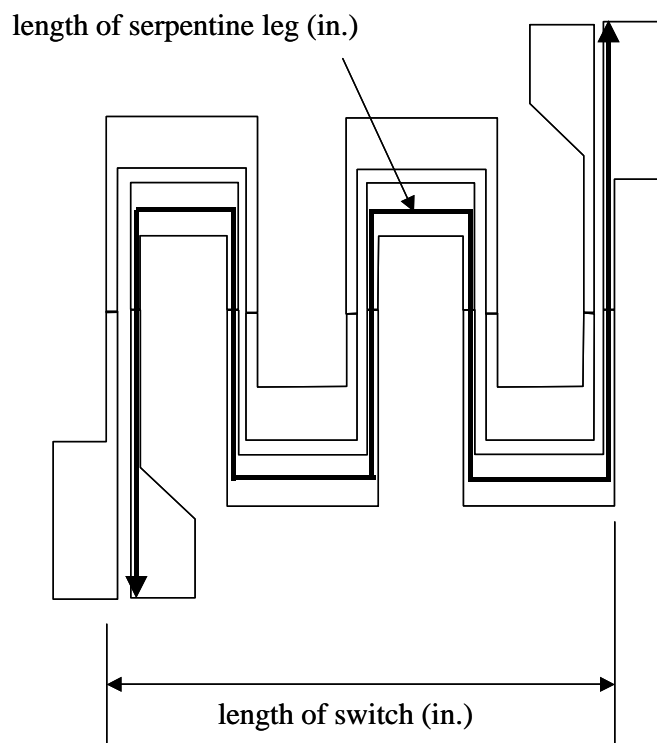
Figure 5.15 Dimensions of Distributed Sensor

5.4.2 Procedures Used to Record the Frequency Response of the Prototype Sensors

Each sensor was excited using a frequency sweep between 1 and 10 MHz. As discussed in Chapter 2, a transmitting antenna was used to drive the total inductance and capacitance of the sensor. Impedance and phase angle data were collected during the tests described in this chapter. The characteristic frequency was taken as the frequency corresponding to the minimum phase angle and the inflection point in the relationship between impedance and driving frequency.

A 4194A HP Impedance/Gain-Phase Analyzer was used to drive the transmitting antenna and acquire the impedance and phase angle data. The transmitting antenna was constructed by wrapping copper wire around a plastic spool, which was sized such that the EAS tag fit within the spool (Fig. 5.16). The cable connecting the antenna to the phase analyzer was selected to minimize the possibility of the resonant frequency of the cable influencing the measured data. The data were acquired using LabView software and later manipulated in a spreadsheet program.
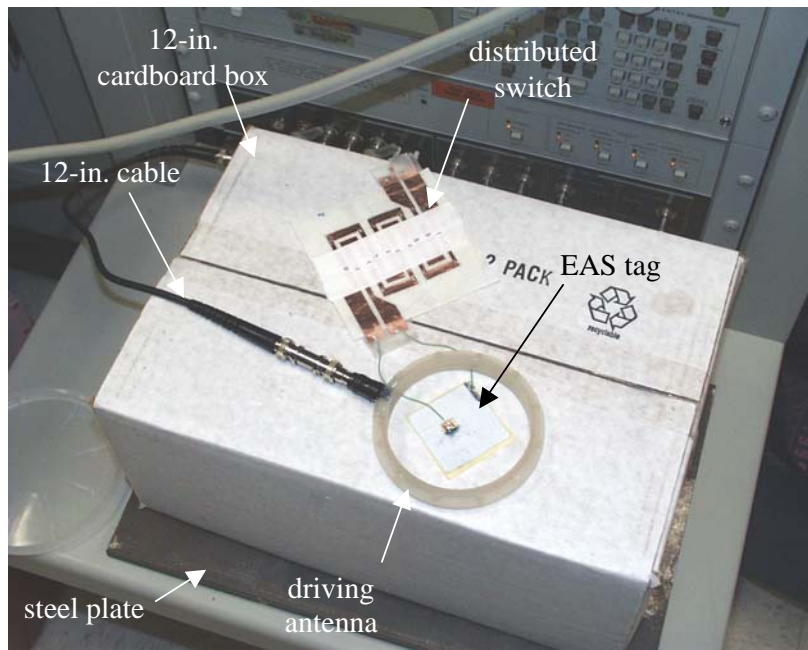
Figure 5.16 Infinity Position for a Distributed Sensor

The frequency response of the prototype sensors does change with the sensor is attached to steel, because the effective inductance is reduced and the total capacitance increases. Therefore, two extreme conditions were considered. The switch was positioned on a 12 by 24-in. 1/2-in. thick steel plate and held in place using a non-conductive weight to simulate field conditions. In one extreme, the entire sensor was supported 12 in. off the surface of the steel plate by a cardboard box (Fig. 5.16). In most cases, the EAS tag was supported 1 cm above the surface of the place, such that the parasitic inductance did not dominate the response (Fig. 5.17). The parasitic inductance and parallel-plate capacitance were essentially zero in this case. These two conditions will be called "field" and "infinity," respectively, in the following discussions.
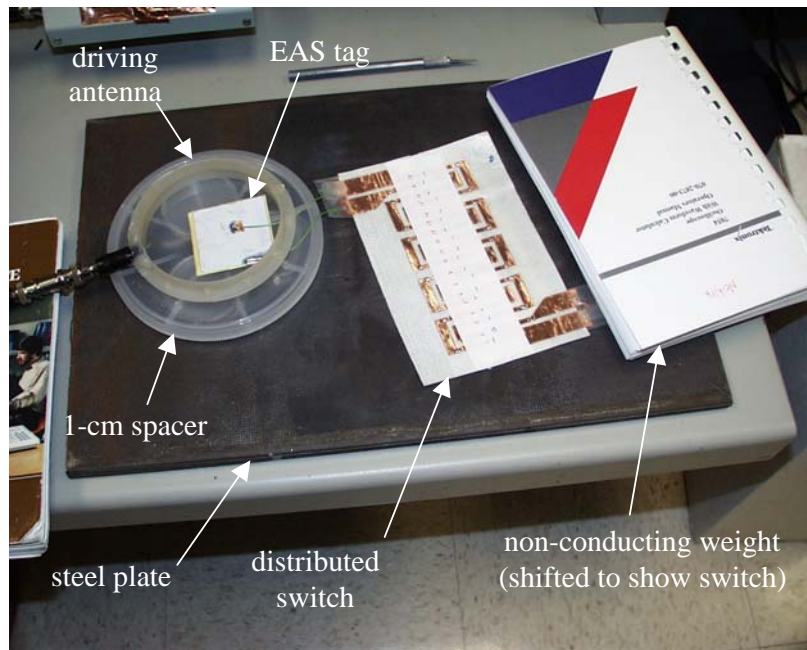
Figure 5.17 Field Position for a Distributed Sensor

During a test in which the copper foil strips were opened in sequence, the following procedure was used. Impedance and phase angle data were recorded at each step.

- Intact sensor is placed in infinity position
- Intact sensor is placed in field position
- Copper foil strip 1 is cut (S_1 opened) to simulate the formation of a crack
- Copper foil strip 2 is cut (S_2 opened) to simulate the propagation of the crack
- Strips are cut in sequence, until all are opened
- Sensor with all strips cut is placed in infinity position

The same basic procedure was used when the copper foil strips were opened in a random order; however, only two strips were cut during the test.

Referring to Fig. 5.1, one of the odd switches, S_i, was opened first, then switch S_{i+1} was opened.

5.5   MEASURED FREQUENCY RESPONSE

The measured frequency response of the fifteen prototype sensors is described in this section. The measured response is also compared with the characteristic frequencies calculated using the electrical circuit model described in Section 5.2. The response of a single point sensor is discussed in 5.5.1, the measured relationships among impedance, phase angle, and driving frequency are presented, and the influence of the parasitic inductance caused by positioning the EAS tag too close to the surface of the steel plate is summarized. These trends are representative of all of the prototype sensors. The response of four point sensors is described in Section 5.5.2, the response of ten distributed sensors with a single added capacitor is described in Section 5.5.3, and the response of a distributed sensor with multiple added capacitors is described in Section 5.5.4.

5.5.1   Variations in Impedance and Phase Angle with Driving Frequency

One of the four point sensors was used to investigate the variations in impedance and phase angle with the driving frequency and the influence of the parasitic inductance on the response. As discussed previously, preliminary tests had indicated that the EAS tag must be separated from the surface of the steel by at least 1 cm in order to obtain the desired response of the sensor. Data representing a 1-cm separation are plotted in Fig. 5.18. The phase angle exhibits a well-defined minimum at a driving frequency of 4.89 MHz and this frequency corresponds to the inflection point in the impedance response. The minimum phase angle is easily distinguished, so it is not necessary to refine the electrical circuit model.

In contrast, the response of the same sensor is shown in Fig. 5.19, but the EAS tag is supported 1 mm from the surface of the steel. Two differences in the response are immediately apparent: the local minimum in the phase angle response is much less pronounced and the characteristic frequency has increased to 6.78 MHz. Therefore, the parasitic inductance has a significant influence on the response of the sensor. If the EAS tag is located too close to the surface of the steel, then it will be difficult to detect the characteristic frequency of the sensor, but if the EAS tag is too far from the switch, it will be more difficult to install in the field and will be more susceptible to damage during construction. Thus, the EAS tags were elevated 1 cm from the surface of the steel in all subsequent tests.
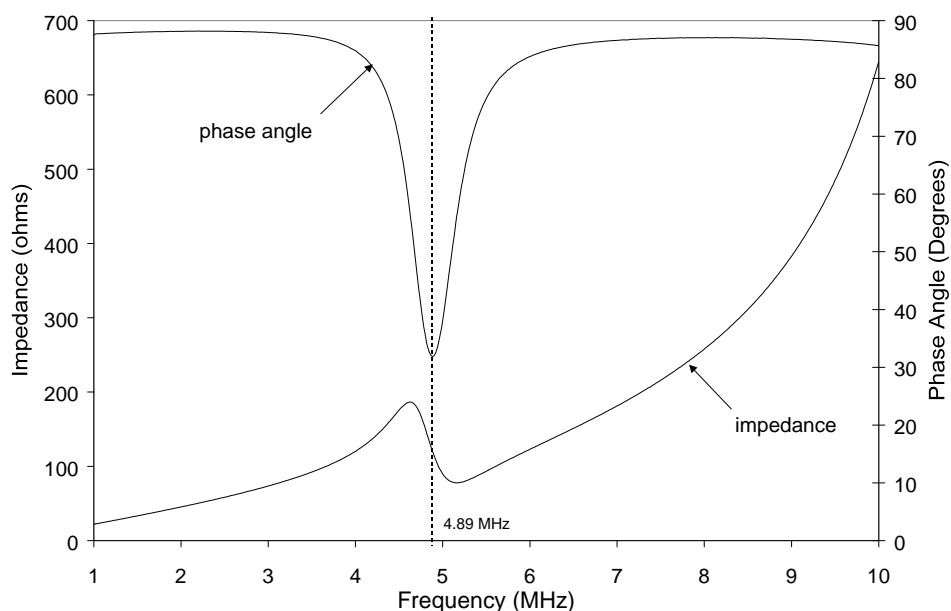
Figure 5.18 Frequency Response of a Point Sensor When the EAS Tag is 1 cm from the Surface of the Steel
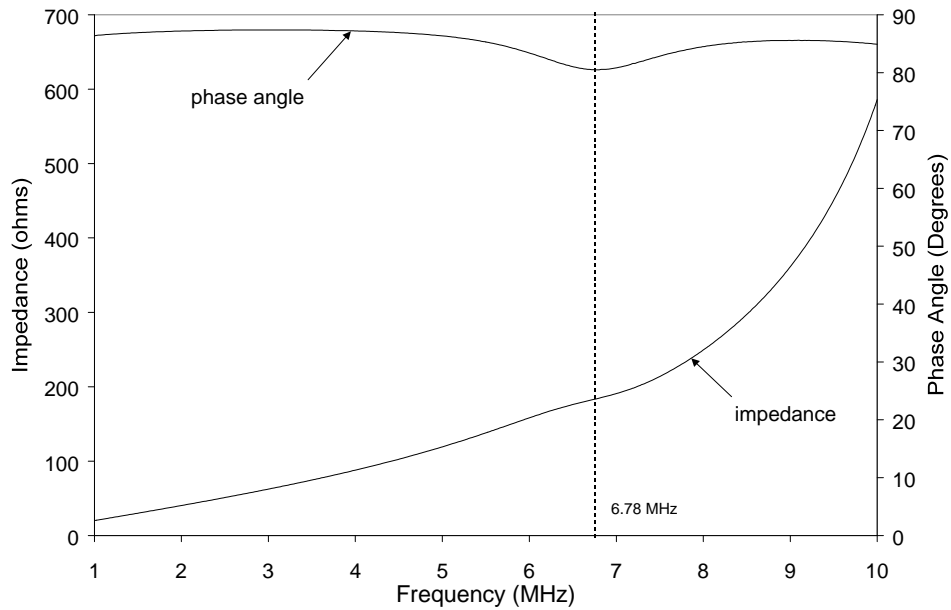
Figure 5.19 Frequency Response of a Point Sensor When the EAS Tag is 1 mm from the Surface of the Steel

5.5.2   Response of Point Sensors

Four point sensors were tested using the procedures described at the beginning of Section 5.5, and the characteristic frequencies were identified using the procedures described in the previous section. The data are presented in Table 5.2

Table 5.2 Measured Frequency Response of Point Sensors

Distance to Steel Plate (in.)	Last Switch Opened	Characteristic Frequency (MHz)			
		Sensor 1	Sensor 2	Sensor 3	Sensor 4
12	0	4.69	4.65	4.49	4.58
0	0	4.89	4.80	4.47	4.78
0	1	8.20	8.20	7.73	8.47
0	2	8.45	8.49	8.04	8.63
12	2	8.13	8.13	8.27	8.09

When the EAS tag is separated from the steel surface by 1 cm, the change in frequency due to the parasitic inductance and parallel-plate capacitors is modest. The characteristic frequency of three of the four point sensors increased slightly when the intact sensor was placed on the steel plate and decreased slightly at the end of the test when the sensor was elevated from the surface of the plate. Point Sensor 3 exhibited the opposite trends, most likely due to a lower inductance in the attached EAS tag.

The measured frequencies of the intact point sensors at the infinity position were lower than 4.6 MHz, the resonant frequency for an intact sensor not in contact with a steel surface (Section 2.2.4). The measured frequencies of the opened sensors at the infinity position were higher than the calculated 8 MHz (Section 2.2.4). The difference between the calculated and the measured frequencies for the intact point sensors at infinity was at most 2.3% and for the opened sensors at most 3.4%.

As expected, the characteristic frequency of the sensors increased dramatically when the first switch was opened: approximately 4.7 MHz to approximately 8.1 MHz. The characteristic frequencies did not change appreciably when the second switch was opened. The characteristics frequencies of the individual sensors at a given switch state did vary slightly. These differences could be due to the variations in the EAS tags, quality of the soldered connections, dimensions of the strips of copper foil tape used to fabricate the switch, or capacitance of the added capacitors. The frequency differences among the sensors were small compared with the differences in frequency before and after the first switch was opened. Therefore, the data from these four point sensors provided proof of the concept that an EAS tag with an external switch can provide information about the state of a welded steel connection.

5.5.3 Response of Distributed Sensors With One Added Capacitor

The distributed sensors were originally developed to increase the area over which a crack could be detected. A secondary objective of determining the extent of crack propagation from the characteristic frequency was later developed. In order to accomplish this second objective, the effective inductance and the total capacitance of the sensor must be determined. The two unknown parameters, ε_r/t and L_{eff}, can be inferred from the measured characteristic frequencies as discussed in Section 5.3.6.

The measured characteristic frequency data for the tests in which the switches were opened sequentially will be presented first, then the unknown electrical parameters will be inferred from the measured data. Average values of L_{eff} and ε_r/t will then be used in the electrical circuit models, and the calculated response will be compared with the measured characteristic frequencies. The measured frequency data for tests in which an arbitrary switch is opened first will be presented. Finally, the amount of variation in the assumed values of A_{ij} is investigated.

(a) Measured Frequency Response When Switches Are Opened in Sequence

A total of seven distributed sensor were tested during this stage of the investigation. The number of pairs of copper strips varied from three to thirteen. The characteristic frequencies were measured at each distributed switch state for each sensor, and the complete set of data is reported in Section B.1. The data are summarized in Table 5.3. The individual sensors are identified by the number of pairs of copper foil strip switches (3P thought 13P).

*Table 5.3 Measured Frequency Response of Distributed Sensors with One
Added Capacitor*

Distance to Steel Plate (in.)	Last Switch Opened *	Characteristic Frequency (MHz)						
		3P	5P	7P	9P	10P	11P	13P
12	0	4.33	4.47	4.53	4.31	4.49	4.49	4.49
0	0	4.35	4.47	4.56	4.08	4.36	4.42	4.42
0	1	7.44	7.14	7.53	6.31	6.58	6.69	6.74
0	all	8.09	8.27	8.76	8.09	8.45	8.49	8.76
12	all	8.16	8.22	8.22	8.25	8.10	8.02	8.18

* switches were opened in sequence

The basic trends in the measured frequencies of the distributed sensors are essentially the same as those observed for the point sensors (Fig. 5.20): the measured frequencies at the infinity conditions were lower than expected for the intact sensor and higher for the opened sensor, an appreciable change in the characteristic frequency was observed when the first switch was opened, and the characteristic frequency continued to increase as the other switches were opened. The variation of the characteristic frequency with the switch state is discussed in Section 5.5.3 (c). The characteristic frequencies did not appear to be sensitive to the length of the distributed sensor.

The measured frequencies of the intact distributed sensors at the infinity position were lower than 4.6 MHz, the resonant frequency for an intact sensor not in contact with a steel surface (Section 2.2.4).   The measured frequencies of the opened sensors at the infinity position were higher than the calculated 8 MHz (Section 2.2.4).   The largest discrepancies between the calculated and the measured frequencies for the point sensors at infinity were from the sensor with nine pairs of switches: 6.3% for the intact switch and 3.1% for the fully opened switch.
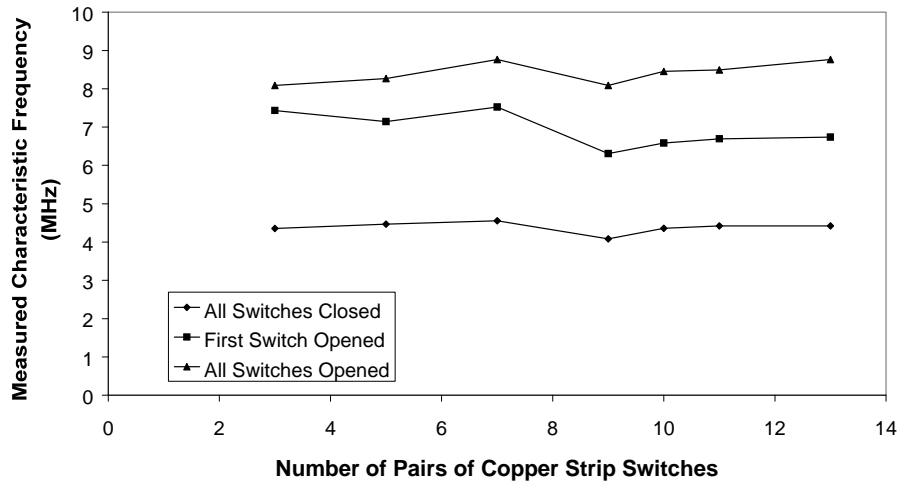
Figure 5.20 Measured Characteristic Frequencies of Distributed Sensors with One Added Capacitor

(b) Electrical Properties of the Distributed Sensors

Two electrical properties, L_{eff} and ε_r/t, must be inferred from the measured characteristic frequencies before the adequacy of the circuit models can be evaluated. As discussed in Section 5.3.6, the dielectric parameter, ε_r/t, can be calculated from any pair of measured characteristic frequencies corresponding to different switch states using Eq. 5.29.

The complete matrices of calculated values for ε_r/t are presented in Tables B.8 through B.14 in Appendix B. A summary of this information is presented in Table 5.4, where the sensors are identified by the number of pairs of switches (3P through 13P). The raw data are characterized by scatter (Fig. 5.21). As will be discussed later, the scatter in the data is attributed to the poor quality of the soldered connections between the aluminum foil in the EAS tag and the attached copper foil terminals.

The data were reduced in order to obtain reasonable values for the dielectric constant. First, the mean and standard deviation of the raw data were calculated. All data points that exceeded the mean plus two standard deviations and were less than zero were eliminated from consideration. The mean and standard deviations of the remaining data were again calculated, and all data outside the range of the mean plus and minus two standard deviations were eliminated from consideration. The remaining data are called the reduced data in Table 5.4 and are plotted in Fig. 5.22. In addition, the data that were eliminated in this data reduction process are shown in shaded cells in Tables B.8 through B.14.

Table 5.4 Summary of Dielectric Parameters Inferred from the Measured Characteristic Frequencies

		Dielectric Parameter, ε_r/t						
		3P	5P	7P	9P	10P	11P	13P
Raw Data	Number of Pairs of Switch States	10	36	78	136	171	210	300
	Maximum	8885	13390	62878	65398	55927	22960	106288
	Mean	4672	6337	5895	6747	7663	5402	6405
	Minimum	-5818	3522	-1212	1745	-3049	-28756	-1705
	Standard Deviation	3874	1862	6807	5304	6115	3535	6444
	Coefficient of Variation	83%	29%	115%	79%	80%	65%	101%
Reduced Data	Number of Pairs of Switch States	8	33	72	126	154	191	280
	Maximum	6664	8651	8323	9346	10039	8257	10672
	Mean	5456	5924	5258	6177	6528	5326	5740
	Minimum	4972	3522	1742	3278	2825	3198	1263
	Standard Deviation	583	1177	1466	999	1203	898	1655
	Coefficient of Variation	11%	20%	28%	16%	18%	17%	29%
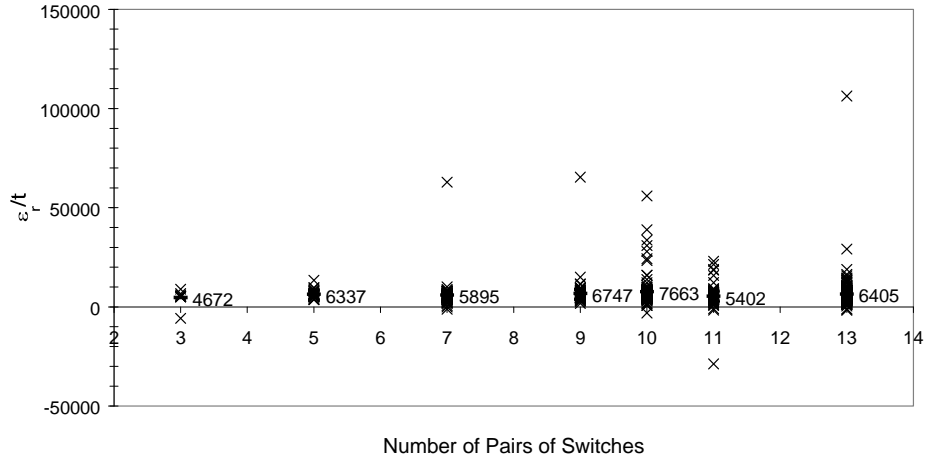
Figure 5.21 Range of Dielectric Parameters Calculated Using the Raw Data
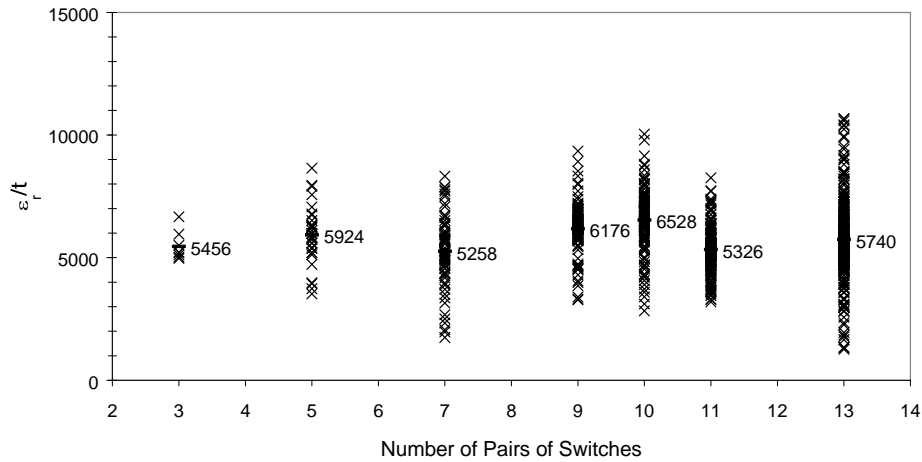
Figure 5.22 Range of Dielectric Parameters Calculated Using the Reduced Data

For most sensors, more than 90% of the potential pairs of switch states were used to calculate the dielectric parameters, and the mean values did not vary appreciably with the length of the distributed sensor.

111

The effective inductance, L_{eff}, was inferred using the mean value of ε_r/t to calculate the parallel-plate capacitance (Eq. 5.24) and in turn the total capacitance (Eq. 5.23) at each switch state for each distributed sensor. The effective inductance was then calculated using Eq. 5.19. The average, standard deviation, and coefficient of variation were calculated for each sensor. Because of the variation in the measured frequency data, there was also some variation in the value of L_{eff} between switch states for each sensor. Table 5.5 summarizes the variability of L_{eff} for the distributed sensors using the mean value of ε_r/t. The data are presented in Fig. 5.23 and given Tables B.15 through B.21 in Appendix B.

Table 5.5 Summary of Effective Inductance Inferred from the Mean Value of the Reduced Data Dielectric Parameter

		Pairs of Switches						
		3P	5P	7P	9P	10P	11P	13P
L_{eff} (μH)	Average	3.57	3.34	2.97	3.46	3.10	3.18	2.87
	Standard Deviation	0.18	0.09	0.12	0.15	0.09	0.06	0.10
	Coefficient of Variation	5%	3%	4%	4%	3%	2%	3%
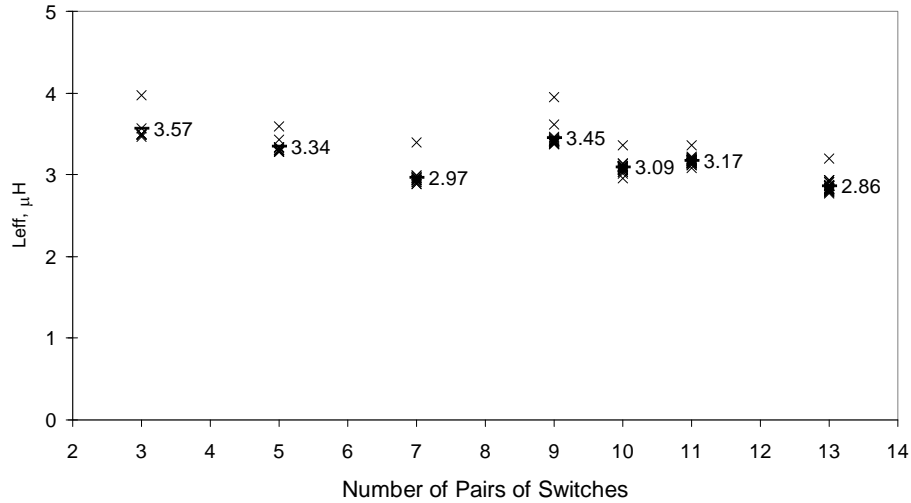
Figure 5.23 Range of Effective Inductance Calculated Using the Mean Value of the Reduced Data Dielectric Parameter

The highest value of L_{eff} occurred in the sensor with three pairs, 3.57 μH, and the lowest value occurred in the sensor with 13 pairs, 2.86 μH. However, no general trend in the average values of L_{eff} is discernable. The coefficient of variation for each sensor was very low, typically less than 5%. These different average values calculated for the effective inductance for each sensor are acceptable, because of the variation in electrical properties of the EAS tags.

(c) Comparison of Calculated Frequency Response Using the Electrical Circuit Model and Measured Characteristic Frequencies

The average values of the electrical constants calculated in the previous section were then used with the electrical circuit models developed in Section 5.3.3 to calculate the frequency response of the sensor at each switch state. The calculated results are plotted using a broken line in Fig. 5.24 through 5.30.

113

In general, the electrical circuit model represented the observed trends in the characteristic frequency very well. However, a few discrepancies were observed consistently.

The electrical circuit model overestimates the characteristic frequency of each sensor when the intact sensor is positioned on the steel plate. The differences between the measured and calculated characteristic frequencies were less than 7%. The sensor with eleven pairs of switches exhibited the lowest discrepancy, 2.9%, and the sensor with nine pairs of switches exhibited the highest discrepancy, 6.8%.

Once the first switch was opened, the electrical circuit model indicates a steady, gradual increase in the characteristic frequency. The measured data followed this trend, but exhibited more scatter. Two possible reasons for this discrepancy is discussed in Section 5.6.
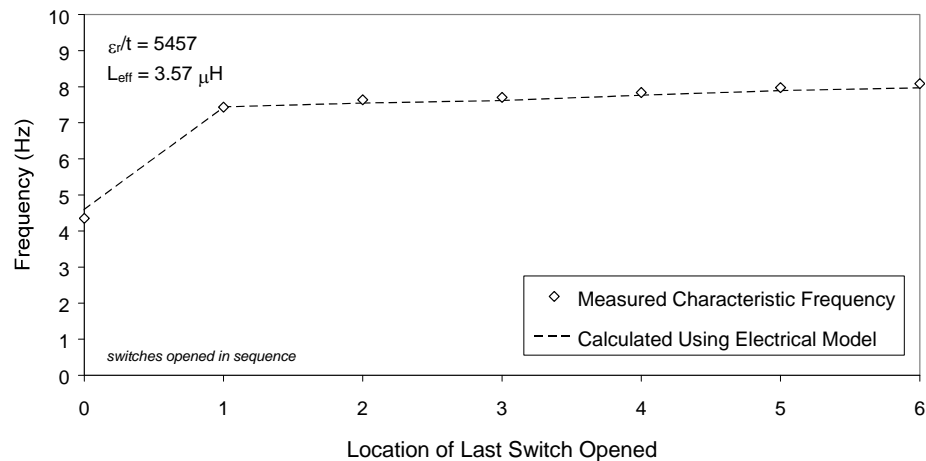
Figure 5.24 Frequency Response of Distributed Sensor with Three Pairs of Switches and One Added Capacitor
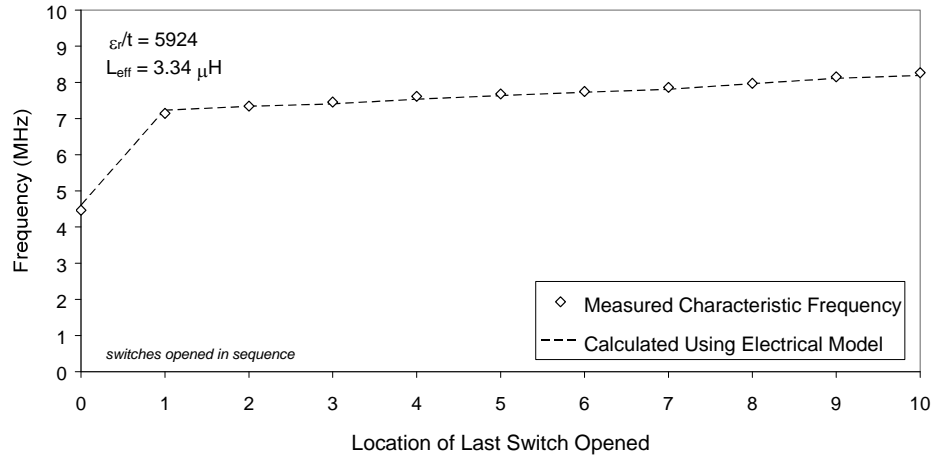
Figure 5.25 Frequency Response of Distributed Sensor with Five Pairs of Switches and One Added Capacitor
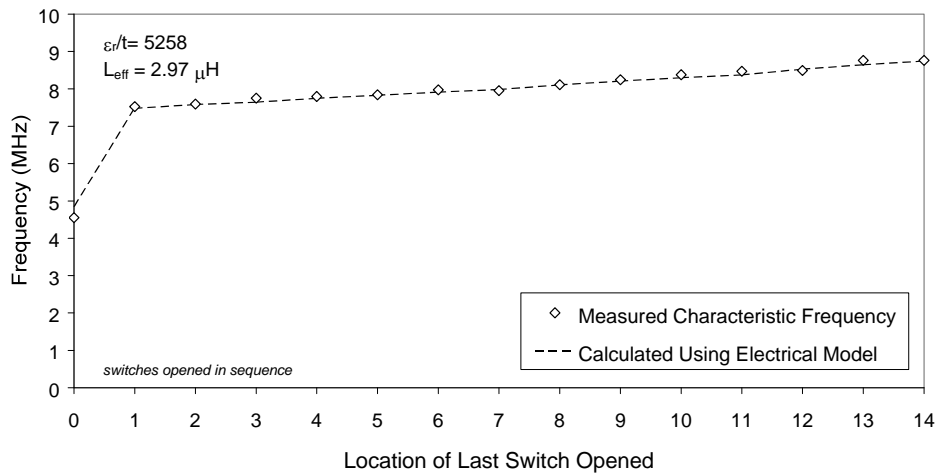
Figure 5.26 Frequency Response of Distributed Sensor with Seven Pairs of Switches and One Added Capacitor
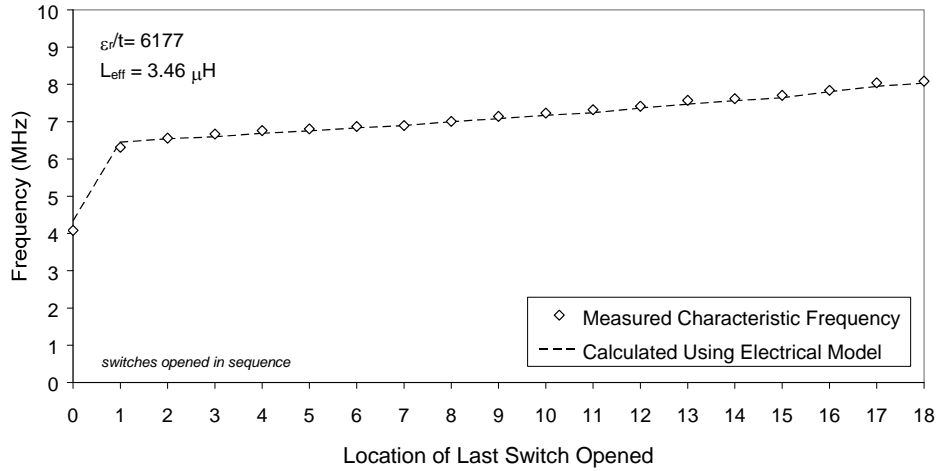
***Figure 5.27 Frequency Response of Distributed Sensor with Nine Pairs of
Switches and One Added Capacitor***
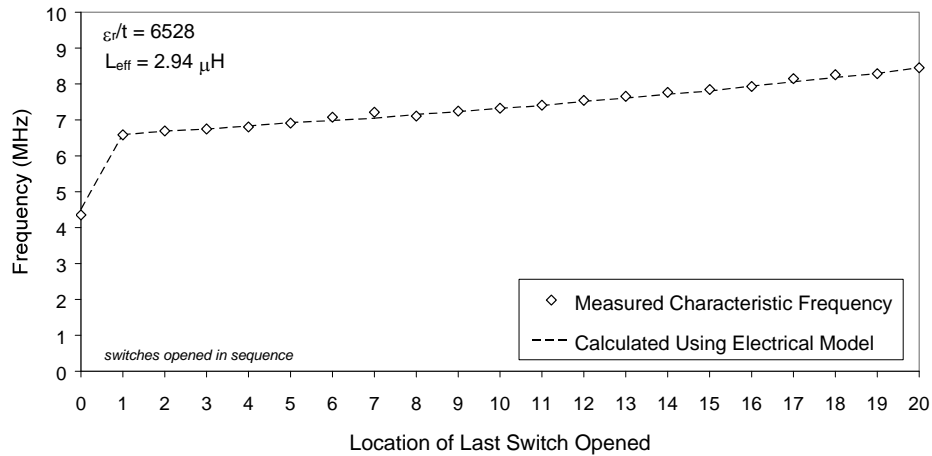
***Figure 5.28 Frequency Response of Distributed Sensor with Ten Pairs of
Switches and One Added Capacitor***
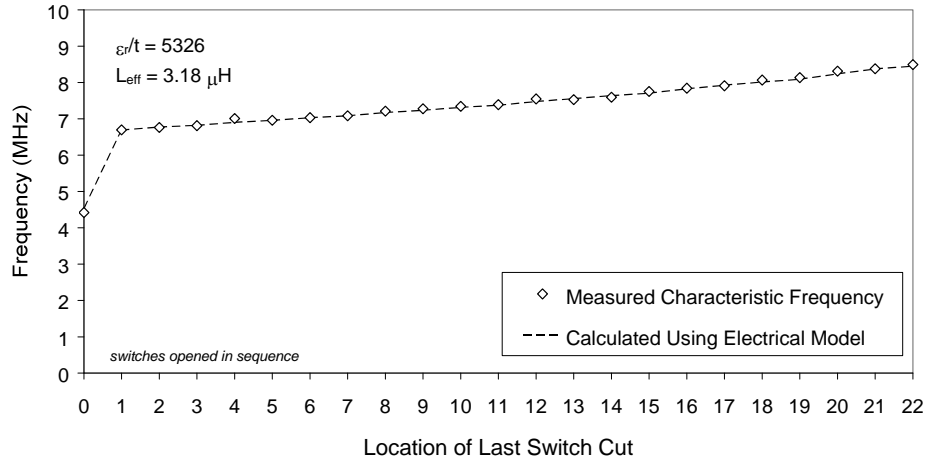
Figure 5.29 Frequency Response of Distributed Sensor with Eleven Pairs of Switches and One Added Capacitor
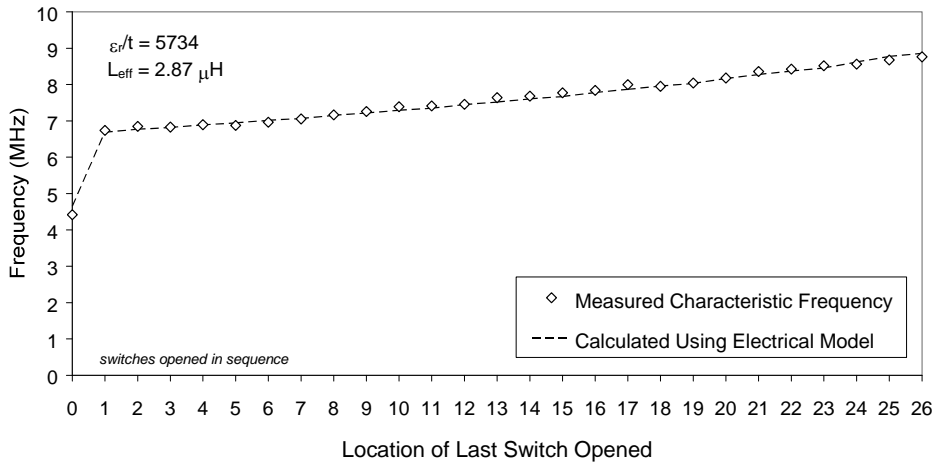
Figure 5.30 Frequency Response of Distributed Sensor with Thirteen Pairs of Switches and One Added Capacitor

(d) Measured Frequency Response When the Location of the Initial Open Switch is Varied

Four additional distributed sensors with five pairs of copper foil strips were fabricated and tested to determine if the change in characteristic frequency associated with opening the switches provided sufficient information to identify the initiation point of the crack. This information would be useful to distinguish those cracks that had propagated the entire length of the sensor from those that had not. The electrical circuit model used to evaluate data from these tests was described in Section 5.3.3 (b).

For the first sensor, switch S_3 was opened first and then switch S_4 was opened. Switches S_5 and S_6 were opened for the second sensor, switches S_7 and S_8 for the third sensor, and switches S_9 and S_{10} for the fourth sensor. The measured frequency data for each of these switch states are reported in Table B.15 and plotted in Fig. 5.31. For comparison, the frequencies calculated using the electrical circuit model when the switches are opened in sequence and when then location of the initial open switch is varied are also shown. The values of L_{eff} and ε_r/t used in all calculations correspond to the average values for the distributed switch with five pairs of switches described in the previous section (Fig. 5.25 and Table B.2).
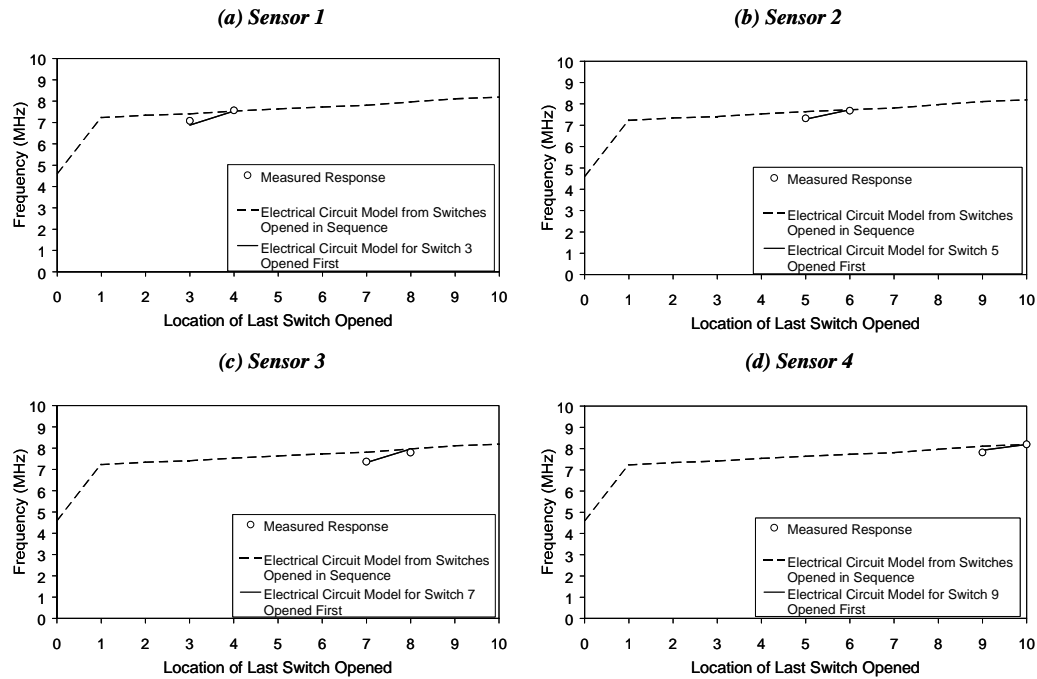
Figure 5.31 Measured Frequency Response of a Distributed Sensor with Five Pairs of Switches When the Location of the Initial Opened Switch is Varied

The electrical circuit models provided a reasonable approximation of the measured frequency response, but the differences in the responses of the four sensors was not sufficiently large that the initiation point for the crack can be identified with confidence. Because all the added capacitance is located at the end of the sensor, the frequency shift associated with the first open switch is significant, but does not change appreciably with the location of the first open switch.

5.5.4   Response of Distributed Sensors with Multiple Added Capacitors

A second design for the prototype distributed sensor was developed to increase the frequency shift that occurs each time a switch is opened. Rather than adding one large capacitor at the end of the switch, multiple smaller capacitors

119

were distributed along the switch (Fig. 5.2). A single distributed sensor with ten pairs of switches and ten added capacitors was tested. The complete set of measured data is presented in Table B.14 and summarized in Fig. 5.32. Data from the sensor with ten pairs of switches and a single added capacitor are also plotted to facilitate comparisons.
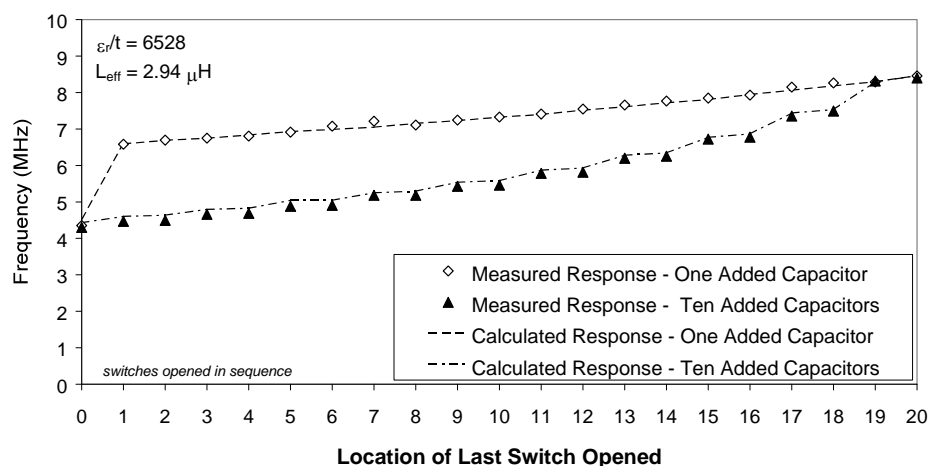
Figure 5.32 Frequency Response of Distributed Sensor with Ten Pairs of Switches with Multiple Added Capacitors

As expected, the measured response of the two sensors was essentially the same when all switches were closed and when all switches were opened. When the first switch was opened, the sensor with ten capacitors experienced a slight change in frequency, while the characteristic frequency of the sensor with one capacitor changed dramatically. As the remaining switches were opened, the incremental change in frequency was larger for the sensor with ten capacitors.

The calculated response for the two sensors is also shown in Fig. 5.32. The electrical circuit model for the sensor with ten capacitors tended to overestimate the measured characteristic frequencies. This variation is a result of using the values of ε_r/t and L_{eff} from the sensor with one capacitor to calculate the

120

electrical model for the sensor with ten capacitors. The values for ε_r/t and L_{eff} could not be directly calculated from the measured frequencies due to the complexity of the capacitance equations from the additional capacitors.

The data shown in Fig. 5.21 suggest that the two types of distributed sensors may be used for different purposes. If the objective is to determine the initiation of a crack, then using a single capacitor is appropriate, because the characteristic frequency will change appreciably when the first switch is opened. However, if the location of a crack is known, and the objective is to monitor the crack propagation, a sensor with multiple capacitors is appropriate, because the incremental frequency changes as switches are opened are larger.

5.6   DISCUSSION OF RESULTS

Despite the agreement between the measured characteristic frequencies and those calculated using the electrical circuit model, two potential sources of error in making these measurements were identified during this investigation.

During the first round of testing of the distributed sensors with one additional capacitor, data from three of the sensors was found to be inconsistent with the expected results. The most common inconsistency was a higher measured frequency when placed on the steel than the expected 4.6 MHz, typically around 6MHz. This increase in frequency was usually resolved by resoldering the copper terminals to the EAS tag. This inconsistent connection acted as an additional resistance on the circuit. Section 5.6.1 investigates the effects of this induced resistance on the frequency response of a distributed sensor with one added capacitor.

In calculating the electrical circuit model, it was assumed that the values of A_{ij}, given in Section 5.4.1, were uniform for all distributed switches. However,

these values of A_{ij} are expected to vary from the calculated values, because these switches were fabricated by hand. Additionally, variation in A_{ij} may have been introduced when the copper foil strip switches were cut. The total capacitance at each switch state for each distributed sensor can be calculated using the measured frequencies and the inferred average values of L_{eff}. From this calculated capacitance, the area of copper foil tape intact at that switch state may be determined. Section 5.6.2 compares these inferred area values to the assumed area values.

5.6.1 Effect of Poor Tag Connection on Measured Characteristic Frequency

During the tag modification process, copper foil terminals were soldered onto the aluminum coil in the EAS tag. This connection would often degrade over time, typically requiring the connection to be resoldered prior to testing. This incomplete electrical connection acts as an added resistor, R_{bad}, between the switch and the EAS tag in the electrical circuit model, shown in Fig. 5.33 (a). The reduced model is shown in Fig. 5.33 (b).
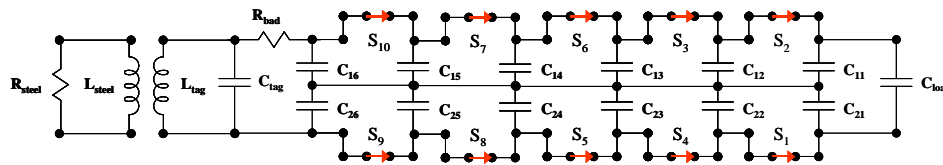
(a) Complete Electrical Circuit Model
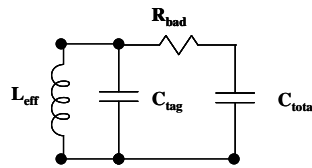
(b) Simplified Electrical Circuit Model

Figure 5.33 Electrical Model of Poor Tag Connection

The resistance, inductance, and capacitance of the circuit are related to each other by the reactance (Eq. 2.8). As discussed in Section 2.2.4, the reactance is dependent on the frequency of the circuit. The total reactance, Z_{total}, for this circuit is:

$$Z_{total} = i \cdot \left(\frac{2\pi f \cdot C_{total}}{\left(2\pi f \cdot C_{total} \cdot R_{bad}\right)^2 + 1} + 2\pi f \cdot C_{tag} - \frac{1}{2\pi f \cdot L_{eff}} \right) + \left(\frac{\left(2\pi f \cdot C_{total}\right)^2 \cdot R_{bad}}{\left(2\pi f \cdot C_{total} \cdot R_{bad}\right)^2 + 1} \right)$$

(5.30)

At resonance, the first term in Eq. 5.30 becomes zero. Setting this term to zero and grouping terms produces Eq. 5.31.

$$\left(2\pi f\right)^4 \cdot C_{tag} \cdot \left(C_{total} \cdot R_{bad}\right)^2 + \left(2\pi f\right)^4 \cdot \left(C_{tag} + C_{total} - \frac{\left(C_{total} \cdot R_{bad}\right)^2}{L_{eff}} \right) - \frac{1}{L_{eff}} = 0$$

(5.31)

As long as the frequency, effective inductance, and total capacitance for a sensor at a given switch state are known, the resistance produced by the incomplete connection may be calculated from Eq. 5.31.

The distributed sensor with one added capacitor and eleven pairs of switches had to be tested twice due to excessive scatter in the measured frequencies. The measured frequencies from both tests, as well as the calculated electrical model frequencies, are summarized in Table 5.6 and shown in Fig. 5.34.

Table 5.6 Summary of the Two Frequency Response Tests for the Distributed
Sensor with Eleven Pairs of Switches and One Added Capacitor

Distance to Steel Plate (in.)	Last Switch Opened *	11P, test 1	11P, test 2	
		Measured Frequency (MHz)	Measured Frequency (MHz)	Calculated Frequency (MHz)
12	0	6.56	4.49	-
0	0	7.00	4.42	4.55
0	1	7.46	6.69	6.69
0	2	7.52	6.76	6.77
0	3	7.52	6.81	6.82
0	4	6.69	7.01	6.90
0	5	7.38	6.96	6.96
0	6	7.49	7.03	7.03
0	7	7.63	7.08	7.08
0	8	7.66	7.21	7.17
0	9	7.08	7.28	7.24
0	10	7.19	7.35	7.32
0	11	7.27	7.39	7.37
0	12	7.38	7.55	7.48
0	13	7.52	7.53	7.55
0	14	7.90	7.59	7.64
0	15	7.93	7.75	7.70
0	16	8.01	7.84	7.83
0	17	8.10	7.91	7.92
0	18	8.18	8.07	8.01
0	19	8.29	8.13	8.09
0	20	8.34	8.31	8.24
0	21	8.43	8.38	8.37
0	22	8.59	8.49	8.45
12	22	8.10	8.02	-

*switches opened in sequence
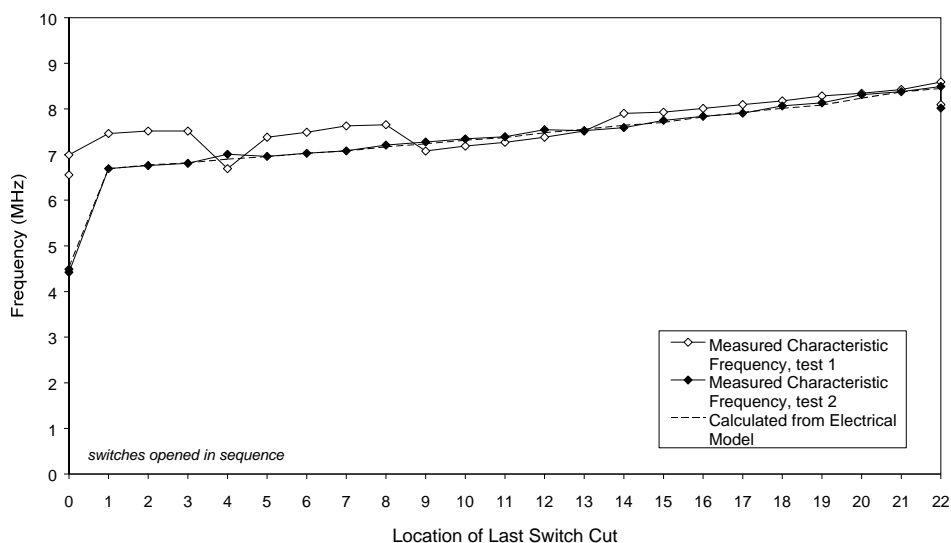
Figure 5.34 Comparison of Two Frequency Response Tests for the Distributed Sensor with Eleven Pairs of Switches and One Added Capacitor

As seen in Fig. 5.34, a large discrepancy between the measured frequencies in the two tests exists. The switch conditions chosen for this investigation are highlighted in Table 5.6. The measured frequency for the intact switch at the infinity condition in the first test is 32% greater than the frequency measured in test 2, and is 37% greater for the intact switch on the steel plate. The discrepancy between the two tests is much less for the subsequent openings of switches 7 and 14: 7% and 4%, respectively.

The solution to Eq. 5.31 for each sensor condition chosen is shown in Fig. 5.35. For the unopened sensor at the infinity position, L_{eff} is L_{tag} and C_{total} is the sum of C_{tag} and C_{load}. For the other switch conditions, L_{eff} was taken as the inferred value used to calculate the electrical circuit model frequencies and the capacitance from addition of the parallel-plate capacitors and C_{load} was used for C_{total}.

125

(a) Infinity Position *(b) Field Position*

(c) Switch S₇ Opened Last *(d) Switch S₁₄ Opened Last*
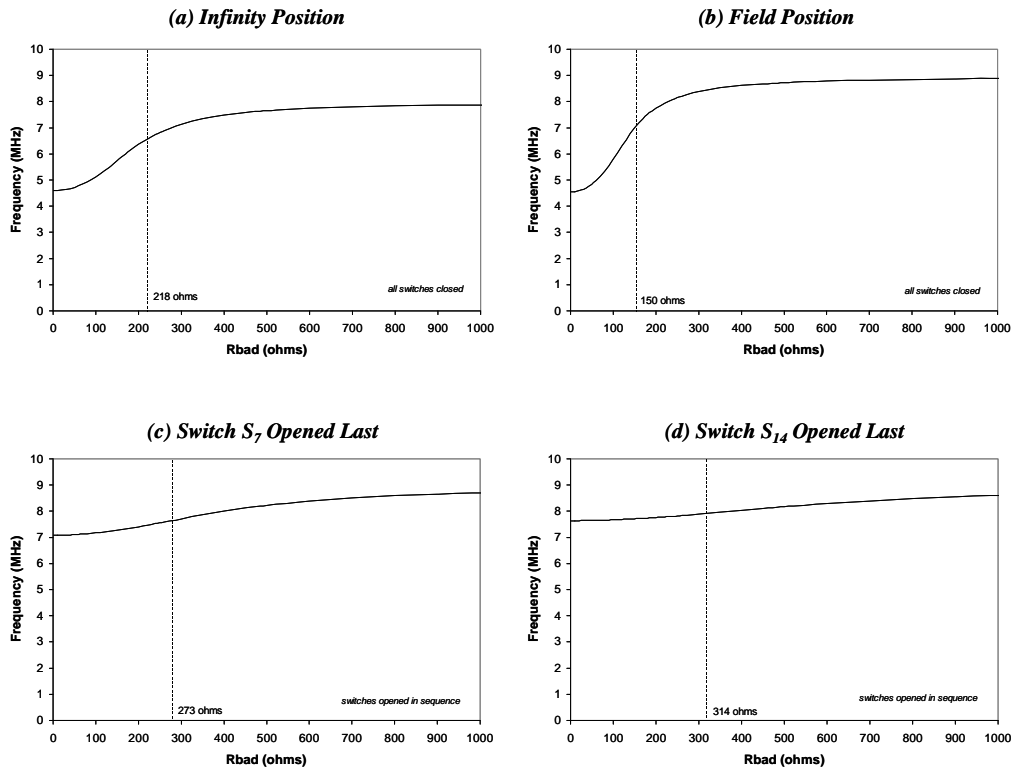
Figure 5.35 Effect of Poor Connection Between EAS Tag and Switch with Nine Pairs of Switches

For test 1, the induced resistance from the incomplete connection for the intact sensor at the infinity position was 218 ohms. When placed on the steel surface, the induced resistance in the intact sensor dropped to 150 ohms. As switches were opened, the resistance increased: when switch S_7 is opened, R_{bad} is measured as 273 ohms; when switch S_{14} is opened, R_{bad} is 314 ohms.

Although the induced resistance increases as the switches are opened, the effect of resistance on frequency flattens out at the same time. Thus, as more switches are opened, the effect of the poor connection on the measured frequency is minimized. However, when the set of switches is intact, the effect of the induced frequency has a dramatic effect on the response of the sensor. Thus,

126

soldering an EAS tag to a point or a distributed switch is not durable enough for field implementation.

5.6.2 Effect of Using Approximate Values of A_{ij}

By substituting the average value of L_{eff} and the measured frequencies in Eq. 5.2, the capacitance, C_{exp}, was calculated for each switch condition for each distributed sensor with one added capacitor. Only sensor states corresponding to all switches being closed and only switch S_1 being opened were not considered, in order to simplify the calculations. The capacitance formed by the copper foil tape, C_{calc}, can be found by subtracting the capacitance of the EAS tag from the C_{exp}. Similarly, C_{cap}, the capacitance of the copper foil using the approximate areas, can be found by subtracting C_{load} from the previously calculated values of C_{total}.

The dielectric constant, ε_r, in Eq. 5.3 is an electrical property of the material separating the copper foil and the steel surface. Therefore, the percent difference between C_{calc} and C_{cap} measures the difference in A/t. Table 5.7 summaries the results of this analysis.

Table 5.7 Percent Difference Between Measured and Calculated Values of A/t

	3P	5P	7P	9P	10P	11P	13P
Percentage of Switch Conditions with A/t less than 5%	0%	50%	58%	38%	83%	75%	63%
Greatest Percent Difference between Calculated and Measured *A/t*	28%	16%	21%	16%	12%	12%	20%

Despite the variation in *A/t*, the difference between C_{exp} and C_{total} is less than 5% for all the distributed sensors. The capacitance formed by the copper foil is very small compared to C_{load}; thus, the variation in *A/t* creates a small shift in the measured characteristic frequency.

5.7   CONCLUSION

Based on the results presented in this chapter, two conclusions may be made: that the prototype sensor is not durable for field implementation and that different combinations of added capacitance may be used to determine the behavior of a crack.   However, it was demonstrated that the electrical circuit model developed for these sensors works.

Soldering the connections to the EAS tag proved to be difficult to achieve and maintain.   The quality of the connection was difficult to assess and was observed to degrade with time and movement.   An investigation of the induced resistance due to the incomplete electrical connection between the EAS tag and the switch is given in Section 5.6.1 for a distributed sensor with eleven pairs of switches.   This investigation confirmed that the frequency response might be drastically altered if this connection is damaged.   Thus, the EAS tag was good for proof of concept of the electrical properties of the prototype sensor, but is not durable enough for field implementation.

The physical properties of the copper foil capacitors, A_{ij} and t, were found to vary considerably.   This is largely due to inconsistencies arising from hand fabrication of the switches: the carpet tape was flattened when the copper foil strips were applied and the copper foil areas were comprised of individual copper foil strips.   Also, the copper foil strip switch was not cut at the boundary of the copper foil areas.

The results of Section 5.5.4 indicate that two types of distributed sensors may be used for different purposes.   If the objective is to determine the initiation of a crack, then using a single capacitor is appropriate.   However, if the location

of a crack is known, and the objective is to monitor the crack propagation, a sensor with multiple capacitors is appropriate.

It is recommended that further testing of the characteristic frequency response of these sensors be conducted. Tests are also needed to determine the behavior of the distributed switch with multiple added capacitors.

CHAPTER 6

Conclusion

6.1   SUMMARY OF TEST RESULTS

The objective of this thesis was to develop a prototype wireless sensor to detect cracks in welded steel moment resisting connections, specifically at the weld toe and root. These devices are intended to provide information quickly and reliably about the condition of the weld after an earthquake to identify the locations that need repairs.

A passive wireless sensor, based on currently available RF technology, was developed and tested. The sensor comprises two elements: a data transmitter and a crack detection device. An EAS tag was modified and used as the data transmitter coil. The crack detection device was a switch fabricated using copper foil and high-strength adhesive tapes. By adding a capacitor to the switch, the electrical circuit of the sensor was modified to transmit two different frequencies: approximately 4.6 MHz when the switch is closed and approximately 8 MHz when the switch is opened. Thus, the sensor is able to provide information about the state of the weld without requiring access to the connection.

The investigation into the electrical behavior and various types of wireless transmitters is presented in Chapter 2. Wireless transmitters have been used for a number of years to provide information about components in difficult environments. To be feasible for the proposed application, the sensor must be durable, affordable, require no external power, and reliable. The EAS sticker was chosen as the data transmitter for the prototype because it initially satisfied these requirements. The crack detection device must also satisfy these requirements.

The development and evaluation of the crack detection switch designs was discussed in Chapters 3 and 4. It was believed that copper foil tape could be cut into a simple shape that would fracture at the desired crack size. The 1-in. wide 3M EMI Copper Foil Shielding Tape 1194 was selected for its electrical properties, ease of soldering, and insulated adhesive backing. This proved unreliable, as the shapes peeled from the weld and surrounding steel during a series of two-dimensional dynamic tests and axial fatigue tests on welded specimens. The crack detection device was then developed into the point switch design. A subsequent modification extended the point switch to the distributed switch design in order to monitor a larger area of the weld. The adhesives chosen to construct the adhesive pads of the final switch design are the high-strength 3M VHB Adhesive Transfer Tape F-9473PC and the thick 3M Polyester Film Tape 8412. Overall, this design performed very well; however, inadequate installation pressure and mill scale effects were found to influence the behavior of the switches. It also was discovered that mill scale must be removed from the steel adjacent to the weld in order for the switch to not delaminate from the connection during loading. The gap size of the switch also was a cause of delamination: the wider the gap size became, the more likely the switch was to delaminate from the surface of the steel.

The electrical circuit model for a complete sensor (transmitter and crack detector) was developed and evaluated in Chapter 5. The measured frequency response of point and distributed sensors was compared with the calculated response using the model. The consequences of distributing capacitors along the length of the switch versus the addition of a single capacitor at the end were also explored. The measured frequencies compared very well with those calculated using the electrical circuit model, thus validating the sensor circuit model. However, better control of the geometric properties of the copper foil parallel-

plate capacitors is needed to eliminate the high amount of scatter in the inferred dielectric constant, ε_r, and its subsequent effect on the effective inductance, L_{eff}. It was concluded that the prototype sensor was not reliable enough to be installed in the field. The soldered connection between the EAS tag and the switch was difficult to fabricate and tended to degrade with time. However, the prototype sensor did demonstrate that the objectives of the investigation could be accomplished.

6.2   RECOMMENDATIONS

A functional passive wireless sensor may be fabricated using the methods described in Appendix A. The results of this thesis demonstrate the need for further research and development of these sensors before installation in a structure in a seismic zone. The four requirements that the sensor must have in order to be implemented are that it is durable, affordable, requires no external power, and reliable.

The durability and reliability requirements are currently not totally satisfied by this design. In order to satisfy these requirements, the following recommendations are proposed:

1. Use high strength 3M adhesive tapes in fabrication of switches. These tapes, when installed properly, allowed the switch to break below the desired failure size of 0.10 in.

2. Remove mill scale from steel surface prior to installation. Minimal preparation is not sufficient for affixing the switch across the weld of a connection. Further investigation of the switches on steel connections is required.

3. Discontinue use the EAS tag. The addition of copper terminals to the aluminum coil was found to be highly unreliable. These modifications tended to

degrade with time and were highly sensitive to movement. Additionally, the electrical properties of the individual EAS tags were not consistent, typically deviating from the specified frequency of 8 MHz.

4. Conduct further experiments on response of distributed sensors. The tests conducted in this thesis indicated that distributed sensors with multiple capacitors distributed along the length of the switch could be used to monitor the propagation of a weld crack. Further investigation of the behavior of these distributed switches is needed.

APPENDIX A

Fabrication of Wireless Sensor Components

A.1   COMPONENTS OF PROTOTYPE WIRELESS SENSOR

There are three main components to the prototype wireless sensor: the EAS tag, the switch, and the added capacitor. Capacitors may be purchased at any electronics store, the EAS tag must be modified to attach to the switch, and the switch is independently constructed. Two different types of switches were fabricated and used in this investigation: a switch that crossed the potential crack once (point sensor) and a switch that crossed the potential crack multiple times (distributed sensor).

A.2   MODIFICATION OF EAS TAG

Electronic Article Surveillance tags are commonly used to control shoplifting in retail stores. Tags may be purchased in various shapes, sizes, and frequencies. EAS tags are composed of an aluminum inductor coil plus a capacitor inside of a layer of thin plastic, with adhesive on the back and a paper cover on the front. The tags used in this project resonate at a frequency of approximately 8.2 MHz and approximately 2-in. by 2-in. in size (Fig. A.1).

In order to incorporate the switch component, wire leads must be attached to the EAS tag. To accomplish this, copper foil tape strips were soldered onto exposed sections of the tag; they are the leads for connecting the wires. This process was complicated by the fact that the inductor coil of the tag is made of aluminum, a difficult metal to solder.
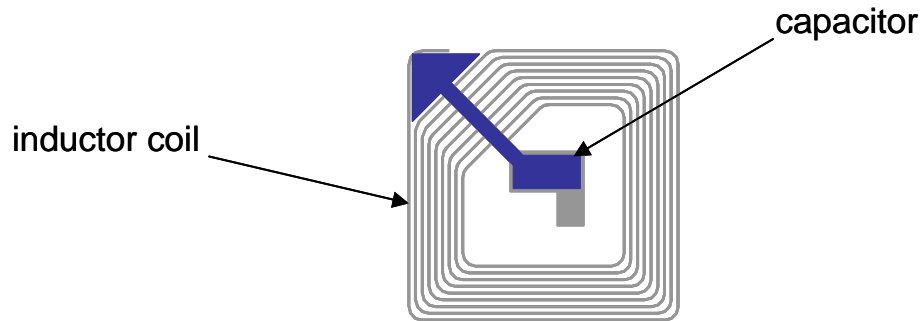
Figure A.1 Diagram of Typical EAS Tag

Attaching the copper terminals is a multi-step process. For the EAS tag to be connected to an external device, leads must be placed across the internal capacitor. The two points chosen are illustrated in Fig. A.2.
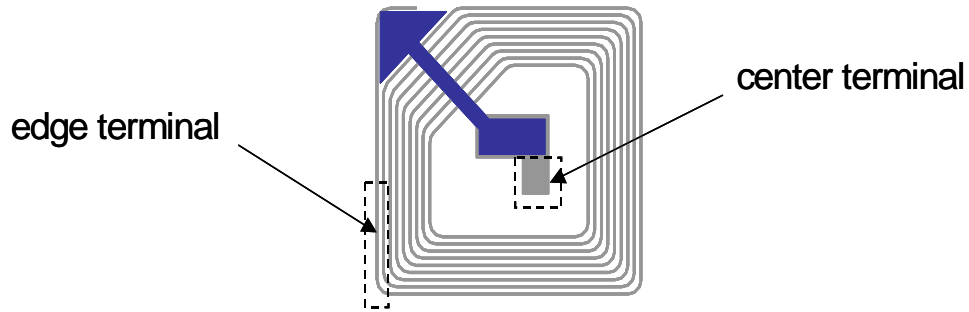
Figure A.2 Location of Copper Terminals

Using a razor blade, the layers of paper and plastic covering the tag were removed from the selected regions. A small area around the center location was removed to better expose the aluminum, as seen in Fig. A.3. The oxidation was removed from the surface by scraping the surface of the exposed aluminum with a razor blade to facilitate soldering.

Figure A.3 EAS Tag with Aluminum Exposed

Two strips were detached from the roll of 1-in. wide 3M EMI Copper Foil Shielding Tape 1194. Each piece was 1/4-in. wide and 1/2-in. long, one folded in half lengthwise and the other widthwise. The lengthwise piece corresponds to the edge region of the tag, the widthwise to the center. The copper strips were attached to the tag, setting the fold parallel to the edge of the aluminum and leaving half of the copper free, as shown in Fig. A.4. The other half of the copper tape was stripped of adhesive using a razor blade.
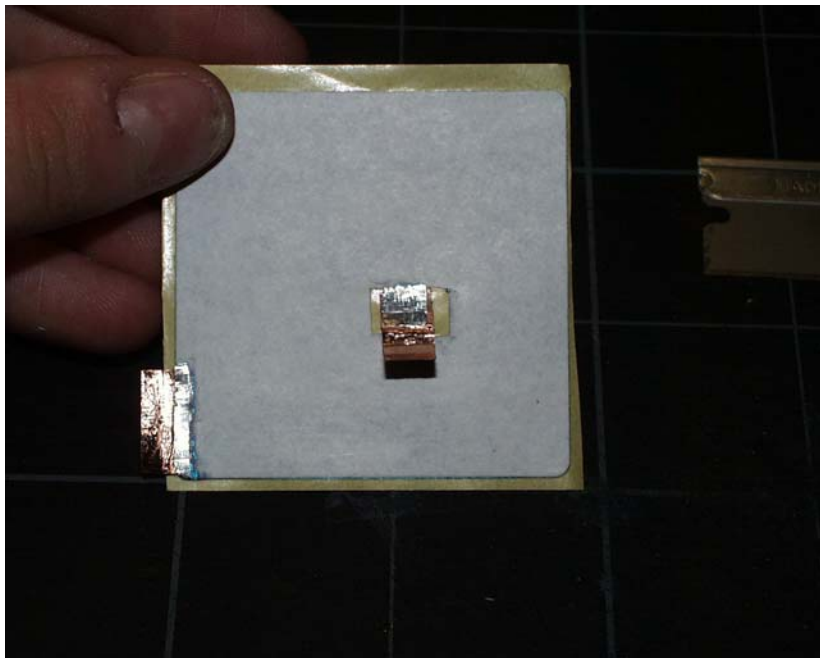
Figure A.4 Copper Strips Affixed to EAS Tag

Aluminum solder paste was spread on the cleaned copper and aluminum surfaces (Fig. A.5). The strips were then folded over along their creases. The copper was then soldered to the exposed aluminum areas. The soldering of the aluminum and copper was aided by applying a small amount of solder to the top of the folded copper, as illustrated in Fig. A.6.

Figure A.5 Aluminum Solder Paste Applied to Copper and Aluminum
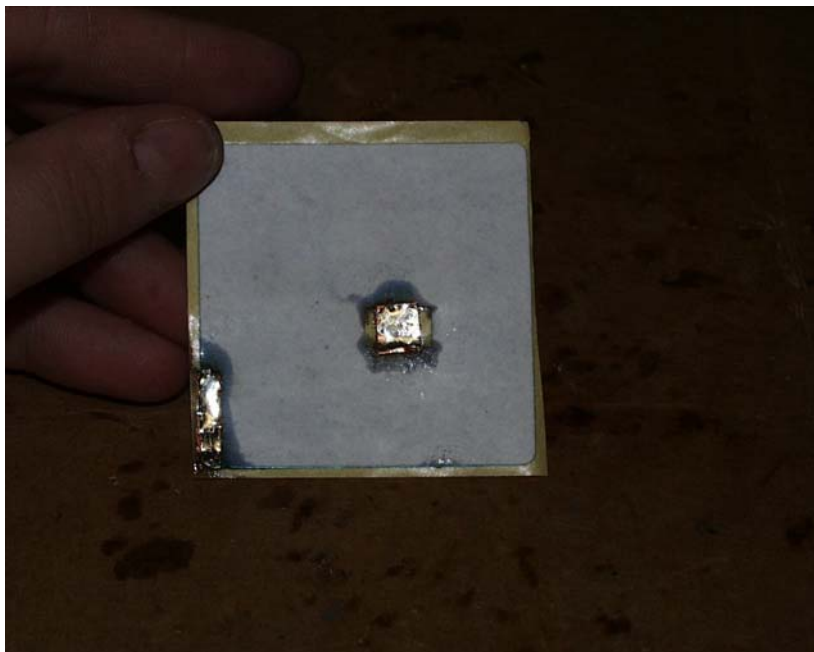
Figure A.6 Copper Soldered to Tag

Finally, two pieces of 28-gage stranded wire, approximately 3-in. in length, were stripped, tinned, and soldered onto the copper terminals (Fig. A.7). The tag was checked with an ohmmeter to verify that the capacitor had not been damaged during the soldering process. An intact tag has a resistance of approximately 1.3 ohms.
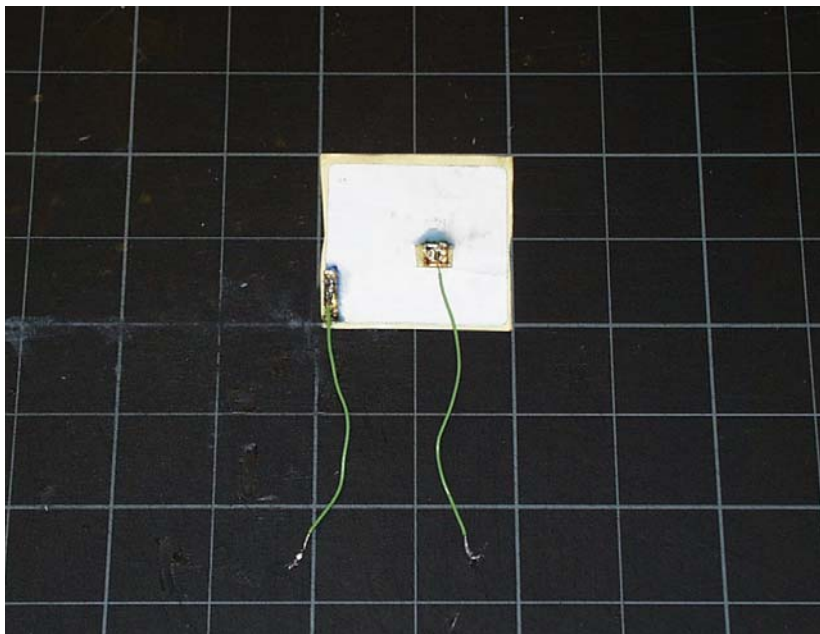
Figure A.7 Complete Modified EAS Tag

A.3   FABRICATION OF A POINT SWITCH

The basic point switch was composed of two 2-in. by 2-in. double-sided tape adhesive pads connected together by two strips of copper foil tape. The pads were covered with clear tape to insulate and secure the strips. The gap of the switch was placed across the weld and breaks when a crack occurs beneath it. The copper strips were 1/8-in. wide where they cross the gap between the two

pads, tapering out to 1/2 in. at the terminals. Typical dimensions of the point switch are given in Fig. A.8.
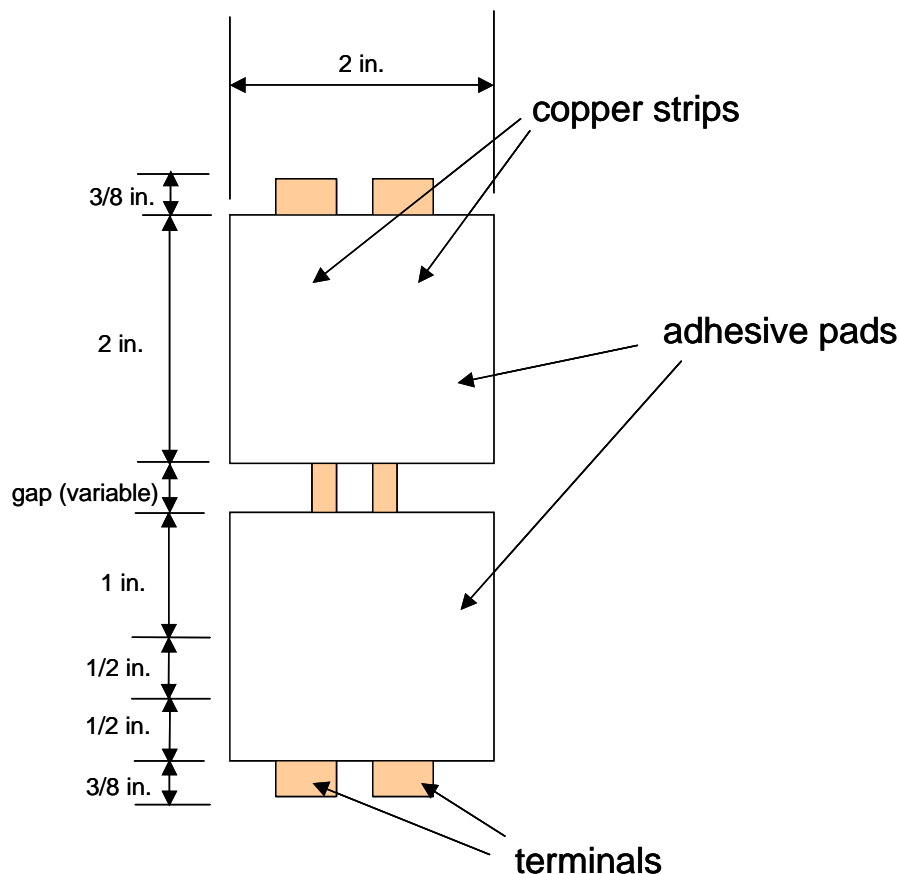
Figure A.8 Typical Dimensions of a Point Switch

These switches may be made using a variety of adhesive tapes and are easily modified to accommodate various weld sizes. For this project, two combinations of 2-in. wide tapes were used: heavy-duty carpet tape with clear packing tape and 3M VHB Adhesive Transfer Tape F-9473PC with 3M Polyester Film Tape 8412. The thicker polyester tape acts as a stiff restraint against the copper strips delaminating from the surface of the VHB tape. The copper tape used for all switches was the 1-in. wide 3M EMI Copper Foil Shielding Tape 1194 with insulated adhesive.

140

The following sections describe the construction procedure for a single crossing switch with a gap of 1/2 in. using the 3M VHB and Polyester tapes.

A.3.1 Creating the Copper Strips

The first step was to cut and shape the two copper strips. On the copper tape backing, a line was drawn down the center of the tape (Fig. A.9).

Figure A.9 Defining Midsection of Copper Tape

Using a utility knife and straight edge, a 7-in. long piece was cut off the roll. This piece was sliced down the middle following the guideline previously drawn. Each strip was trimmed as shown in Fig. A.10. The strip was folded over at the ends where indicated in Fig. A.10, using a straight edge to create a flap, as shown in Fig. A.11. The backing was lifted up to affix the flap to the strip, creating the terminals (Fig. A.12). The strip was flattened with a roller or flat

141

edge and the excess backing trimmed. The complete copper strip is shown in Fig.
A.13.
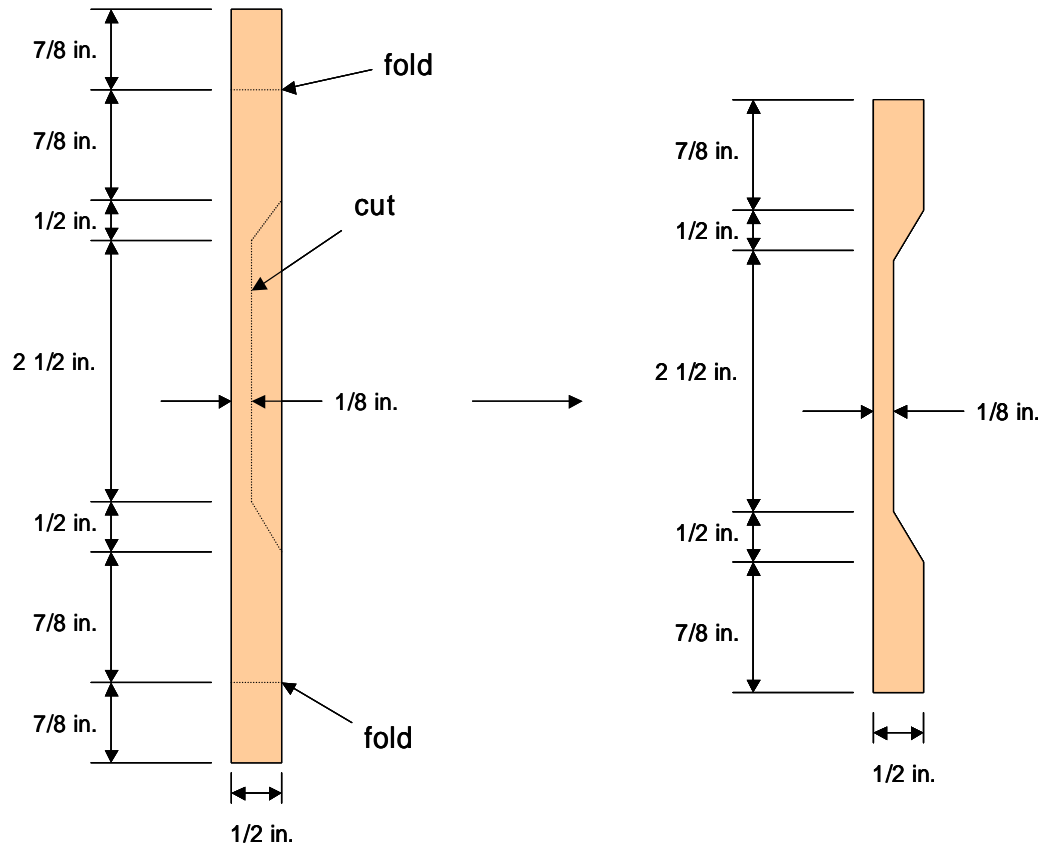
Figure A.10 Pattern for Creating Strip
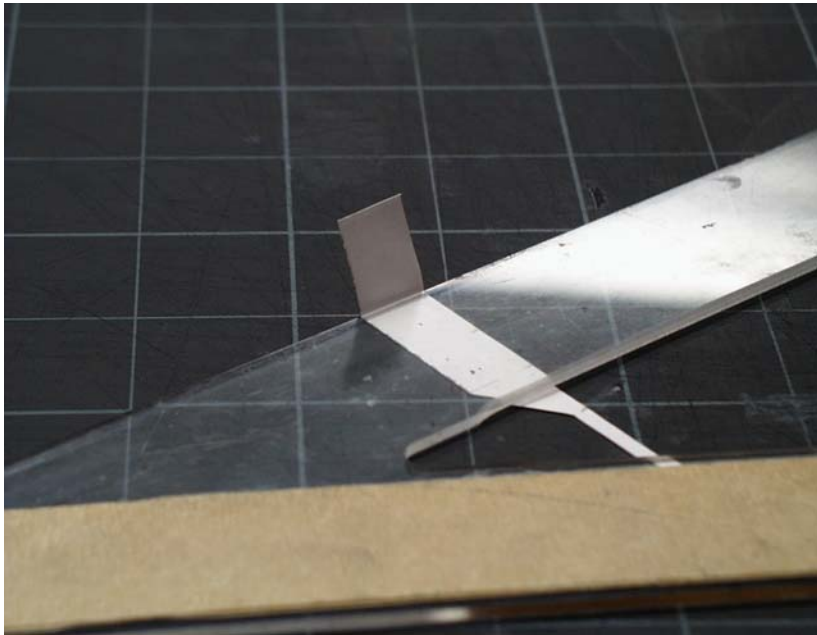
Figure A.11 Creasing the Copper Strip
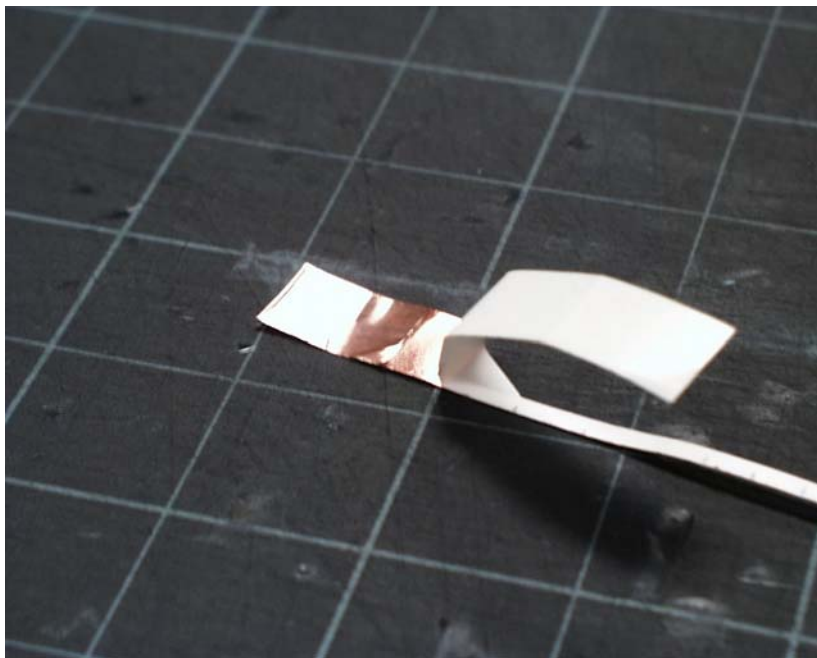
Figure A.12 End Piece Folded Over

143

Figure A.13 Completed Copper Strip

A.3.2 Attaching Copper Strips to Adhesive Pads

Once the copper strips had been prepared, the next step was to place them on the adhesive tape. A sheet of transparency paper with guidelines for various gap spaces between the adhesive pads and the placement of the copper strips was used as a pattern (Fig. A.14). A piece of low tack masking tape, secured with masking tape, was placed over the area of the gap to protect the copper strips (Fig. A.15). Two pieces of double-sided 3M VHB tape were placed on the transparency and held in place with masking tape (Fig. A.16). The backing was removed from the copper strips and placed onto the adhesive at 1/8 in. apart with a 3/8-in. overhang at the ends, as shown in Fig. A.17. Covering the exposed adhesive with a piece of tape backing, the copper strips were firmly pressed into place using a roller.
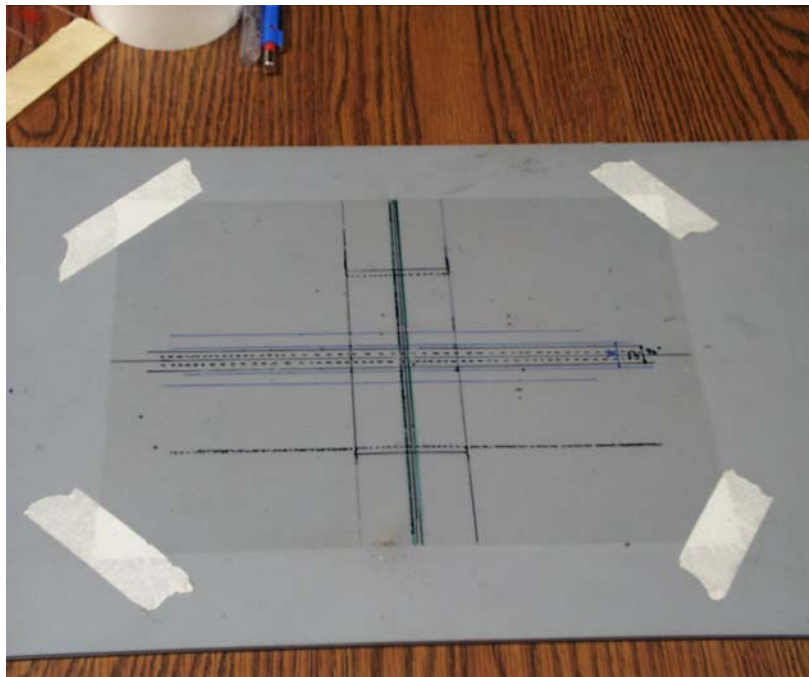
Figure A.14 Pattern for Adhesive and Copper Strip Placement
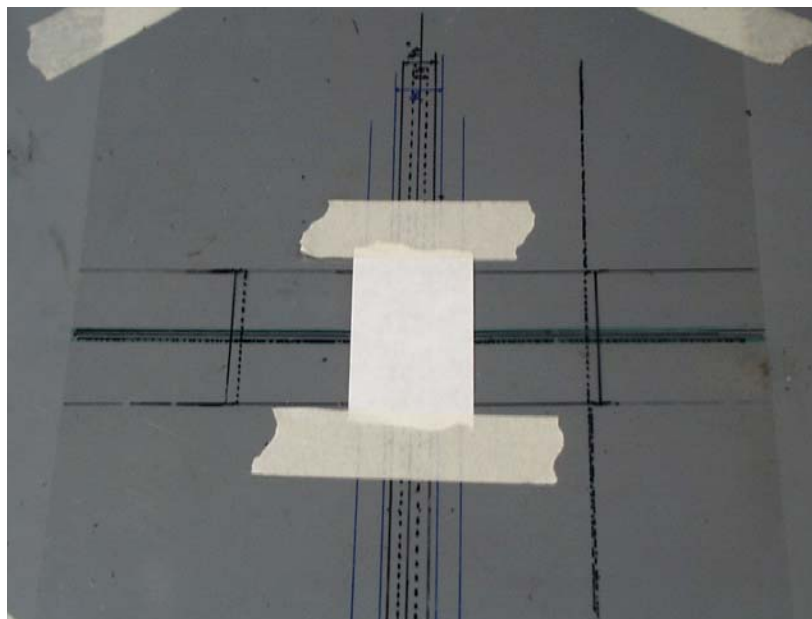
Figure A.15 Placement of Low Tack Tape
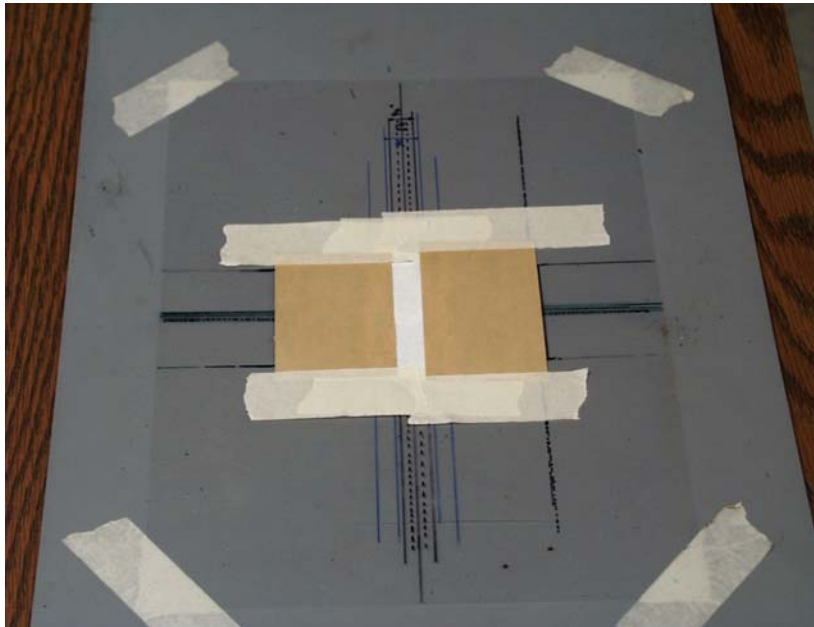
Figure A.16 Placement of Adhesive Tape
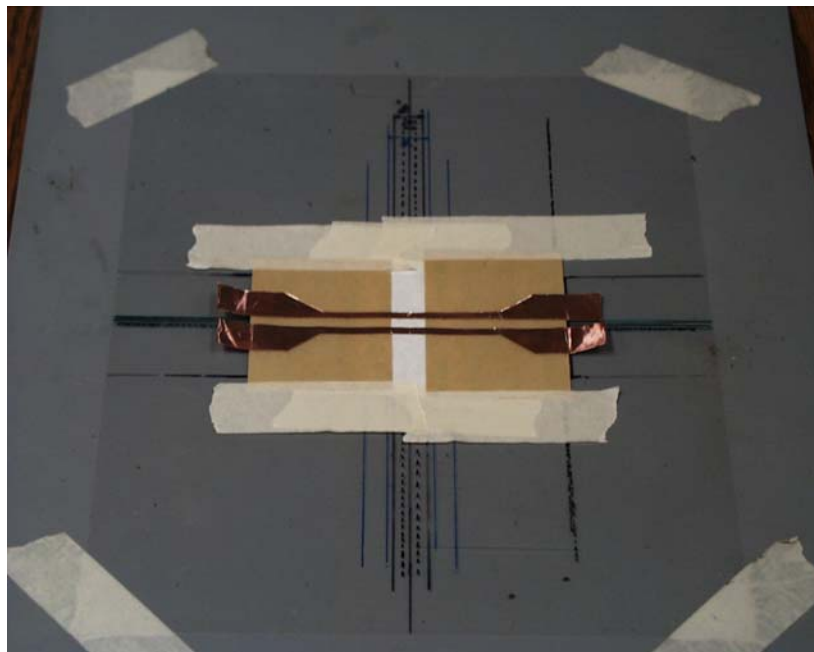
Figure A.17 Copper Strips Placed on Adhesive

146

Two lengths of the 3M Polyester tape were cut and placed over the exposed adhesive, as shown in Fig. A.18. Using the roller, the tape was firmly pressed onto the copper strips and the adhesive. The 2-in. width of the adhesive pad was marked on the tape strips where indicated by the pattern. A piece of low-tack masking tape was placed over the gap to protect the copper strips on the front (Fig. A.19).
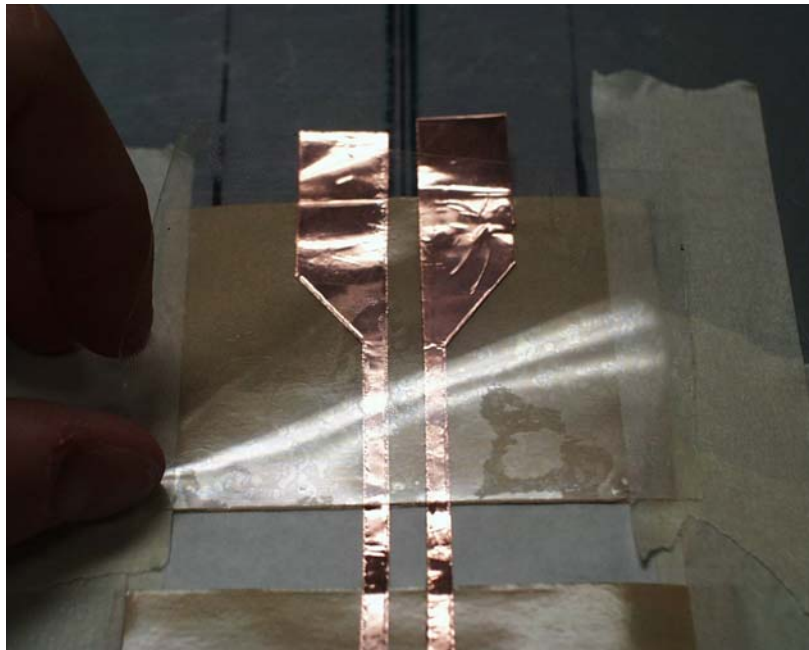
Figure A.18 Applying the Polyester Tape

147
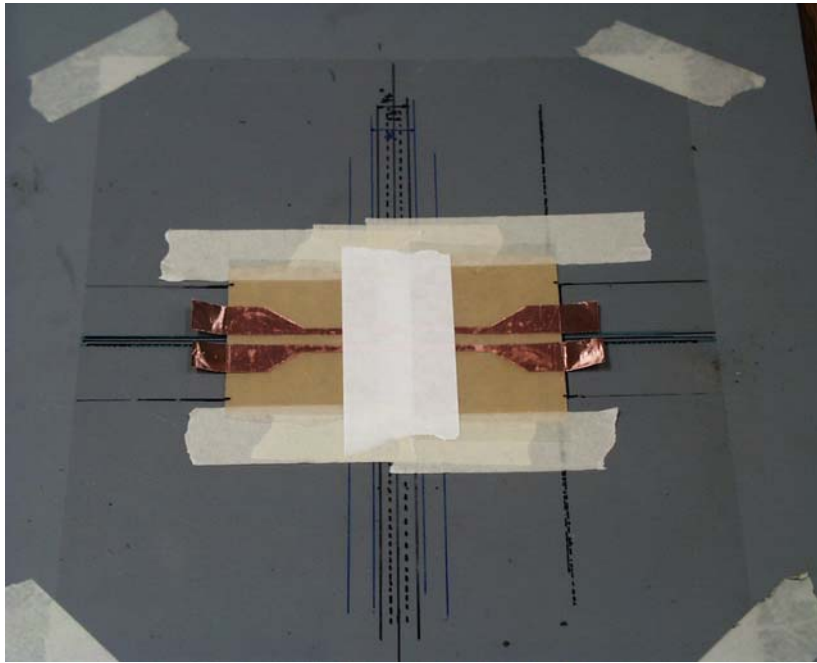
Figure A.19 Low-tack Tape Placed over Gap

A.3.3   Completion of Switch

The entire assemblage was removed from the pattern and the excess tape is trimmed at the marks using a straight edge. The completed point switch is shown in Fig. A.20. To assemble the sensor, a modified EAS tag and a 200-pF capacitor were soldered to the terminals of the switch. The fully assembled prototype wireless sensor using a single crossing switch is shown in Fig. A.21.

Figure A.20 Completed Point Switch
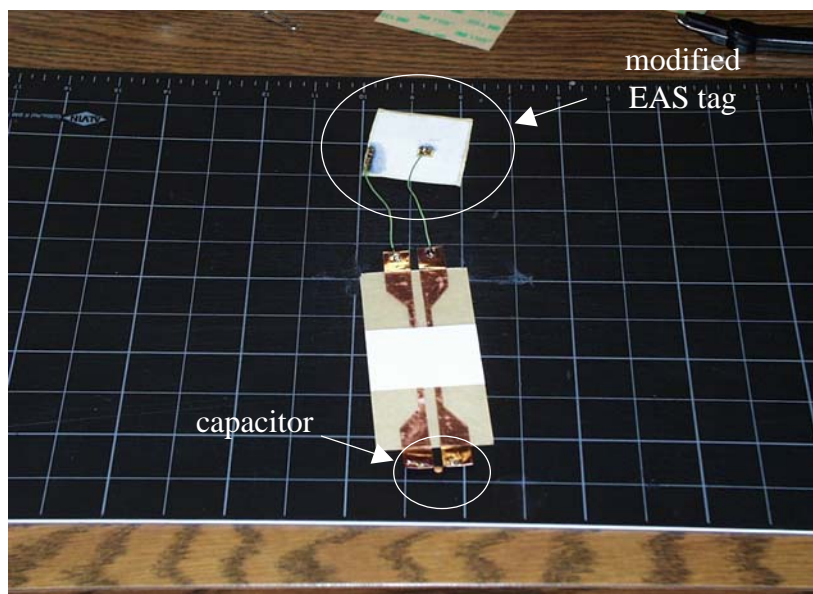
Figure A.21 Assembled Wireless Sensor with Point Switch

A.4 FABRICATION OF DISTRIBUTED SWITCH

The distributed switch was composed of two 2-in. wide strips of double-sided tape adhesive pads connected together by pairs of 1/8-in. wide copper foil tape strips, all covered with clear tape. The copper tape strips were arranged into a serpentine pattern and connected electrically with dots of solder. The pairs of strips cross the gap between the adhesive pads. Figure A.22 illustrates this pattern for a switch with five pairs of copper strips. This serpentine shape allows for longer switches to be created, monitoring a longer section of the weld.
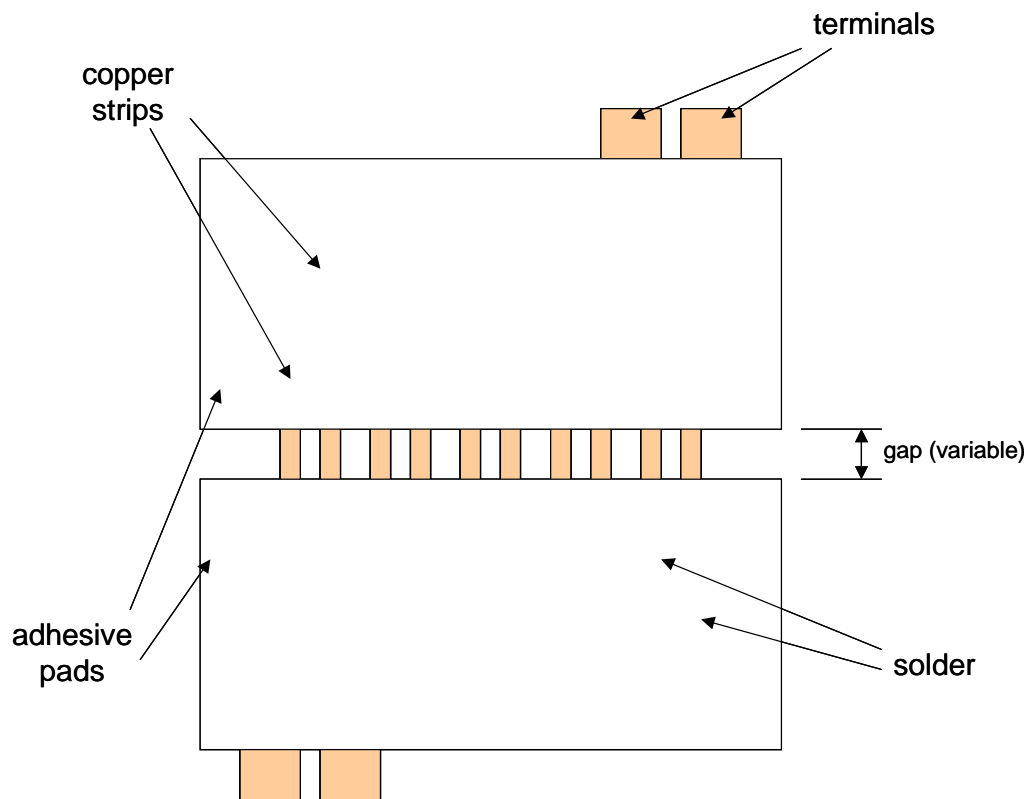
Figure A.22 Distributed Switch with Five Pairs of Strips

Similarly to the point switch, distributed switches may be made using a variety of adhesive tapes and are easily modified to accommodate various weld sizes. Two combinations of 2-in. wide tapes were used: heavy duty carpet tape

with clear packing tape and 3M VHB Adhesive Transfer Tape F-9473PC with 3M Polyester Film Tape 8412. The thicker polyester tape acts as a stiff restraint against the copper strips delaminating from the surface of the VHB tape. The copper tape used for all switches was the 1-in. wide 3M EMI Copper Foil Shielding Tape 1194 with insulated adhesive.

The following sections describe the construction procedure for a distributed switch with five pairs of copper strips and a gap size of 1/4 in., using heavy-duty carpet tape with packing tape.

A.4.1 Fabrication of Copper Foil Shapes

Each switch was composed of the same basic copper foil shapes: 1/8-in. wide strips, 1/2-in. and 1-in. long strips, and tapered and straight terminal pieces. These pieces were prepared in advance for ease of assembly, as shown Fig. A.23 through A.26. Where indicated, the piece was folded and flattened as described in Section A.3.2.
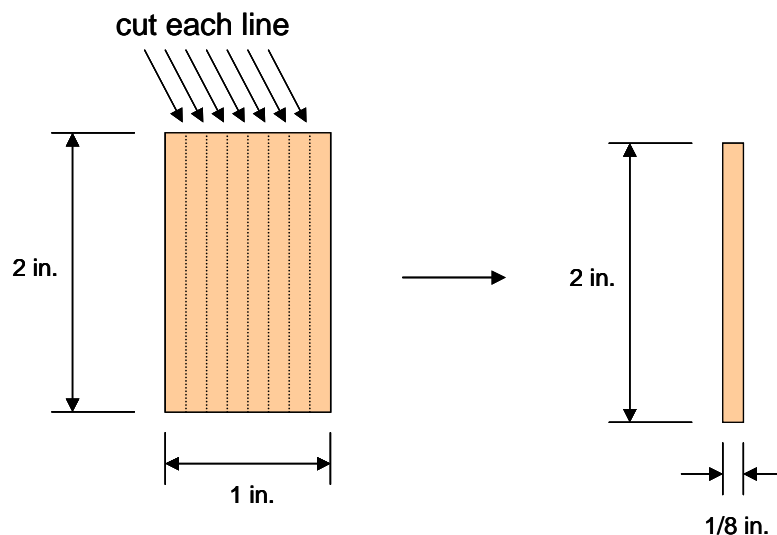
Figure A.23 Creation of 1/8 in. Wide Strips
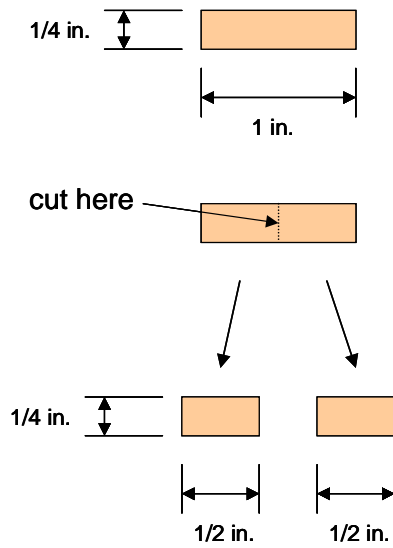
Figure A.24 Creation of 1/2-in. and 1-in. Wide Strips
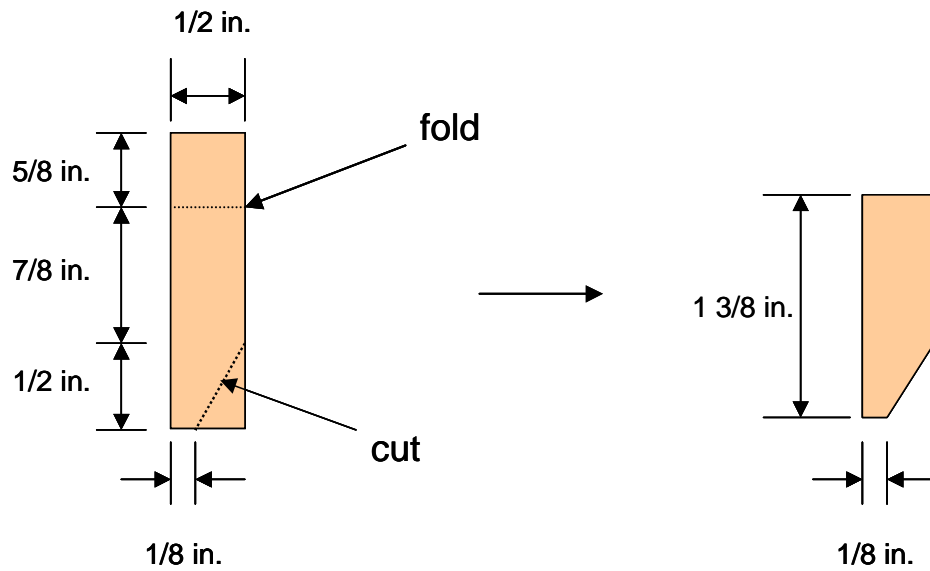
Figure A.25 Creation of Tapered Terminal Strip

152

1/2 in.

fold

1/2 in.

1/2 in.

1/2 in.

2 in.

2 in.
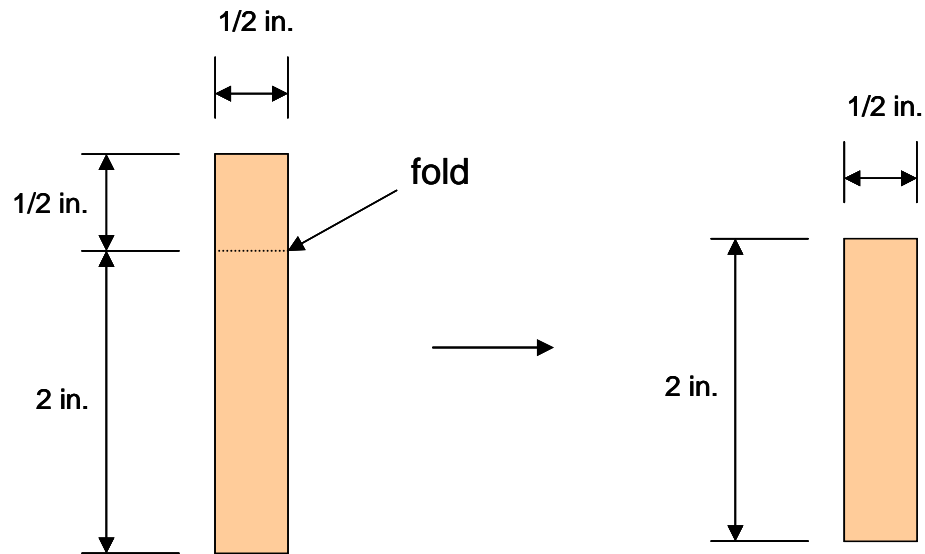
Figure A.26 Creation of Straight Terminal Piece

A.4.2 Arrangement of Strips in Serpentine Pattern

To make a distributed switch, the copper strips were arranged either on transfer tape or directly on the adhesive. When fabricating a distributed switch on carpet tape, it was easiest to first arrange the copper strips on low tack masking tape as a means of transferring the copper to the adhesive. Because the 3M VHB tape is tackier than the carpet tape, the low tack masking tape method cannot be used. In this case, the strips were placed onto the adhesive pads directly, which follows the same steps as the low tack tape method, but was a more difficult to execute.

Two pieces of low tack masking tape, approximately 8 in. long, were taped into position on the transparency sheet pattern, as shown in Figure 2.27. For this example, the low tack tape was placed along the 1/4 in. gap lines. A guideline was drawn on each strip 1/2 in. from the edge of the gap.

153
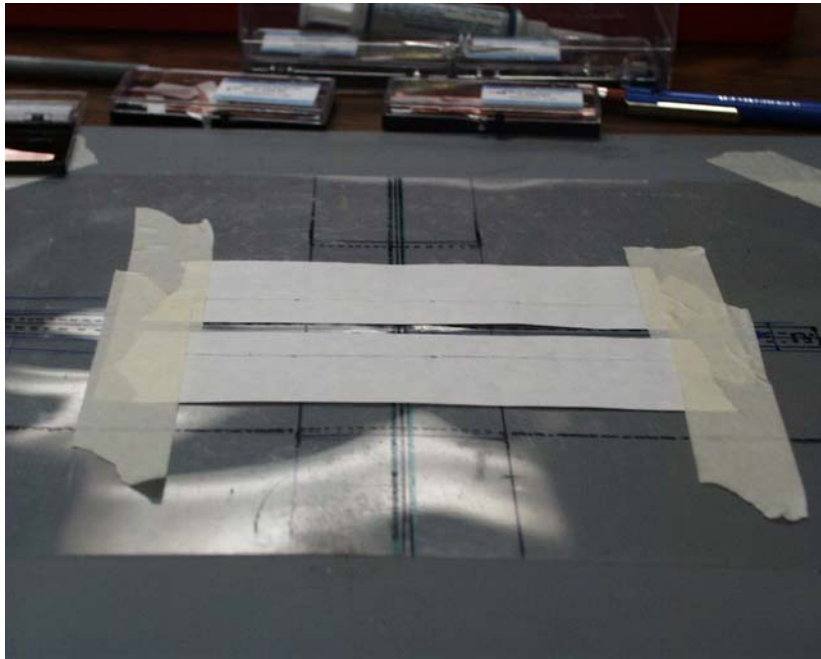
Figure A.27 Positioning of Low-tack Masking Tape

Starting with the top half, a straight terminal piece was positioned with the non-terminal end along the guideline. A tapered terminal piece was placed 1/8 in. away from the straight terminal, as shown in Figure A.28. Two 1/8-in. wide copper strips were laid down parallel along the line of the interior edges of the terminal pieces, letting them overlap approximately 3/16 in. At the end of the 1/8-in. wide strip on the right, a 1/2-in. wide copper strip was placed perpendicular to and underneath, positioning the longer edge along the outside of the guideline. A 1-in. wide copper strip was placed perpendicular to and underneath the other 1/8-in. strip, positioning it 1/8 in. beneath the 1/2-in. wide copper strip (Fig. A.29).
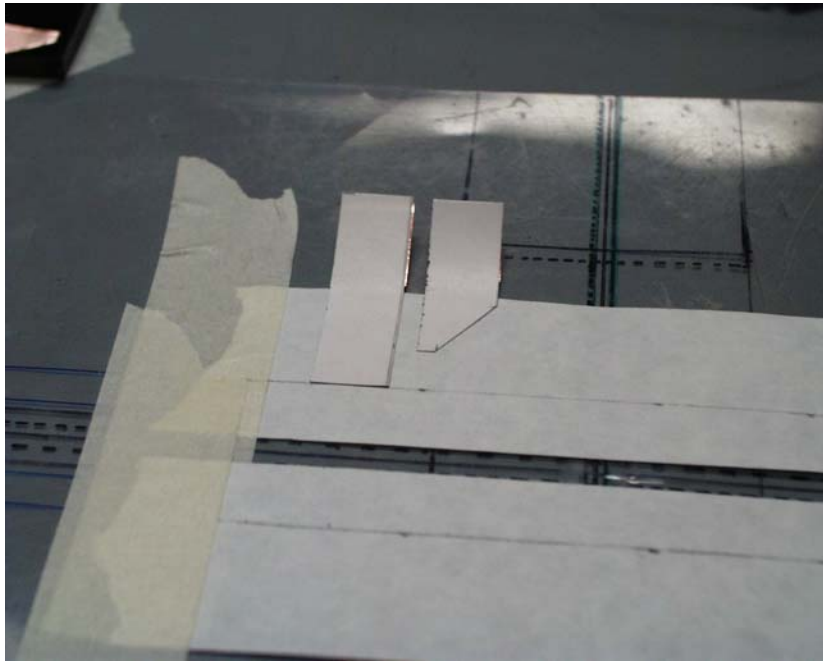
Figure A.28 Terminal Pieces Positioned on Low-tack Tape
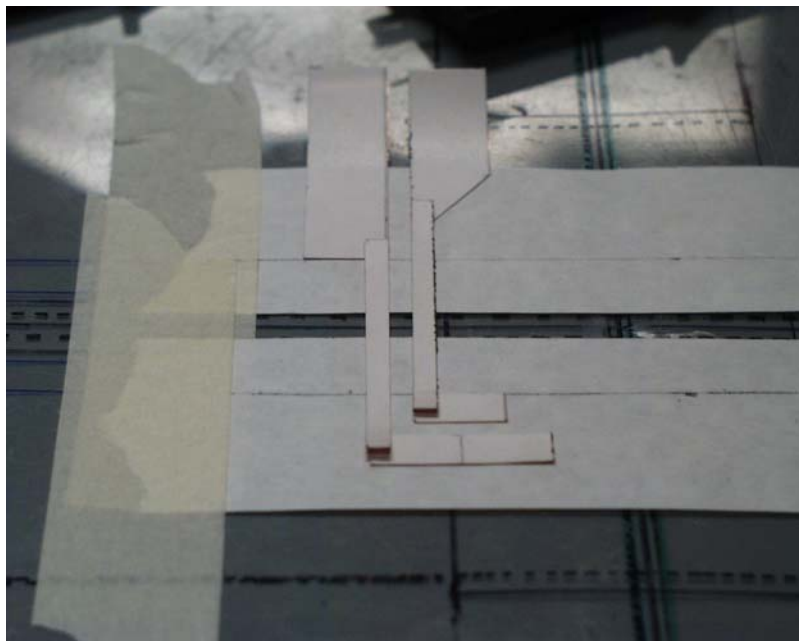
Figure A.29 Placement of Copper Strips

Overlapping the 1/2-in. piece by about 3/16 in., a 1/8-in. copper strip was positioned parallel to the first two 1/8 in. strips. Another 1/8-in. piece was placed similarly on the 1-in. wide piece. At the ends of these strips, a 1/2-in. strip was placed perpendicular to the outer 1/8-in. strip and a 1-in. strip to the other 1/8-in. strip. The 1/8-in. strips were adjusted so they lay on top of the 1/2-in. and 1-in. strips with an overlap of 3/16 in. Again, two 1/8-in. strips were positioned on the 1/2-in. and 1-in. strips as before (Fig A.30). The pattern is repeated two more times to create the next two pairs of strips. To end the serpentine, the two terminal pieces were placed at the ends of the 1/8-in. wide strips as at the start of the serpentine. The completed layout is shown in Fig. A.31. The backing was then removed from the copper tape, pieces of unattached tape backing were placed on top, and the whole assembly flattened with a roller. The copper strips were now ready to be transferred onto carpet tape (Fig. A.32).
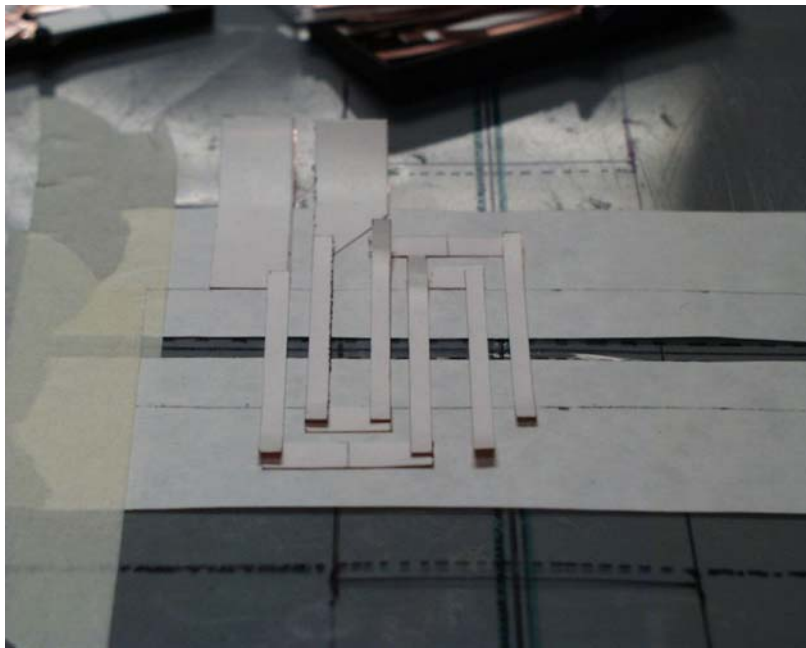
Figure A.30 Three Pairs of Strips in Serpentine Pattern

156
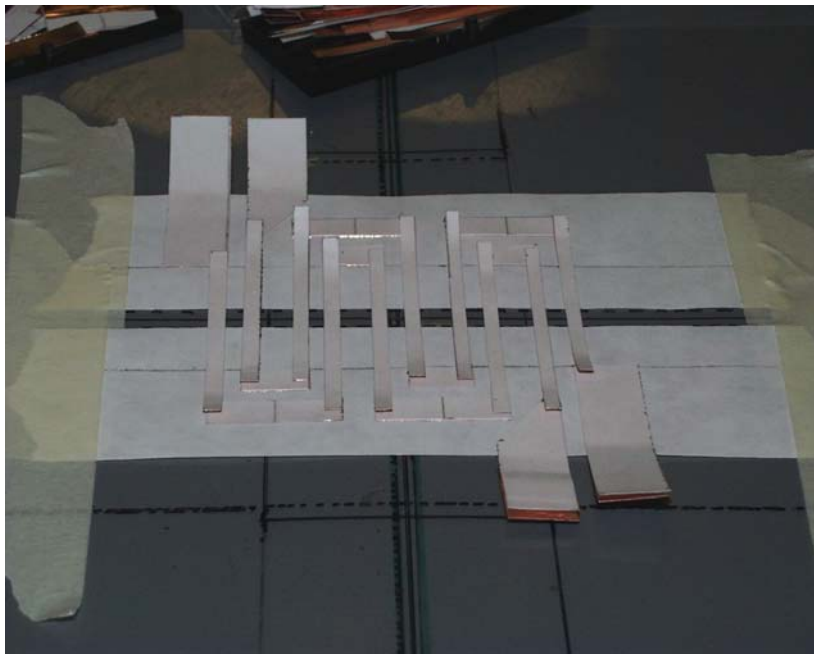
Figure A.31 Completed Layout of Serpentine on Low-tack Masking Tape
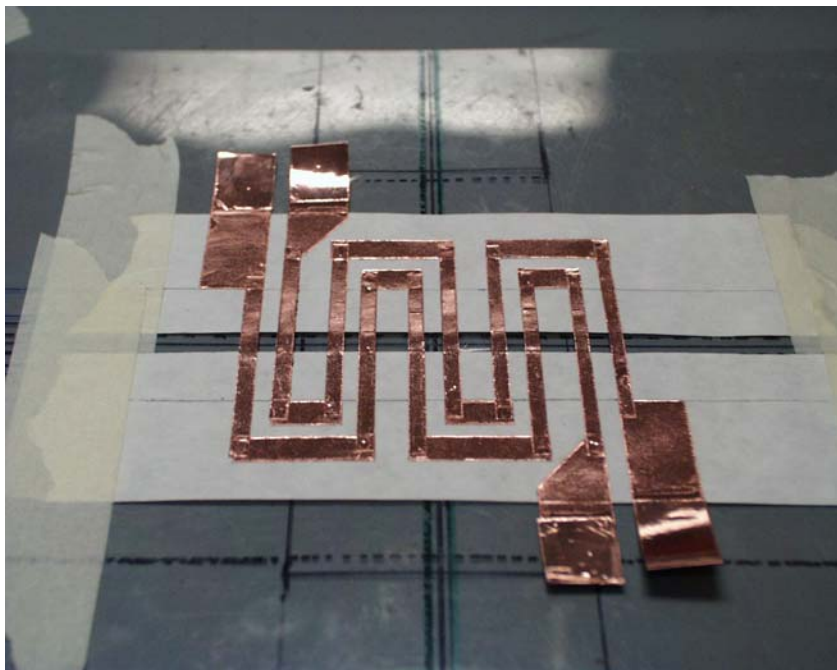
Figure A.32 Backing Removed from Copper Strips

157

A.4.3 Transferring Copper Strips to Adhesive Pads

Two pieces of carpet tape, approximately 8 in. in length, were set on top of each low tack tape strip, aligning the edge of the carpet tape with the gap edge of the low tack masking tape (Fig. A.33). The copper strips were gently pressed onto the carpet tape with a blunt instrument, such as a pencil eraser. A piece of low tack copper tape was laid over the gap region and secured in place with regular masking tape (Fig. A.34). The entire assembly as carefully peeled off the transparency sheet pattern and turned over (Fig. A.35). Folding over the edges of the regular masking tape, the low tack masking tape was removed from the carpet tape, as shown in Fig. A.36. Strips of unattached tape backing were placed on top of the exposed tape and the copper pieces flattened down with a roller. The completed transfer is shown in Fig. A.37.
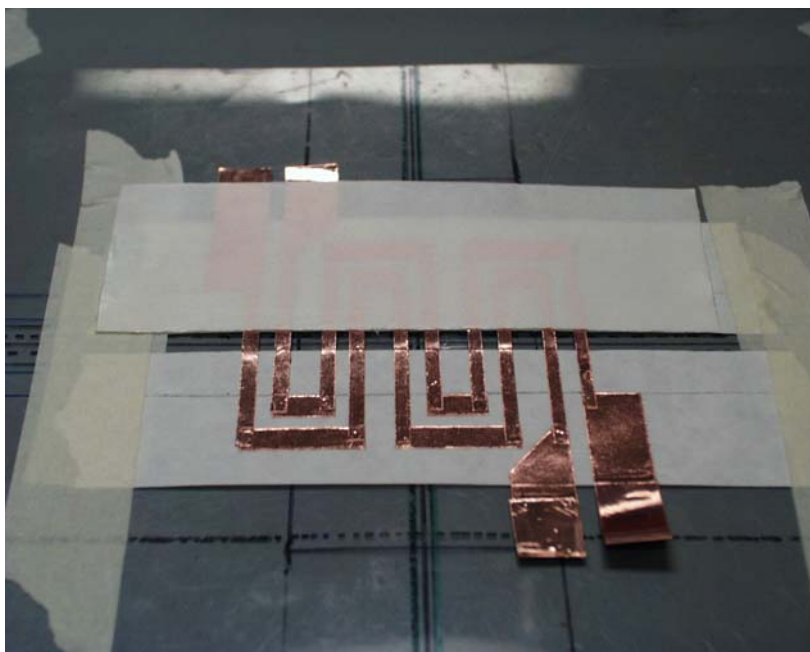
Figure A.33 Carpet Tape Placed on Top of Low-tack Tape
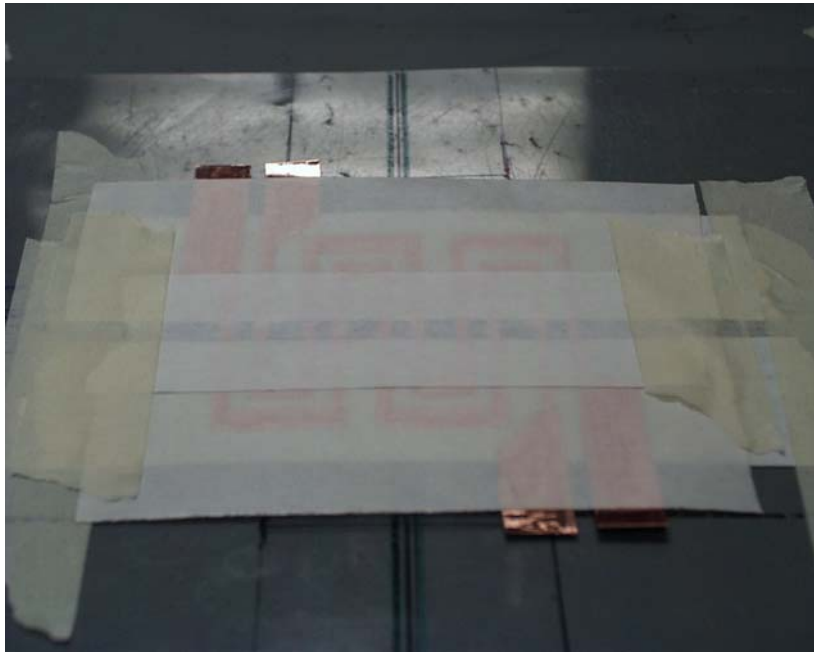
Figure A.34 Low-tack Tape Placed over Gap

Figure A.35 Tape Assembly Removed from Pattern
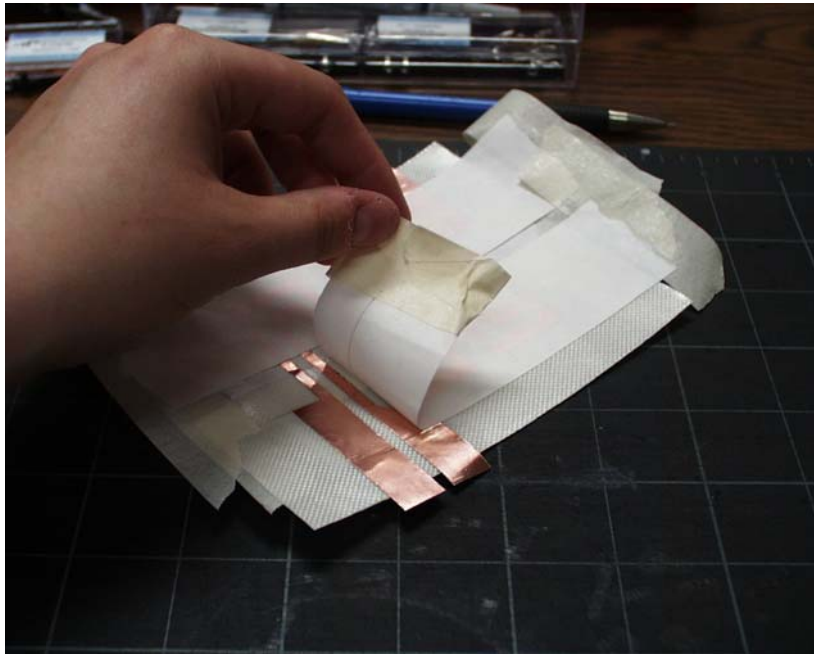
Figure A.36 Removing Low-tack Masking Tape

Figure A.37 Completed Transfer of Copper Strips to Carpet Tape

A.4.4 Electronic Connection of Copper Strips

In order for the switch to act as an electrical circuit, the copper strips must be soldered together. A small drop of solder was placed at each of the overlapping points being careful to not burn the tape. Next, a loop of stranded wire was soldered onto one of the terminal sets. The other terminals have wires soldered to each one and the wires were then connected to an ohmmeter. For a distributed switch with five pairs of copper strips, the ohmmeter gives a reading of 0.4 ohms for a complete circuit (Fig. A.38). The resistance ranges from approximately 0.3 ohms for shorter switches to 0.5 ohms for longer switches. Once the switch has been checked, the wires were removed from the terminals.
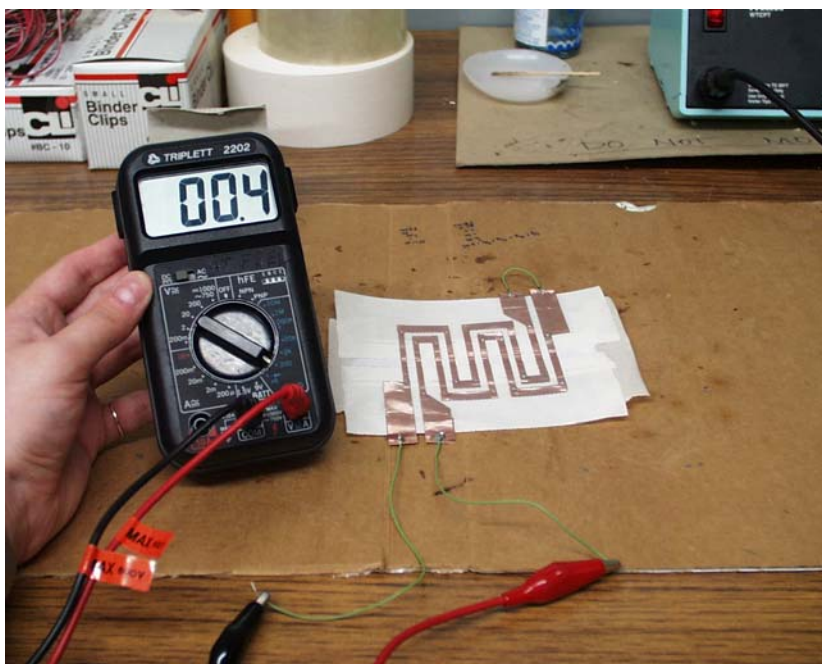
Figure A.38 Complete Circuit Reading for Switch with Five Pairs of Copper Strips

A.4.5 Completing the Switch

A layer of packing tape was placed on top of the exposed carpet tape (Fig. A.39). The adhesive pads were then flattened using a roller. The ends of the switch were cut approximately 1/4 in. from the outermost terminal edge with a straight edge and utility knife (Fig. A.40). A piece of low tack tape was placed over the gap to protect the tops of the copper strips during installation, as shown in Figure A.41. To make a prototype sensor using this switch, a 200-pF capacitor was soldered to one terminal set and a modified EAS tag to the other (Fig. A.42).

Figure A.39 Packing Tape on Top of Carpet Tape

162

Figure A.40 Ends Trimmed from Switch
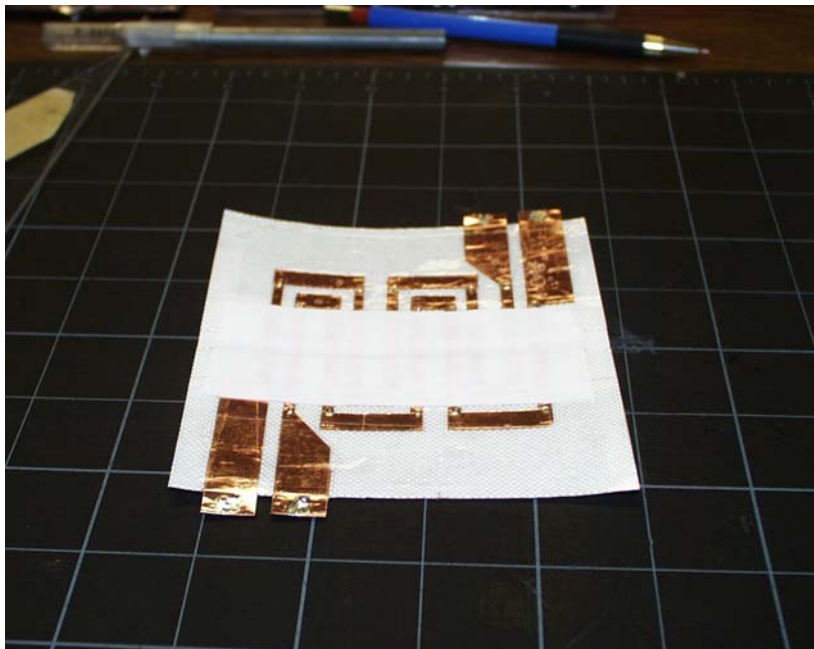
Figure A.41 Low-tack Tape Covering Copper Strips Across Gap

163
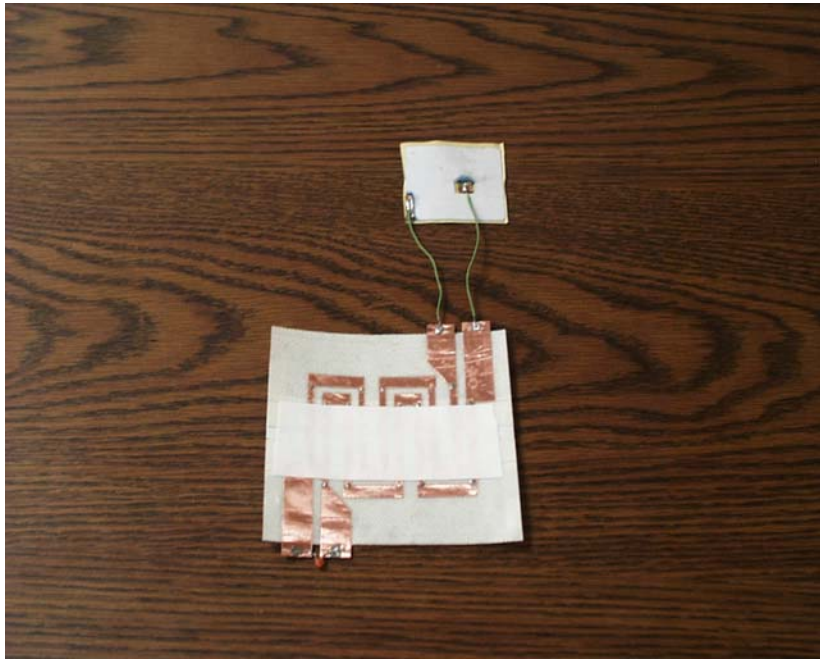
Figure A.42 Complete Five-Crossing Distributed Sensor

A.5   GENERAL INSTALLATION PROCEDURE FOR SWITCH

To install the switches across a weld, the steel surface was first cleaned with acetone. Next, the low-tack tape on the back of the switch was removed from the copper strips. The backing was detached from an adhesive pad and placed on the steel, positioning the gap edge of the switch flush with the edge of the weld. The backing was then removed from the back of the other adhesive pad and attached to the steel, again aligning the edge of the pad with the weld edge. Both pads were pressed to the steel surface using a roller or putty knife. Finally, the low tack tape protecting the copper strips was removed from the front of the switch.

APPENDIX B

Frequency Response of Distributed Sensors

B.1   RESPONSE OF DISTRIBUTED SENSORS WITH ONE ADDED CAPACITOR

The data presented in Tables B.1 through B.7 represent the measured characteristic frequencies for the distributed sensor when the switches are opened in sequence. The frequencies calculated using the electrical circuit model and average values of L_{eff} and ε_r/t are also reported.

Table B.1 Frequency Response of Distributed Sensor with Three Pairs of Switches

Distance to Steel Plate (in.)	Last Switch Opened *	Characteristic Frequency (MHz)	
		Measured	Calculated $\varepsilon_r/t = 5457$ $L_{eff} = 3.57\ \mu H$
12	0	4.33	-
0	0	4.35	4.59
0	1	7.44	7.44
0	2	7.64	7.55
0	3	7.71	7.62
0	4	7.84	7.76
0	5	7.98	7.89
0	6	8.09	7.97
12	6	8.16	-

* switches opened in sequence

Table B.2 Frequency Response of Distributed Sensor with Five Pairs of Switches

Distance to Steel Plate (in.)	Last Switch Opened *	Characteristic Frequency (MHz)	
		Measured	Calculated $\varepsilon_r/t = 5924$ $L_{eff} = 3.34\ \mu H$
12	0	4.47	-
0	0	4.47	4.62
0	1	7.14	7.22
0	2	7.35	7.34
0	3	7.46	7.40
0	4	7.62	7.53
0	5	7.68	7.63
0	6	7.75	7.72
0	7	7.86	7.80
0	8	7.98	7.96
0	9	8.16	8.11
0	10	8.27	8.19
12	10	8.22	-

* switches opened in sequence

Table B.3 Frequency Response of Distributed Sensor with Seven Pairs of Switches

Distance to Steel Plate (in.)	Last Switch Opened *	Characteristic Frequency (MHz)	
		Measured	Calculated $\varepsilon_r/t = 5258$ $L_{eff} = 2.97\ \mu H$
12	0	4.53	-
0	0	4.56	4.87
0	1	7.53	7.48
0	2	7.59	7.58
0	3	7.75	7.64
0	4	7.80	7.75
0	5	7.84	7.83
0	6	7.98	7.92
0	7	7.95	7.98
0	8	8.11	8.11
0	9	8.25	8.21
0	10	8.38	8.30
0	11	8.47	8.37
0	12	8.49	8.53
0	13	8.76	8.64
0	14	8.76	8.75
12	14	8.22	-

* switches opened in sequence

167

Table B.4 Frequency Response of Distributed Sensor with Nine Pairs of Switches

Distance to Steel Plate (in.)	Last Switch Opened *	Characteristic Frequency (MHz)	
		Measured	Calculated $\varepsilon_r/t = 6177$ $L_{eff} = 3.46\ \mu H$
12	0	4.31	-
0	0	4.08	4.36
0	1	6.31	6.45
0	2	6.56	6.54
0	3	6.67	6.59
0	4	6.76	6.69
0	5	6.81	6.75
0	6	6.87	6.83
0	7	6.90	6.89
0	8	7.01	7.00
0	9	7.14	7.08
0	10	7.23	7.17
0	11	7.32	7.24
0	12	7.41	7.37
0	13	7.57	7.47
0	14	7.62	7.56
0	15	7.71	7.64
0	16	7.84	7.80
0	17	8.04	7.95
0	18	8.09	8.03
12	18	8.25	-

* switches opened in sequence

Table B.5 Frequency Response of Distributed Sensor with Ten Pairs of Switches

Distance to Steel Plate (in.)	Last Switch Opened *	Characteristic Frequency (MHz)	
		Measured	Calculated $\varepsilon_r/t = 6528$ $L_{eff} = 2.94\ \mu H$
12	0	4.49	-
0	0	4.36	4.54
0	1	6.58	6.59
0	2	6.69	6.69
0	3	6.75	6.74
0	4	6.80	6.83
0	5	6.91	6.93
0	6	7.08	6.99
0	7	7.22	7.05
0	8	7.11	7.15
0	9	7.24	7.23
0	10	7.33	7.32
0	11	7.41	7.40
0	12	7.55	7.52
0	13	7.66	7.61
0	14	7.77	7.72
0	15	7.85	7.80
0	16	7.93	7.94
0	17	8.15	8.06
0	18	8.26	8.18
0	19	8.29	8.29
0	20	8.45	8.46
12	20	8.10	-

* switches opened in sequence

Table B.6 Frequency Response of Distributed Sensor with Eleven Pairs of Switches

Distance to Steel Plate (in.)	Last Switch Opened *	Characteristic Frequency (MHz)	
		Measured	Calculated $\varepsilon_r/t = 5326$ $L_{eff} = 3.18 \, \mu H$
12	0	4.49	-
0	0	4.42	4.55
0	1	6.69	6.69
0	2	6.76	6.77
0	3	6.81	6.82
0	4	7.01	6.90
0	5	6.96	6.96
0	6	7.03	7.03
0	7	7.08	7.08
0	8	7.21	7.17
0	9	7.28	7.24
0	10	7.35	7.32
0	11	7.39	7.37
0	12	7.55	7.48
0	13	7.53	7.55
0	14	7.59	7.64
0	15	7.75	7.70
0	16	7.84	7.83
0	17	7.91	7.92
0	18	8.07	8.01
0	19	8.13	8.09
0	20	8.31	8.24
0	21	8.38	8.37
0	22	8.49	8.45
12	22	8.02	-

* switches opened in sequence

Table B.7 Frequency Response of Distributed Sensor with Thirteen Pairs of Switches

Distance to Steel Plate (in.)	Last Switch Opened *	Characteristic Frequency (MHz)	
		Measured	Calculated $\varepsilon_r/t = 5734$ $L_{eff} = 2.87\ \mu H$
12	0	4.49	-
0	0	4.42	4.67
0	1	6.74	6.69
0	2	6.85	6.77
0	3	6.83	6.81
0	4	6.90	6.89
0	5	6.87	6.95
0	6	6.96	7.02
0	7	7.05	7.07
0	8	7.17	7.15
0	9	7.26	7.21
0	10	7.39	7.29
0	11	7.41	7.35
0	12	7.46	7.45
0	13	7.64	7.52
0	14	7.68	7.60
0	15	7.77	7.67
0	16	7.84	7.78
0	17	8.00	7.87
0	18	7.95	7.96
0	19	8.04	8.03
0	20	8.18	8.17
0	21	8.36	8.27
0	22	8.43	8.37
0	23	8.52	8.45
0	24	8.56	8.62
0	25	8.67	8.77
0	26	8.76	8.86
12	26	8.18	-

* switches opened in sequence

B.2   SOLUTION MATRICES FOR THE DIELECTRIC PARAMETER

The solution matrices for ε_r/t are presented in Tables B.8 through B.14 for the distributed sensors with three, five, seven, nine, ten, eleven, and thirteen pairs of switches. The switch state listed in the first column corresponds to state a and those listed in the first row correspond to state b.

Table B.8 Values of ε_r/t Calculated from the Distributed Sensor with Three Pairs of Switches

	2	3	4	5
3	5114			
4	5018	4972		
5	5202	5225	5500	
6	-5818	5959	6664	8885

Table B.9 Values of ε_r/t Calculated from the Distributed Sensor with Five Pairs of Switches

	2	3	4	5	6	7	8	9
3	13390							
4	9511	7905						
5	7065	5739	3522					
6	6238	5199	3735	3974				
7	6783	5990	5208	6325	9745			
8	5984	5365	4723	5116	5589	3935		
9	6287	5815	5416	5850	6334	5599	7562	
10	6515	6106	5803	6251	6736	6220	7951	8651

Table B.10 Values of ε_r/t Calculated from the Distributed Sensor with Seven Pairs of Switches

	2	3	4	5	6	7	8	9	10	11	12	13
3	62878											
4	7083	1742										
5	5298	2056	2503									
6	6390	3960	5770	10123								
7	4559	2674	3149	3507	-1212							
8	5147	3707	4400	5021	3357	7206						
9	5559	4349	5087	5725	4724	7504	7878					
10	5951	4897	5653	6289	5605	7880	8323	8812				
11	6007	5060	5759	6322	5755	7596	7775	7715	6516			
12	4946	4175	4568	4831	4271	5225	4710	3878	2334	657		
13	5913	5228	5728	6089	5720	6740	6641	6389	5840	5663	1972	
14	5285	4667	5037	5282	4903	5658	5392	4996	4352	3956	6719	0

Table B.11 Values of ε_r/t Calculated from the Distributed Sensor with Nine Pairs of Switches

	2	3	4	5	6	7	8	9	10	11	12	13	14	15	16	17
3	65397.54															
4	11619.55	5773.96														
5	8029.98	4675.16	3395.63													
6	6929.74	4666.07	4053.15	4648.26												
7	5761.95	3988.61	3316.26	3278.33	1745.30											
8	5954.74	4605.32	4296.82	4561.00	4519.20	6595.30										
9	6953.74	5776.65	5777.26	6355.29	6980.77	9529.54	14989.75									
10	6842.46	5846.36	5859.79	6326.82	6771.41	8329.88	9556.83	6225.33								
11	7076.33	6178.30	6245.03	6715.54	7176.87	8529.80	9494.74	7482.36	9346.23							
12	6476.17	5740.15	5735.76	6029.43	6251.76	7008.91	7128.63	5680.55	5446.62	3856.99						
13	6969.16	6314.14	6376.25	6702.85	6985.84	7721.40	7981.33	6988.90	7218.18	6677.81	11337.73					
14	6454.98	5871.61	5881.39	6115.35	6285.62	6810.99	6850.44	5963.36	5906.74	5319.79	6373.12	2536.91				
15	6523.41	5984.55	6003.91	6227.51	6392.75	6872.07	6916.31	6157.73	6145.50	5700.59	6654.54	4518.66	7373.08			
16	6299.90	5837.51	5842.44	6017.05	6134.21	6497.70	6485.56	5876.17	5829.97	5485.44	6000.72	4736.26	5708.80	4971.50		
17	6586.87	6177.48	6205.09	6380.47	6508.79	6846.50	6872.78	6389.19	6406.82	6176.80	6727.94	5953.61	6902.65	6790.26	8919.39	
18	6360.99	5977.15	5990.08	6140.01	6241.76	6533.60	6527.74	6072.73	6058.06	5830.14	6234.40	5511.87	6179.23	5959.00	6663.62	3142.31

Table B.12 Values of ε_r/t Calculated from the Distributed Sensor with Ten Pairs of Switches

	2	3	4	5	6	7	8	9	10	11	12	13	14	15	16	17	18	19
3	6489																	
4	4200	3111																
5	7200	7468	24237															
6	10811	12118	27876	30909														
7	13827	15858	33605	38914	55927													
8	5462	5335	6109	4308	707	-3049												
9	6804	6839	7994	6572	3715	662	23379											
10	6490	6490	7289	6179	4070	1902	9795	5013										
11	6624	6634	7357	6407	4633	2825	9147	6111	7798									
12	6843	6867	7500	6733	5326	3902	8810	6911	8026	8168								
13	7015	7047	7631	6965	5756	4534	8762	7298	8207	8349	8583							
14	6947	6972	7464	6889	5859	4828	8248	7093	7669	7640	7351	6439						
15	6862	6881	7312	6793	5873	4958	7901	6912	7334	7255	6914	6235	5985					
16	6394	6390	6707	6255	5468	4699	6937	6123	6304	6126	5640	4974	4329	3399				
17	7087	7111	7466	7070	6375	5686	7930	7253	7572	7549	7427	7219	7470	7998	15930			
18	6971	6987	7296	6938	6315	5700	7648	7055	7300	7258	7113	6908	7017	7260	10039	5821		
19	6490	6490	6733	6400	5826	5268	6896	6352	6490	6396	6162	5887	5787	5752	6811	3592	1426	
20	6468	6467	6681	6386	5881	5392	6809	6342	6457	6377	6185	5968	5902	5891	6631	4699	4240	6282

Table B.13 Values of ε_r/t Calculated from the Distributed Sensor with Eleven Pairs of Switches

	2	3	4	5	6	7	8	9	10	11	12	13	14	15	16	17	18	19	20	21
3	12201																			
4	4828	2669																		
5	18464	21391	-28756																	
6	5987	5132	7312	-1645																
7	6409	5744	7728	646	8848															
8	5228	4680	5418	1298	4074	2366														
9	6530	6119	7254	3317	7219	6760	22960													
10	6144	5785	6576	3518	6280	5829	9170	4283												
11	6217	5899	6616	3908	6383	6033	8451	5290	6897											
12	5365	5075	5482	3448	5049	4683	5537	3604	3294	1853										
13	6225	5989	6507	4564	6335	6117	7314	5832	6397	6249	18856									
14	5124	4888	5173	3622	4810	4539	5041	3841	3739	3198	4203	-957								
15	5169	4952	5221	3790	4900	4661	5128	4086	4048	3646	4623	1282	5757							
16	5453	5268	5536	4268	5302	5120	5581	4754	4827	4604	5619	3665	6999	7701						
17	5400	5232	5469	4331	5254	5092	5486	4774	4837	4655	5453	3975	6222	6359	4891					
18	5276	5120	5325	4291	5117	4966	5298	4665	4708	4542	5171	3957	5612	5582	4397	3880				
19	5752	5613	5847	4848	5702	5582	5966	5398	5514	5417	6172	5161	6950	7154	6916	8257	15778			
20	5306	5176	5349	4494	5183	5064	5333	4844	4892	4779	5257	4437	5552	5528	4970	4995	5456	2178		
21	5494	5380	5548	4771	5415	5316	5574	5151	5215	5133	5586	4915	5899	5913	5567	5712	6184	4490	7386	
22	5454	5345	5502	4768	5373	5279	5518	5121	5179	5102	5512	4897	5779	5781	5457	5560	5914	4536	6387	4712

1

Table B.14 Values of ε_r/t Calculated from the Distributed Sensor with Thirteen Pairs of Switches

	2	3	4	5	6	7	8	9	10	11	12	13	14	15	16	17	18	19	20	21	22	23	24	25
3	-1211																							
4	1344	4496																						
5	416	1263	-1099																					
6	1777	3002	2259	9422																				
7	3068	4708	4803	14288	29147																			
8	4067	5681	6071	11961	13549	9528																		
9	4803	6437	6986	12083	13199	10660	12487																	
10	5942	7690	8478	13370	14613	12943	15688	18863																
11	5365	6712	7153	10242	10417	9014	8803	7551	1656															
12	4727	5679	5856	7644	7401	6379	5678	4588	1840	1948														
13	6120	7277	7685	9892	9954	9077	8980	8440	6523	9176	106288													
14	5606	6517	6762	8327	8214	7484	7164	6593	5104	6150	10672	2348												
15	5885	6770	7026	8504	8419	7766	7521	7053	5812	6862	10585	4864	10378											
16	5451	6153	6307	7392	7242	6701	6401	5973	4989	5561	7058	3901	4795	2804										
17	6042	6761	6959	8052	7959	7477	7279	6947	6128	6807	8508	5892	7464	6724	16428									
18	5036	5568	5647	6409	6240	5813	5524	5171	4434	4754	5442	3568	3899	2984	3102	-1705								
19	5194	5708	5793	6518	6368	5974	5718	5402	4739	5061	5737	4084	4488	3788	4280	1204	8055							
20	5249	5712	5787	6421	6286	5943	5721	5452	4891	5173	5738	4410	4779	4282	4772	2968	6478	5740						
21	5662	6123	6216	6840	6732	6422	6247	6020	5531	5836	6440	5272	5726	5371	6070	4790	8173	8206	11999					
22	5513	5929	6005	6558	6450	6165	5992	5780	5333	5591	6086	5061	5423	5102	5611	4548	6891	6671	7301	3599				
23	5563	5959	6032	6553	6451	6184	6024	5827	5414	5658	6119	5183	5524	5242	5716	4802	6818	6631	7056	4829	6471			
24	5094	5419	5460	5877	5768	5530	5366	5180	4811	4983	5296	4515	4727	4464	4713	3957	5190	4898	4664	3046	2831	1338		
25	5006	5298	5330	5699	5596	5381	5229	5060	4727	4876	5140	4457	4634	4405	4607	3973	4964	4717	4506	3347	3285	2572	4053	
26	5057	5339	5371	5724	5627	5423	5280	5121	4809	4952	5206	4567	4740	4531	4732	4156	5082	4868	4710	3736	3764	3276	4798	6206

1

B.3   SOLUTIONS FOR EFFECTIVE INDUCTANCE

The solutions for the effective inductance of a distributed sensor at each switch state are presented in Tables B.15 through B.21. The mean value of ε_r/t, the mean value minus the standard deviation of ε_r/t, and the mean value plus the standard deviation of ε_r/t were used to calculate L_{eff}.

Table B.15 Values of L_{eff} Calculated from the Distributed Sensor with Three Pairs of Switches

Leff (μH)

Switch Last Opened	ε_r/t - Std. Dev.	ε_r/t	ε_r/t + Std. Dev.
0	4.01	3.97	3.92
1	3.66	3.57	3.49
2	3.56	3.48	3.41
3	3.56	3.49	3.42
4	3.55	3.50	3.44
5	3.54	3.50	3.45
6	3.50	3.46	3.42
Average	3.63	3.57	3.51
Std. Dev.	0.18	0.18	0.18
C.O.V.	4.90%	5.06%	5.25%

Table B.16 Values of $\mathbf{L_{eff}}$ ***Calculated from the Distributed Sensor with Five Pairs of Switches***

Leff (µH)

Switch Last Opened	ε_r/t - Std. Dev.	ε_r/t	ε_r/t + Std. Dev.
0	3.70	3.59	3.48
1	3.65	3.42	3.23
2	3.54	3.34	3.16
3	3.49	3.30	3.13
4	3.45	3.27	3.12
5	3.46	3.30	3.16
6	3.47	3.33	3.19
7	3.43	3.30	3.17
8	3.45	3.34	3.23
9	3.40	3.31	3.22
10	3.36	3.28	3.21
Average	3.49	3.34	3.21
Std. Dev.	0.10	0.09	0.10
C.O.V.	2.97%	2.73%	3.09%

Table B.17 Values of L_{eff} Calculated from the Distributed Sensor with Seven Pairs of Switches

Leff (μH)

Switch Last Opened	ε_r/t - Std. Dev.	ε_r/t	ε_r/t + Std. Dev.
0	3.56	3.39	3.24
1	3.25	2.94	2.68
2	3.26	2.96	2.72
3	3.17	2.89	2.66
4	3.20	2.94	2.71
5	3.22	2.96	2.75
6	3.16	2.93	2.73
7	3.22	2.99	2.80
8	3.17	2.97	2.79
9	3.13	2.94	2.78
10	3.08	2.91	2.77
11	3.06	2.90	2.77
12	3.12	3.00	2.88
13	3.00	2.89	2.80
14	3.05	2.96	2.88
Average	3.18	2.97	2.80
Std. Dev.	0.13	0.12	0.14
C.O.V.	4.12%	4.05%	4.93%

179

Table B.18 Values of L_{eff} Calculated from the Distributed Sensor with Nine

Pairs of Switches

Leff (µH)

Switch Last Opened	ε_r/t - Std. Dev.	ε_r/t	ε_r/t + Std. Dev.
0	4.10	3.95	3.81
1	3.89	3.61	3.38
2	3.69	3.44	3.23
3	3.62	3.38	3.17
4	3.61	3.39	3.19
5	3.63	3.41	3.21
6	3.64	3.42	3.23
7	3.67	3.46	3.27
8	3.65	3.46	3.28
9	3.59	3.40	3.24
10	3.57	3.40	3.25
11	3.55	3.38	3.23
12	3.57	3.42	3.28
13	3.50	3.37	3.25
14	3.54	3.41	3.30
15	3.52	3.40	3.30
16	3.52	3.43	3.34
17	3.46	3.38	3.31
18	3.48	3.41	3.35
Average	3.62	3.46	3.29
Std. Dev.	0.09	0.15	0.15
C.O.V.	2.57%	4.25%	4.66%

Table B.19 Values of* L_{eff} *Calculated from the Distributed Sensor with Ten Pairs of Switches

Leff (μH)

Switch Last Opened	ε_r/t - Std. Dev.	ε_r/t	ε_r/t + Std. Dev.
0	3.52	3.36	3.22
1	3.40	3.10	2.86
2	3.38	3.10	2.86
3	3.37	3.10	2.86
4	3.40	3.13	2.90
5	3.37	3.11	2.89
6	3.26	3.02	2.81
7	3.19	2.96	2.76
8	3.37	3.14	2.94
9	3.30	3.08	2.89
10	3.31	3.10	2.91
11	3.29	3.09	2.91
12	3.26	3.07	2.91
13	3.23	3.06	2.90
14	3.22	3.06	2.91
15	3.22	3.06	2.93
16	3.25	3.11	2.98
17	3.15	3.03	2.92
18	3.15	3.04	2.94
19	3.19	3.10	3.01
20	3.18	3.10	3.04
Average	3.29	3.10	2.90
Std. Dev.	0.07	0.09	0.10
C.O.V.	2.08%	2.76%	3.40%

Table B.20 Values of L_{eff} ***Calculated from the Distributed Sensor with Eleven Pairs of Switches***

Leff (µH)

Switch Last Opened	ε_r/t - Std. Dev.	ε_r/t	ε_r/t + Std. Dev.
0	3.49	3.36	3.24
1	3.43	3.18	2.96
2	3.44	3.19	2.98
3	3.43	3.19	2.98
4	3.31	3.08	2.89
5	3.40	3.17	2.98
6	3.40	3.18	2.99
7	3.39	3.18	2.99
8	3.35	3.15	2.97
9	3.34	3.14	2.97
10	3.34	3.15	2.99
11	3.34	3.16	3.00
12	3.29	3.12	2.97
13	3.37	3.20	3.06
14	3.37	3.22	3.08
15	3.28	3.14	3.01
16	3.30	3.17	3.05
17	3.31	3.19	3.08
18	3.24	3.14	3.04
19	3.24	3.14	3.05
20	3.20	3.12	3.05
21	3.24	3.18	3.11
22	3.20	3.15	3.09
Average	3.36	3.18	3.00
Std. Dev.	0.05	0.06	0.08
C.O.V.	1.48%	1.92%	2.63%

Table B.21 Values of L_{eff} ***Calculated from the Distributed Sensor with Thirteen***

Pairs of Switches

Leff (μH)

Switch Last Opened	ε_r/t - Std. Dev.	ε_r/t	ε_r/t + Std. Dev.
0	3.46	3.20	2.97
1	3.29	2.83	2.47
2	3.25	2.80	2.46
3	3.31	2.86	2.51
4	3.31	2.87	2.53
5	3.37	2.93	2.59
6	3.34	2.91	2.58
7	3.29	2.88	2.56
8	3.25	2.86	2.55
9	3.22	2.84	2.54
10	3.16	2.79	2.51
11	3.18	2.82	2.54
12	3.20	2.86	2.58
13	3.10	2.78	2.52
14	3.12	2.81	2.56
15	3.09	2.79	2.55
16	3.11	2.83	2.59
17	3.04	2.78	2.56
18	3.13	2.87	2.66
19	3.10	2.86	2.66
20	3.08	2.86	2.67
21	3.01	2.81	2.64
22	3.01	2.83	2.67
23	2.99	2.83	2.68
24	3.05	2.91	2.78
25	3.05	2.94	2.83
26	3.03	2.93	2.84
Average	3.22	2.87	2.57
Std. Dev.	0.09	0.10	0.12
C.O.V.	2.88%	3.49%	4.65%

B.4 RESPONSE OF DISTRIBUTED SENSORS WHEN THE LOCATION OF THE INITIAL OPEN SWITCH IS VARIED

Four additional distributed sensors with five pairs of switches and one added capacitor were tested. In each case, the location of the initial open switch was varied. The measured and calculated data are reported in Tables B.22 through B.25. The values of L_{eff} and ε_r/t for the four distributed sensors were assumed to be the same for the sensor which was opened in sequence starting with switch S_1. These values were not calculated because insufficient data were collected to estimate these parameters.

Table B.22 Response of Distributed Sensor with Five Pairs of Switches When Switch S_3 is Opened First

Distance to Steel Plate (in.)	Last Switch Opened	Characteristic Frequency (MHz)	
		Measured	Calculated $\varepsilon_r/t = 5924$ $L_{eff} = 3.34\ \mu H$
12	0	4.49	-
0	0	4.38	4.63
0	3	7.08	6.87
0	4	7.57	7.54
12	4	8.11	-

Table B.23 Response of Distributed Sensor with Five Pairs of Switches When Switch S_5 is Opened First

Distance to Steel Plate (in.)	Last Switch Opened	Characteristic Frequency (MHz)	
		Measured	Calculated $\varepsilon_r/t = 5924$ $L_{eff} = 3.34\ \mu H$
12	0	4.40	-
0	0	4.35	4.63
0	5	7.32	7.28
0	6	7.68	7.73
12	6	8.11	-

Table B.24 Response of Distributed Sensor with Five Pairs of Switches When

Switch S₇ is Opened First

Distance to Steel Plate (in.)	Last Switch Opened	Characteristic Frequency (MHz)	
		Measured	Calculated $\varepsilon_r/t = 5924$ $L_{eff} = 3.34\ \mu H$
12	0	4.42	-
0	0	4.35	4.63
0	7	7.37	7.32
0	8	7.80	7.97
12	8	8.16	-

Table B.25 Response of Distributed Sensor with Five Pairs of Switches When

Switch S₉ is Opened First

Distance to Steel Plate (in.)	Last Switch Opened	Characteristic Frequency (MHz)	
		Measured	Calculated $\varepsilon_r/t = 5924$ $L_{eff} = 3.34\ \mu H$
12	0	4.44	-
0	0	4.40	4.63
0	9	7.82	7.92
0	10	8.20	8.19
12	10	8.22	-

B.5   RESPONSE OF A DISTRIBUTED SENSOR WITH TEN PAIRS OF SWITCHES AND TEN ADDED CAPACITORS

The measured frequency response of a distributed sensor with ten pairs of switches and ten added capacitors is summarized in Table B.23. The electrical circuit model described in Section 5.3.5 was used to calculate the response. The values of L_{eff} and ε_r/t for the distributed sensor with ten pairs of switches and one added capacitor were assumed to be the same for this sensor and were used to

calculate the electrical circuit model values. These values were not calculated because of the complexity of the capacitor equations for the sensor with ten added capacitors.

Table B.26 Frequency Response of Distributed Sensor with Ten Pairs of Switches and Ten Added Capacitors

Distance to Steel Plate (in.)	Last Switch Opened *	Characteristic Frequency (MHz)	
		Measured	Calculated $\varepsilon_r/t = 6528$ $L_{eff} = 2.94\ \mu H$
12	0	4.27	-
0	0	4.30	4.43
0	1	4.47	4.60
0	2	4.49	4.63
0	3	4.66	4.79
0	4	4.69	4.83
0	5	4.88	5.04
0	6	4.91	5.04
0	7	5.18	5.25
0	8	5.18	5.29
0	9	5.43	5.54
0	10	5.46	5.58
0	11	5.79	5.87
0	12	5.81	5.93
0	13	6.20	6.28
0	14	6.25	6.34
0	15	6.72	6.77
0	16	6.78	6.86
0	17	7.35	7.44
0	18	7.49	7.53
0	19	8.32	8.29
0	20	8.40	8.46
12	20	7.96	-

* switches opened in sequence

References

Arce, Gabriela. *Impact of Higher Strength Steels on Local Buckling and Overstrength of Links in Eccentrically Braced Frames*. Thesis. University of Texas at Austin, 2002.

Engelhardt, Michael D. and Thomas A. Sabol. "Lessons Learned from the Northridge Earthquake: Steel Moment Frame Performance." *A New Direction in Seismic Design*. Tokyo, 1995.

Engelhardt, Michael D. and Thomas A. Sabol. "Developments in Seismic Resistant Steel Moment Connections Since the 1996 Northridge Earthquake." *Progress in Structural Engineering and Materials* 1 (1997): 68-77.

Okazaki, Taichiro. "Development of Link-to-Column Connections for Steel Eccentrically Braced Frames." Diss. University of Texas at Austin, 200x.

SAC Joint Venture. *Interim Guidelines: Evaluation, Repair, Modification and Design of Welded Steel Moment Frame Structures*. Report No. SAC-95-02. Sacramento, CA: The SAC Joint Venture, 1995.

SAC Joint Venture. *Technical Report: Analytical and Field Investigations of Buildings Affected by the Northridge Earthquake of January 17, 1994*. Report No. SAC-95-04, Part 2. Sacramento, CA: The SAC Joint Venture, 1995.

SAC Joint Venture. *Technical Report: Surveys and Assessment of Damage to Buildings Affected by the Northridge Earthquake of January 17, 1994*. Report No. SAC-95-06. Sacramento, CA: The SAC Joint Venture, 1995.

Sabol, Thomas A. and Michael D. Engelhardt. "Welded Steel Moment Frame Test Programs." *Proceedings Structures Conference '96*. Chicago: American Society of Civil Engineers, 1996.

Serway, Raymond A. *Physics for Scientists & Engineers*. 4th ed. Vol. 2. Philadelphia: Saunders Golden Sunburst Series, 1996. 970-979.

Spadea, Joseph R. *Fatigue Strength of Fillet-Welded Transverse Stiffeners With Undercuts*. Thesis. University of Texas at Austin, 2002.

Vita

Lisa J. Novak was born in South Bend, Indiana on May 18, 1978, to Robert J. and Loraine J. Novak. Her family moved to Atlanta, Georgia shortly thereafter, where her sister Karen was born in 1981. That same year, the family moved to Guaynabo, Puerto Rico. In 1986, the Novaks moved to Champaign, Illinois. Lisa graduated from University High School in Urbana, Illinois in 1996. She attended the University of Illinois at Urbana-Champaign from 1996 to 2000, graduating in May 2000 with a Bachelor of Science in Civil Engineering. During her time at Illinois, Lisa participated in two undergraduate research projects, served a term as Editor for the Alpha Chapter of Chi Epsilon, and was an undergraduate teaching assistant in the Department of Mathematics for three years. In September 2000, she began her graduate research at Ferguson Structural Engineering Laboratory at the University of Texas at Austin under the supervision of Dr. Sharon L. Wood. Lisa graduated with a Master of Science in Civil Engineering in August 2002.

Permanent Address: 1817 Maynard Dr.

Champaign, IL 61822

United States of America

This thesis was typed by the author.